Metamorphic evolution of the Hırkadağ and Kırşehir massifs, Central Turkey,

based on geothermobarometry of HT metapelitic rocks

MSc Thesis
Kalijn Peters
Supervisor:
Prof. Dr. R.L.M. Vissers

Faculty of Geosciences
Department of Structural geology and tectonics
Utrecht University

August 2010

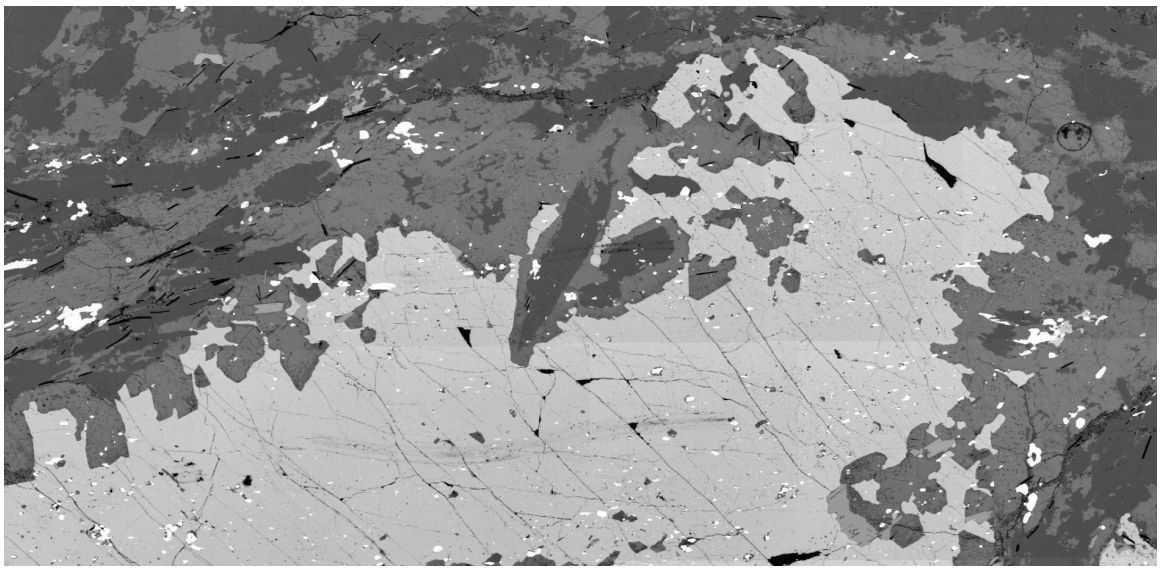

Abstract

The Central Anatolian Crystalline Complex (CACC) in Turkey is a continental domain of Pan-African origin that collided with the Eurasian continent during the Alpine orogeny. The crystalline rocks are characterized by intense Late Cretaceous deformation, high-temperature metamorphism and intrusion.

This study focuses on the metamorphic history recorded in regionally metamorphic garnet-sillimanite schists from the Hırkadağ massif in the centre of the CACC and garnet-sillimanite schists and biotite-clinopyroxene schists from the Kırşehir massif in the northwest of the CACC. The principal aim is to elucidate PTt histories of selected samples of pelitic rocks from both massifs on the basis of microstructurally controlled mineral chemistry data.

Petrography and mineral and bulk rock major element compositions are used to calculate and interpret TheriakDomino PT-pseudosections. The general mineral assemblage observed in the pelitic schists from the Hirkadag massif is Grt + Bt + Sil + Plag + Qtz + Spl ± Kfs ± Crd ± Wh mica + Ilm. The mineral assemblage of the garnet-sillimanite schist of Kırşehir is similar to the metapelitic rocks of the Hirkadag massif, but the microstructure is finer grained and lacks spinel: Grt + Bt + Sil + Plag + Qtz + Kfs + Wh mica. The biotite-clinopyroxene schists of the Kirsehir massif show a banded structure with pelitic bands, calc-silicate bands and intermediate zones, showing the mineral assemblage: Bt + Sil + Plag + Kfs + Qtz ± Cpx ± Wh mica ± Spl. Important reactions include replacement of garnet by cordierite (decompression) and growth of hercynite (high temperature). The two assemblages can be linked in a clockwise PT path.

Peak temperature conditions are best preserved in the cordierite-bearing garnet-sillimanite schists and less well in the biotite-clinopyroxene schists. PT domains calculated with TheriakDomino show approximately isothermal decompression from ~9.5 kbar to 3 kbar at temperatures of 800 °C for the samples of the Hırkadağ massif and decompression from about 8 kbar down to 5 kbar at 700 °C for the Kırşehir samples. Peak metamorphic conditions calculated with the garnet-biotite and Ti-in-biotite thermometers and GASP and GPMB barometers show lower peak temperatures: 620-740 °C at about 8 kbar for the Hırkadağ massif and 620 °C at 6 kbar for the Kırşehir massif.

The presence of melt as inferred by the high-temperature low-pressure metamorphic conditions and shown in TheriakDomino pseudosections is supported by microstructural relationships.

Attempts to date the metamorphism of the Hırkadağ and Kırşehir massifs using monazite U-Pb dating are unfortunately unsuccessful, because concentrations of radiogenic Pb are below the detection limits of the available electron microprobe at Utrecht University. These low concentrations are likely due to the relative young (Cretaceous, <100 Ma) age commonly assigned to the metamorphism and intrusion of the CACC.

The inferred HT/LP history calls for a highly anomalous thermal state of the pertinent crust, possibly indicating ascent of asthenospheric mantle to shallow levels.

Contents

1. Introduction

1.1 Setting

The Central Anatolian Crystalline Complex (CACC) in Turkey is a continental domain of Pan-African origin that collided with the Eurasian continent during the Alpine orogeny (see figure 1). The crystalline rocks in the CACC are characterised by intense Late Cretaceous deformation, low to moderate pressure and moderate to high temperature metamorphism (6-7 kbar at 750 °C; Whitney and Dilek, 2001; Whitney et al., 2001) and granitic, granodioritic and syenitic intrusions.

Whitney and Dilek (2001) have studied the metamorphic evolution of the Hırkadağ massif, situated in the centre of the CACC. They propose one single clockwise PT path based on upper amphibolite facies rock samples from different locations and rock types. An earlier garnet-sillimanite assemblage yielding metamorphic conditions of 670-710 °C, ~7 kbar has been overprinted by high-temperature, low-pressure metamorphism (3 kbar, >650 °C) as indicated by secondary cordierite + spinel (Whitney et al., 2001). According to Whitney and Dilek (2001) this HT LP event may be due to isothermal decompression at high temperatures or may be related to magmatism.

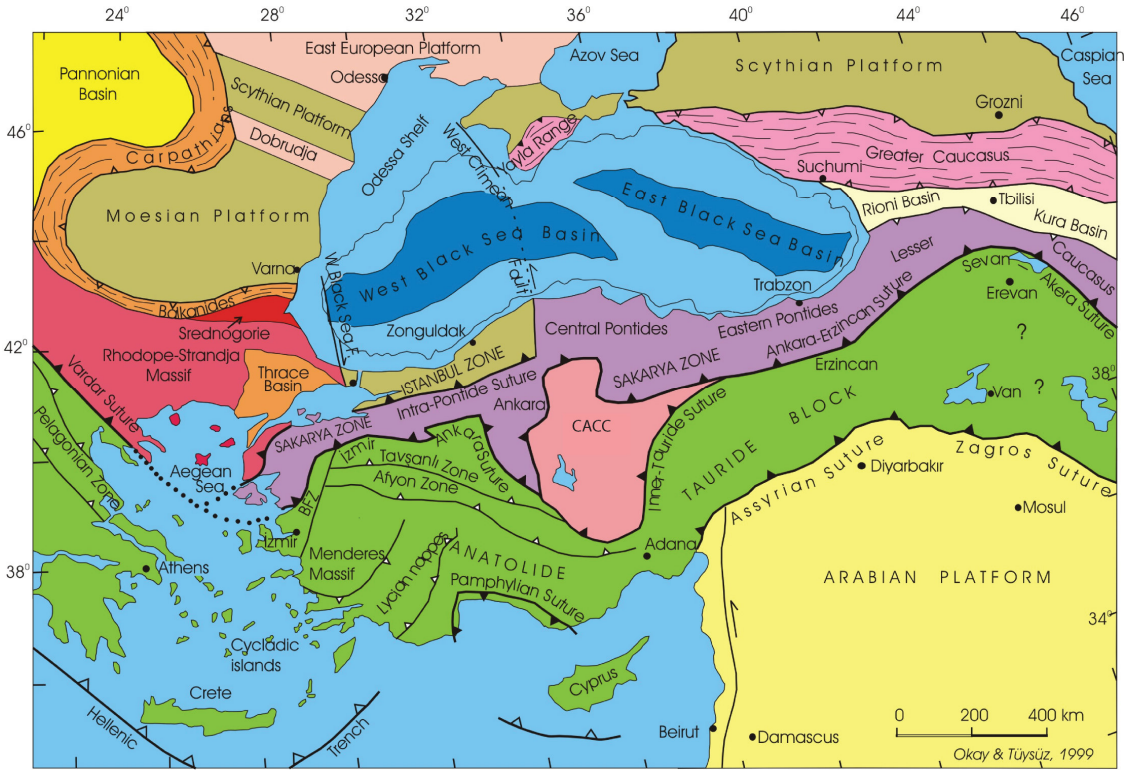

Figure 1. *Tectonic map of the Eastern Mediterranean region (modified after Okay and Tüysüz, 1999). The CACC is indicated in pink in the centre of Turkey.*

The northern part of the basement of the CACC (Kırşehir massif and Akdağ massif) has been suggested to have been exhumed primarily by erosion since the Late Cretaceous (Fayon et al., 2001; Whitney and Hamilton, 2004; Whitney et al., 2001) while the southern part of the CACC (Niğde massif) is supposed to have been exhumed by mainly extensional tectonic processes (Gautier et al., 2008; Whitney and Dilek, 1998). The Hırkadağ massif is situated in the centre of the CACC. Processes involved in its exhumation are as yet unclear, but current structural studies indicate that extensional unroofing may have been important (Lefebvre, personal communication).

1.2 Aim of the project

The aim of this research project is to unravel the metamorphic evolution of the Kırşehir and Hırkadağ massifs in the Central Anatolian Crystalline Complex. In a previous study, Whitney and Dilek (2001) have presented a PT path based on different samples from different locations. This research focuses on the construction of PT paths for several samples and on the question whether or not these samples experienced a same metamorphic history. As a consequence, we tried to find actual PT paths for individual samples from both the Hırkadağ and the Kirshir massifs. Questions pertinent to this objective are:

- did the Kırşehir and Hırkadağ massifs experience the same metamorphic event(s) or did they undergo different events at specific metamorphic conditions?
- are the peak metamorphic conditions preserved in the mineral assemblages in such a way that they can be determined with the use of geothermobarometry?
- can the inferred HT conditions be related to the highest pressures, or did peak temperatures and pressures not occur simultaneously?
- what is the age of the metamorphism in the metapelitic rocks and to which part of the PT path does this age correspond?
- what may be the cause of the HT, LP metamorphism?

In order to answer these questions, geothermobarometry and U-Th-Pb monazite age dating are applied. The scope of geothermobarometry is to deduce the metamorphic history by determining the PT-conditions of peak metamorphism and constructing a PT path, whilst an attempt is made to determine the age of the metamorphism via monazite dating.

1.3 Research approach

In this study samples of metapelitic rocks are investigated from both the Kırşehir and Hırkadağ massifs collected and provided by Prof. Dr. Vissers and MSc. P.C. Wehrens.

Thin sections were made from the metapelitic rock samples and these were studied with the optical microscope to assess the mineral assemblage, to obtain a rough indication of metamorphic grade and to identify appropriate microstructures for electron microprobe analyses. The chemical composition of minerals useful for thermobarometry was analysed with use of the electron microprobe, whilst XRF analyses provided the bulk rock composition. XRD analyses of aluminosilicates were done in order to find possible polymorphs of aluminosilicates that could further constrain the construction of PT paths.

Geothermobarometry was used to determine precise PT conditions of the protolith assemblage, peak metamorphism and retrograde assemblages. These PT conditions form the basis for the inferred PT path.

The geochronology of the metapelitic rocks was planned to be investigated by monazite U-Th-Pb. For this purpose the electron microprobe was used in order to obtain data for determining the ages of peak metamorphism and the time that the metamorphic minerals crystallized (reflected by the cooling age). Zoning in the monazites would provide ages reflecting polyphase metamorphism and potentially yields ages of prograde metamorphism.

The results of metamorphic and geochronological research are discussed and combined in order to construct a complete PTt path that reflects the metamorphic history of both the Kırşehir and Hırkadağ massifs. Finally, the results of this study are compared with results of previous studies, and will be incorporated in the larger-scale structural context of the CACC.

2. Geological setting

The geology of Turkey is controlled by the closure and northward subduction of the Neo-Tethyan Ocean in the Late Cretaceous to Early Tertiary. This closure and ongoing continental collision of the African and Eurasian plates have formed the east-west oriented orogenic belts of Turkey: the Pontides in the north, the Anatolides in central Turkey, the Taurides to the south, and the Border folds to the southeast (figure 2; Ketin, 1966). Ketin (1966) suggested that the tectonic-orogenic evolution of Anatolia proceeded gradually from the north to the south, starting in the Pontides and with the last movements in the Border fold region.

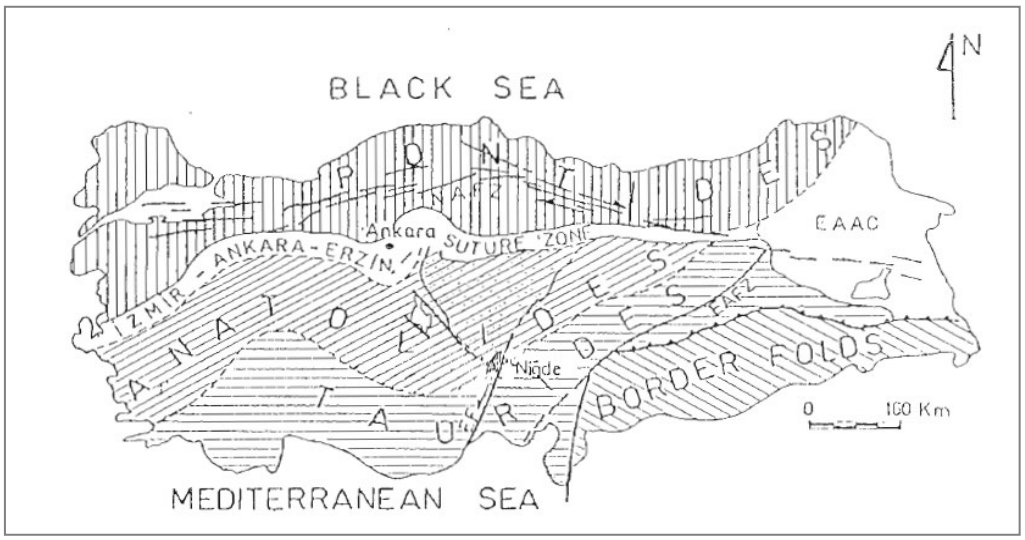

Figure 2. *Schematic map showing the main tectonic units of Turkey (from Ketin, 1966; in Kuşcu, 1992): the Pontides, Anatolides, Taurides and Border folds. EF: Ecemis fault zone, NAFZ: North Anatolian Fault Zone, EAAC: Eastern Anatolian Accretionary Complex.*

The Izmir-Ankara-Erzincan Suture zone (IAES) is a remnant of the Neo-Tethys. The Anatolide tectonic belt is characterised by high grade metamorphism south of the IAES and comprises two continental domains, that probably represent continental fragments of the Pan-African plate: the Menderes massif in western Turkey and the Central Anatolian Crystalline Complex (CACC) in the centre (figure 3).

2.1 Central Anatolian Crystalline Complex

The CACC (figure 4) is a triangular continental fragment bounded by the Izmir-Ankara-Erzincan Suture zone to the north, the Central Anatolian Fault Zone to the east and the Tuz Gölü Fault to the west (Whitney et al., 2003). The CACC consists of dominantly meta-sedimentary rocks, Late Cretaceous granitoids (Köksal et al., 2004), ophiolites and a cover of Cenozoic sediments and

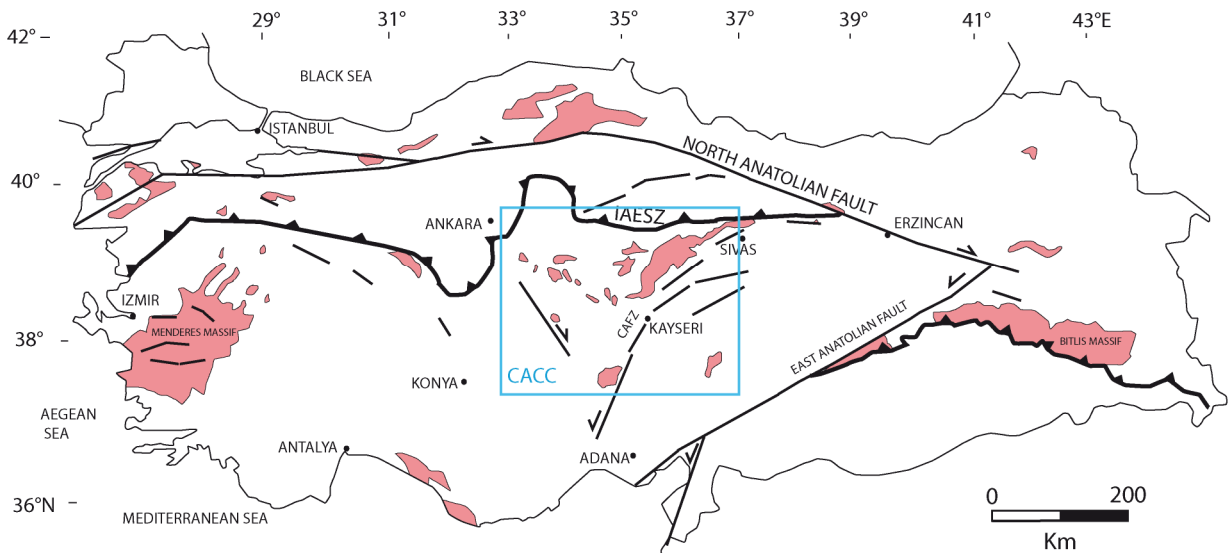

Figure 3. *Simplified geological map of Turkey after Whitney et al., 2001 (modified by Lefebvre). The locations of the metamorphic massifs are given in pink with the Central Anatolian Crystalline Complex (CACC) indicated with a blue box. IAESZ=Izmir-Ankara-Erzincan suture zone from which the geometry is not well constrained. CAFZ=Central Anatolian Fault Zone.*

volcanics. Three separate metamorphic massifs are defined, based on their geographic location: the Kırşehir massif in the northwest, the Akdağ massif in the northeast and the Niğde massif to the south (Whitney et al., 2001). The Hırkadağ block is a NW-SE trending massif in the central part of the CACC that consists of metamorphic rocks and felsic intrusives. According to Whitney and Dilek (2001), the Hırkadağ block is related to the Kırşehir massif, although it is isolated from that main massif by deformed Oligocene-Miocene sediments and younger volcanic rocks.

The geochronological data available at present (including limited zircon and monazite U-Pb SHRIMP data; Whitney et al., 2003; Whitney and Hamilton, 2004) propose Mesozoic ages of 90-85 Ma for peak temperature metamorphism and ages of 85-75 Ma for the intrusive plutons (e.g. Köksal et al., 2004). Apatite fission track ages in the northern massifs ranging from 47-32 Ma (Fayon et al., 2001) are in conflict with geological field data showing that Eocene limestones (48-40 Ma) unconformably overly the metamorphic and plutonic basement rocks.

2.2 Kırşehir massif

The Kırşehir massif in the northwest of the CACC (figure 5) consists of metamorphic rocks that range in grade from greenschist facies (chlorite zone) to upper amphibolite facies (sillimanite-K-feldspar zone; Whitney et al., 2001). In the Kaman area the metamorphic grade increases from southeast to

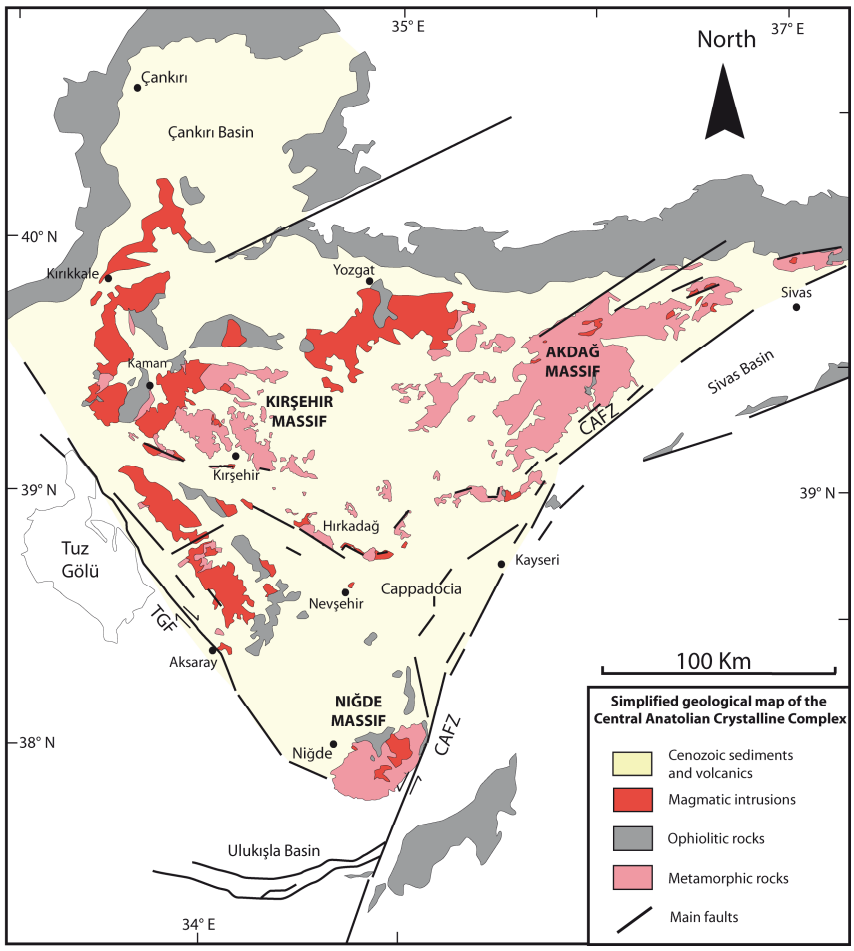

Figure 4. *Simplified geological map of the CACC from Whitney et al. (2003). Metamorphic rocks are indicated in pink. The Kırşehir and Hırkadağ massifs are located in the northwest and centre of the CACC, respectively.*

northwest, with estimated PT conditions of 400-700 °C at low pressures (1.5-2 kbar; Seymen, 1981) that are probably underestimated as garnet was stable (Whitney et al., 2001). According to Whitney et al. (2001) these variations in metamorphic grade were observed in both the Kaman and the Hırkadağ block. Wehrens (2008), however, suggests that in the Hırkadağ block the metamorphic conditions seem uniformly distributed throughout the area and no metamorphic field gradient could be established. The Kırşehir massif comprises marble and calcsilicate rocks interlayered with metapelitic schist, amphibolite (± garnet) and quartzite and is intruded by calc-alkaline and alkaline, subduction related granitiods (Whitney and Hamilton, 2004; Akiman et al., 1993). Field relations (e.g. xenoliths of high-grade gneiss and schist in the granitoids) show that the intrusions post-dated the peak of regional metamorphism and the event that formed the main foliation (Whitney and Hamilton, 2004). The metamorphic rocks are divided into three lithostratigraphic units: the Kalkanlidağ (gneiss, biotite schist, pyroxene schist, amphibole schist, quartzite, quartz schist and

calcsilicate schist), Tamadağ (marble, schist and gneiss) and the Bozcaldağ (marble and metachert-bearing marble) Formations (Seymen, 1981).

The massif is surrounded by Mesozoic ophiolites at the NE-NW, by Miocene to Pliocene sedimentary rocks of the Tuz Gölü Basin and Pliocene volcanic rocks to the SW and by Pliocene to recent volcanic rocks to the NE (Teklehaimanot, 1993).

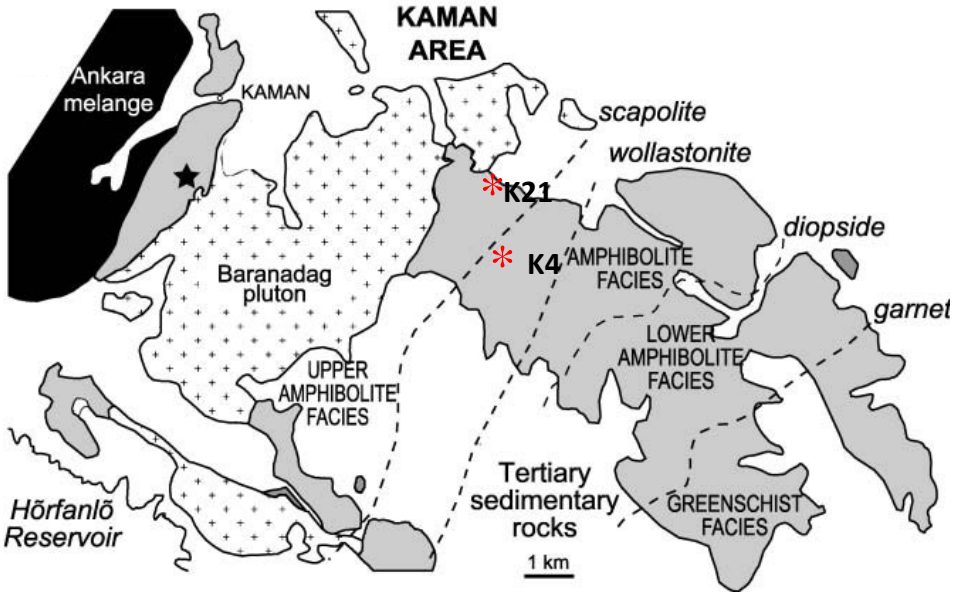

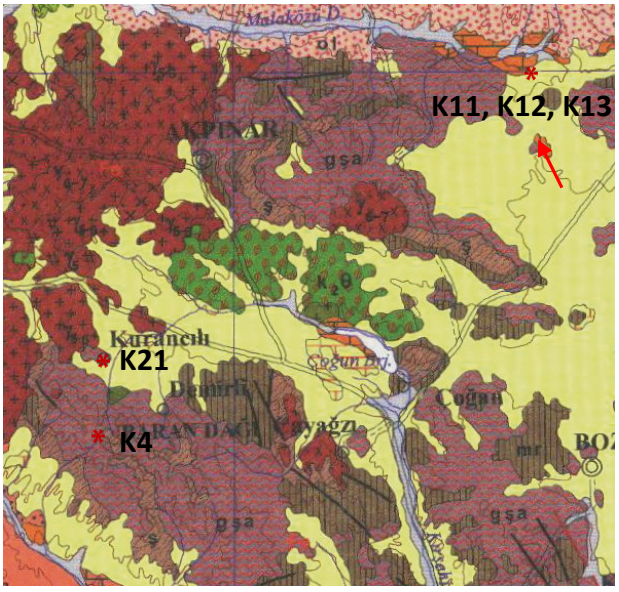

Figure 5. *Schematic geological map of the Kırşehir massif with a) the Kaman area in the Kırşehir massif from Whitney et al. (2001). Regional metamorphic isograds and facies are shown as well as the sample location for geochronoly (star; after Seymen, 1981; Whitney et al., 2001).Sample location of samples studied in this research are indicated with an asterix.b) The Kırşehir massif with sample locations: the two samples in the SW are also indicated in a), the other sample is taken from the crystalline basement that is covered by Eocene limestones. UTM coordinates of sample locations for the Kırşehir massif are given in Appendix 1.*

2.3 Hırkadağ massif

The Hırkadağ block is located between Gülşehir and Hacıbektas north of the Kızılırmak River, that marks a major tectonic boundary between the northern and southern part of the CACC (Dilek et al.,

1999). Recent studies of the Hırkadağ block are scarce and include a study by Teklehaimanot (1993), by Whitney and Dilek (2001) and more recently a structural and metamorphic study by Wehrens (2008). The block is bounded by high-angle normal faults in the northeast and southwest (Whitney et al., 2001). The rocks exposed in the study area are divided into four units: (1) the Paleozoic-Mesozoic Central Anatolian Metamorphic rocks, (2) the Cenomanian Ü□kapılı Granodiorite, (3) Elmadere Olistostrome (Tertiary) and (4) Eocene-Quaternary cover units (Teklehaimanot, 1993). According to the work of Göncuoğlü (1977; see also Teklehaimanot, 1993) the metasedimentary Central Anatolian Metamorphic rocks can be divided in the Gümüşler, Kaleboynu and Aşigediği Formations and are distributed throughout the area as a normal conformable sequence (Wehrens, 2008).

In the southern part of the Hırkadağ massif an alteration of up to ten meters thick quartzite beds interlayered with quartz-rich garnet-sillimanite schists, calcsilicates and banded marble are observed (Wehrens, 2008). These lithologies are identified as remnants of the Gümüşler Formation (Teklehaimanot, 1993). The central part of the studied area is dominated by the Kaleboynu Formation of mainly calcsilicates interbedded with marble and quartzite beds. Metapelitic garnet-sillimanite schist is associated with the quartzite. The northern part is characterised by the occurrence of marbles and minor amounts of calcsilicates and are identified as the Aşigediği Formation (Teklehaimanot, 1993). Felsic intrusives of the Ü□kapılı Granodiorite occur in minor amounts in the central part and in larger amounts in the northern part of the area (Teklehaimanot, 1993). A schematic geologic map with sample locations is given in figure 6.

At least four deformation phases have been recognised in the Hırkadağ massif (Wehrens, 2008):

- A Dm-1 phase indicated by relicts of an old crenulation cleavage as shown by the angular relations between biotite grains in the garnet-sillimanite schist.
- Dm: tight to isoclinal z-shaped folds (cm-scale) of garnet-sillimanite schists in a matrix of calcsilicates with an axial plane foliation (main foliation) that is present in both the garnet-sillimanite schist and in the calcsilicate.
- Dm+1: tight meter-scale folds refolding the main foliation and the development of an extensional mylonitic zone, reflecting vertical shortening.
- Dm+2: large scale (hundreds of meters) open folds that also affected the sediments to the north of the Hırkadağ area (Wehrens, 2008; Köksal and Göncüoğlu, 1997).

Ongoing study of the Hırkadağ massif (Lefebvre, personal communication) suggests that the extensional mylonitic zone is probably part of a detachment fault. Observations that support this

hypothesis include the occurrence of a fault plane that in the present-day orientation seems to have a thrust movement, but after reconstruction shows a low-angle normal movement; the occurrence of both brittle (brecciated marble) and ductile (shear zone) deformation and recrystallised marble, indicating an increasing temperature, that could correspond to the lower part of the detachment fault.

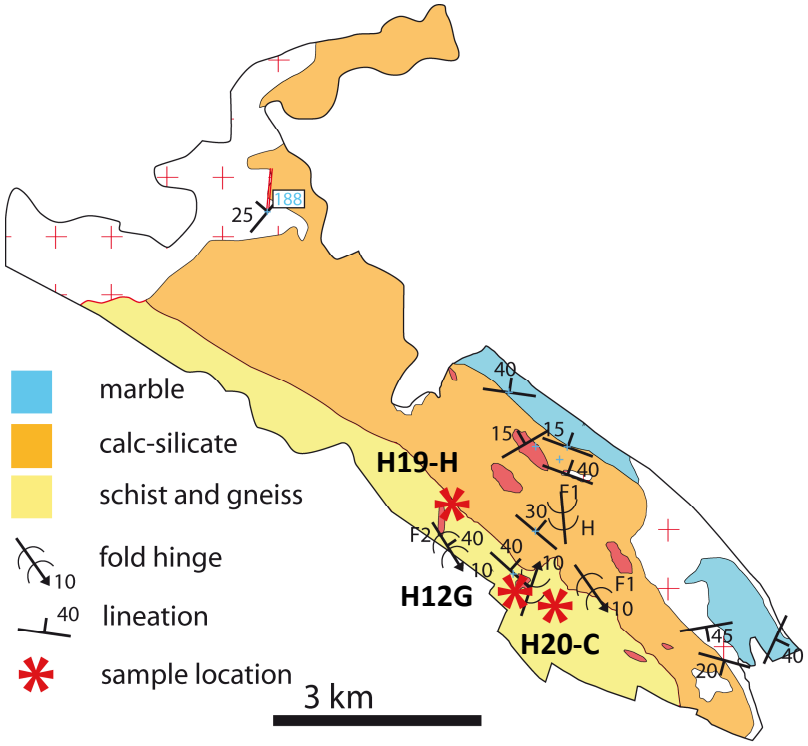

Figure 6. *Schematic geological map of the Hırkadağ block (after Whitney et al., 2003, Teklehaimanot, 1993; modified by Lefebvre). Lithologies are shown as well as main foliation. The sample locations are indicated with a red asterix.*

3. Metamorphism

3.1 Introduction

3.1.1 A review of general concepts

During metamorphism, the mineralogical and chemical composition as well as the structure of a rock change. Protoliths of metamorphic rocks include the entire range of sedimentary, igneous and metamorphic rocks with all possible chemical compositions. The process of metamorphism is driven by large-scale geodynamic processes such as global plate movements, subduction of oceanic and/or continental lithosphere and continent-continent collision that change the physical and/or chemical conditions and result in transient pressures and temperatures. The occurrence of the maximum pressure and maximum temperature conditions are often diachronous (England and Thompson, 1984). The changes in bulk rock composition and the composition of individual minerals are caused by chemical reactions.

Metamorphism often occurs episodically and therefore it is important to identify groups of minerals that have coexisted in chemical equilibrium at one stage during the metamorphic evolution of the rock: the mineral assemblage. The mineral assemblage defines the metamorphic grade, the particular pressure and temperature at which this group of minerals is in chemical equilibrium. In one rock, more than one mineral assemblage might be preserved (early assemblages survive as metastable relics), corresponding to different stages of metamorphism, like prograde, peak and retrograde conditions. The succession of mineral assemblages that follow and often replace one another during the metamorphic evolution is called the mineral paragenesis (Bucher and Frey, 2002). Since it is hardly possible to demonstrate that a given mineral assemblage once coexisted in chemical equilibrium, it is assumed in this study that minerals belong to one assemblage when the grains are in direct contact (without reaction textures in between) and when there is textural evidence that groups of minerals coexist, e.g. in a corona texture.

3.1.2 Geothermobarometry-background

An important aspect of studying the metamorphism of a rock, is the determination of the pressure and temperature at which the rock transformed. These pressure and temperature can be assessed by various methods.

A rough indication of the pressure and temperature conditions can be obtained via a characteristic mineral assemblage plotted on a petrogenic grid. This yields a space in the petrogenic grid, corresponding to the PT range in which the mineral assemblage formed. Since more than one

mineral assemblage can be preserved in one rock, different spaces on the petrogenic grid can be defined (for the metastable mineral assemblages), together forming (part of) the PT-path the rock experienced. However, petrogenic grids are typically constructed for simplified chemical systems, whereas real rocks may be more complex. Therefore it is important to consider the relation between the chemical system represented by the grid and the chemical system of the rock. Extra components influence the stability of the minerals in the grid, like MnO and CaO in garnet when analysed with use of a KFMASH grid, resulting in predictions about PT-conditions that do not reflect natural conditions.

A more accurate technique of determining the pressure and temperature at which the rock formed, is termed geologic thermometry and barometry or, in short, geothermobarometry (Bucher and Frey, 2002). The P-T conditions of the least hydrated state of a rock along a metamorphic evolution path can be inferred from mineral equilibria (both stable and metastable) together with the chemical composition of the minerals in a specific rock sample (especially the distribution of elements between coexisting minerals; Bucher and Frey, 2002). The basic idea of geothermobarometry is to find one or more suitable equilibrium mineral assemblages from which at least two reactions among the phase components can be formulated. The equilibrium conditions of the reactions are presented as lines on a P-T diagram and the intersection of these lines defines the pressure and temperature at which the assemblage was in equilibrium. Geothermometers are equilibria that have little pressure dependence and a corresponding low ΔV (volume change), high ΔS (entropy) and ΔH (enthalpy) and steep slopes in P-T diagrams. Similarly, geobarometers are equilibria that are relatively insensitive to temperature with high ΔV and low to moderate ΔS and ΔH and have gentle slopes in P-T diagrams (see Spear and Peacock, 1989). The obtained P-T data should be interpreted with great care and common sense, since geothermobarometry relies on several assumptions that cause potential pitfalls, including:

- the fundamental assumption that a mineral assemblage represents equilibrium conditions. It is impossible to prove that minerals in an individual rock achieved equilibrium and therefore it is desirable to find different generations of sub-assemblages in the same rock, each preserved in a state of small-scale equilibrium. From these sub-assemblages it might be possible to infer pressures and temperatures at different stages of the metamorphic evolution, resulting in the construction of a P-T(-t) path (Bucher and Frey, 2002).
- The assumption that reequilibration on cooling and the closure temperature as applied to thermobarometry do not affect the stable mineral assemblages (Spear and Peacock, 1989).

- Interpretation of the significance of the results with respect to the precision and accuracy of the measurements.
- The significance of the results with respect to the calibration (Spear and Peacock, 1989; Bucher and Frey, 2002). Since most geothermobarometers are based on mineral equilibria that were calibrated using simple mineral compositions while most minerals in rocks contain additional components that form complex solid solution series, accurate knowledge of activity-composition relations is required. However, the connection between activity and composition is often complex and poorly understood for most minerals, resulting in the usage of different solution models and thus multiple P-T estimates for one mineral equilibrium.
- The estimation of the amount of ferrous (Fe^{2+}) versus ferric (Fe^{3+}) iron. With the electron microprobe only the total iron content can be measured. Assuming that all iron is ferrous can lead to an overestimation of the temperature. For relatively simple minerals with low ferric iron like garnets in pelites, the ferric and ferrous iron contents can be calculated assuming charge balance and some site occupancy model for a mineral, but for more complex minerals with partially vacant cation sites and variable H_2O content like amphiboles and micas, these calculations are often questionable and the assumption that $Fe_{total}=Fe^{2+}$ is recommended (Bucher and Frey, 2002).

Finally, the estimated pressures and temperatures for different mineral assemblages of a rock can be plotted in a P-T diagram and the interpretation of these points together with light microscopy study of the microstructure lead to the construction of a PT-path showing the metamorphic history of the analysed samples. When the age of the minerals is determined, the time can be added to the PT-path, resulting in a PTt-path that provides more information about the metamorphic evolution of the area.

3.2 Methods

In order to obtain information about the metamorphic history of the rocks, several techniques were used as will be described below.

First, thin sections of about 30 µm thick were made at the University of Ankara and studied with use of the optical microscope. This was done to determine the mineral assemblage from which a rough

indication of the metamorphic grade could be made. The optical microscope was also used to select spots for chemical analyses with the electron microprobe (EMP).

The chemical analyses were carried out using the JEOL JXA-8600 Superprobe at the Faculty of Geosciences at the University of Utrecht. The acceleration voltage during the analyses was 15 kV at a beam current of 20 nA with a spot size of ~1-3 µm (depending on the height, z, of the sample). Both the energy dispersive detection system (EDS) for quick recognition of the different minerals and the wavelength dispersive spectrometers (WDS) for accurate chemical analyses were used. Table 1 shows the standards used during the analyses.

Table 1 *WDS analyses set-up for the JEOL JXA-8600 Superprobe. Diffraction crystals that are used: Tithium Fluoride (LIF), Pentaerythritol (PET) and Thallium Acid Phatalate (TAP).*

Element	Crystal used for diffraction	Calibration standard	Counting time (s)
Si	TAP	diopside	30
Ti	PET	TiO	30
Al	TAP	corundum	30
Fe	LIF	hematite	50
Mn	LIF	tephroite	50
Mg	TAP	forsterite	30
Ca	PET	diopside	50
Na	TAP	jadeite	30
K	PET	KTiPO5	30
Cr	PET	chromium	50

For the chemical analyses, uncovered polished thin sections with a thickness of about 30 µm were made at the University of Utrecht. In a selection of six thin sections, minerals that are useful for thermobarometric calculations were identified, photographed and their chemical composition was measured. To determine if the garnets were chemically zoned, linescans were made to show possible chemical variations from core to rim. Heterogeneity in a mineral reflects changing PT- and chemical conditions during its growth, which is often indicative for different stages of the metamorphism (e.g. the prograde or retrograde path). Furthermore, it is important to know if a mineral is homogeneous or not, because for thermobarometric calculations equilibrium has to be assumed. For example, if a garnet is heterogeneous, the core composition is in equilibrium with inclusions in the core and reflects PT conditions during first growth, while the rim is in equilibrium

with inclusions in the rim and neighbouring minerals (matrix) and will reflect the pressure and temperature during later stages of garnet growth.
The electron microprobe was also used for BSE images showing the textures of the mineral assemblages as well as zoning patterns while the minerals have a characteristic greyscale (the larger the atomic number, the lighter the greyscale) and the localisation of monazites and zircons that were useful for dating. The chemical composition of the different minerals analysed was used to estimate PT conditions.

For calculation of the pressure and temperature experienced by these rock samples, the following programmes were used: a mineral recalculation Excel spreadsheet of Dave Waters available from his website and combined with ferric iron estimations according to Schumacher (1991) and Droop (1987), to normalize the analyses to a given number of oxygen atoms and recalculate to an ideal cation proportion. In a first attempt, the program PT Gibbs of Brandelik and Massone (2004) was used to calculate PT conditions, since this program is user-friendly and capable to determine the P-T conditions of a large number of mineral equilibria with complex solid solution models. Several geothermobarometers were selected, based on the minerals garnet, biotite, sillimanite, plagioclase, K-feldspar, spinel, cordierite and clinopyroxene.
However, this Excel-based computer programme is easy to use for (ultra)mafic rocks, but if used for metapelitic rocks, the user is urged to do additional calculations, since solid solution models for minerals typical for metapelitic rocks are not incorporated in the programme. These calculations involve the determination of the activity for a number of minerals (see Appendix 2 for background of mineral activity). These activity calculations are based on the database of Holland (1998), while in PT GIBBS the database of Berman (1988) is used. The combination of different databases in geothermobarometric calculations will not improve the results. Besides, the calculation of the activity of minerals will also enhance the uncertainty in the results, because the connection between activity and mineral composition is often complex and poorly understood (Spear and Peacock, 1989). To obtain the best possible results and avoid complex calculations (e.g. activity calculations), we have chosen to use a more sophisticated programme: TheriakDomino. TheriakDomino is a programme collection written by C. de Capitani and K. Petrakakis (version used in this study: 01.08.09) to calculate equilibrium assemblages and equilibrium phase diagrams (pseudosections). Theriak is used to calculate stable mineral assemblages and phase compositions for a given bulk rock composition and specific PT conditions and with Domino we calculated PT pseudosections and

equilibrium phase compositional isopleths. We have chosen TheriakDomino because calculations are relatively quick due its approach to equilibrium by Gibbs free energy minimisation rather than solving complex and large equations systems. We used a Holland & Powell-based database (tcdb55c2d), because this can deal with melting, whereas a database based on Berman can not at this stage. An introduction about the practical aspects of using TheriakDomino is given in Appendix 3.

3.2.1 Ferric iron estimation

The relative proportion of ferric (trivalent) and ferrous (divalent) iron cannot be determined directly by microprobe analyses. Various workers have therefore proposed recalculation schemes to estimate the ferric iron content of silicate minerals. Most of these schemes are based on a stoichiometric charge balance (e.g. Droop, 1987; Schumacher, 1991). This approach assumes that if the number of cations of the recalculated mineral formula taking all iron as ferrous is less than stoichiometric, this is caused by the presence of ferric iron (Brouwer, 2000). This approach is only useful for minerals with a relative simple crystal structure with low ferric iron, like almandine, and would give unreliable results for more complex minerals with an unknown water content or partially vacant cation sites.

Therefore, in this study only the ferric iron content of garnet and clinopyroxene is estimated according to the analysis of Schumacher (1991) and used for end-member calculations. The other minerals have been assumed to contain ferrous iron only. In calculations with TheriakDomino all iron is assumed to be ferrous iron (Fe^{2+}), since the bulk rock composition is used as input and no difference can be made for separate minerals.

In order to find polymorphs of sillimanite, X-ray diffraction (XRD) analyses were done on sillimanite aggregates. For example, the presence of the former HP polymorph kyanite would be a valuable addition to the PT path. For this analysis, cm-scale sillimanite aggregates were drilled by a microdrill equipped with a DREMEL 2 mm diameter diamond drillhead. The powder samples were analysed using a X-ray diffrectometer operating with a Cu-K alpha (λ=1.54) X-ray tube.

3.3 Petrography

The metapelitic rocks were selected, because they were expected to preserve the peak metamorphic conditions.

10 samples were studied with use of the optical microscope and 6 samples were selected for analyses with the electron microprobe. The selection was based on the presence of minerals useful for the calculation of pressure and temperature and the state of weathering of the rock sample. Overview pictures of the thin sections as well as BSE images of analyses spots are given in Appendix 4 and 5, respectively. A basic overview of the mineralogy and microstructure is given in tables 2 and 3. For a list with mineral abbreviations used in the text, the reader is referred to Appendix 6.

3.3.1 Mineral assemblages

In Appendix 7 hand specimen of samples selected for PT analyses are shown. The general mineral assemblage observed in the pelitic schists from the Hirkadag massif is Grt + Bt + Sil + Plag + Qtz + Spl ± Kfs ± Crd ± Wh mica + Ilm. The mineral assemblage of K4 (Kırşehir) is similar to the metapelitic rocks of the Hirkadag massif, but the microstructure is finer grained and lacks spinel: Grt + Bt + Sil + Plag + Qtz + Kfs + Wh mica. The other samples of the Kirsehir massif show a banded structure with pelitic bands, calc-silicate bands and intermediate zones. These samples do not include garnet and are also relatively fine grained showing the mineral assemblage: Bt + Sil + Plag + Kfs + Qtz ± Cpx ± Wh mica ± Spl. Based on textural relationships such as mineral reactions, in most samples more than one metastable mineral assemblage could be defined:

Sample H12-G (Hırkadağ):

1. Sillimanite + plagioclase + garnet + biotite ± quartz
2. Spinel (as reaction product of sillimanite)
3. K-feldspar + plagioclase + quartz (in light-coloured zones in between the foliation that is formed by sillimanite, biotite, spinel and fine grained plagioclase and quartz)

Sample H19-H (Hırkadağ):

1. garnet + K-feldspar + sillimanite (fibrolite in foliation) ± muscovite ± quartz + ilmenite

2a. sillimanite (in plagioclase) + biotite + plagioclase + spinel (in domain around garnet)

2b. Spinel (as the reaction product of fibrolitic sillimanite)

Sample H20-C (Hırkadağ):

1. garnet + biotite + sillimanite + quartz ± plagioclase + ilmenite
2. cordierite + spinel + quartz + K-feldspar

	Sample	Main minerals									Accessory phases									
		grt	spl	bt	sil	plag	Kfs	cpx	qtz	crd	chl	white mica	sca	ilm	mag	zi	ep	cnd	ru	ti
Hırkadağ massif	H12-C	x		m	x	x			x	x		x		x		x	x			x
	H12-G	x	x	x	m	x	x		x	x*		x*		x		x				
	H19-H	x	x	x	x	x	x		x			x		x				x		
	H20-C	x	m	m	x	x	x		x	x		x		x		x				
	H17-C	x	x	x	x	x			x	x			x	x						
Kırşehir massif	*K4*	x		x	x	x	x		x		x*	x	x						x	
	K11			x	x	x	x	x	x		x*	x		x		x	x			x
	K12		x	x		x			x					x		x				
	K13	x*		x	x	x	x	x	x		x*				x	x			x	x
	K21			x	x	x	x		x		x*			x				x		

Table 2. *Basic overview of the mineralogy. Boxes marked with an 'x' mean that the above mineral occurs in the corresponding sample. An 'x*' means that the mineral is observed with use of the optical microscope, but not found in the corresponding thin section used for EMP analyses. When minerals below the heading ' main minerals' occur as minor phases, they are indicated with an 'm'. The samples used for EMP analyses are italic. A list with abbreviations of mineral names is given in Appendix 4.*

	Sample	Remarks
Hırkadağ massif	**H12-C**	foliation defined by altered crd and sil together with qtz and fds; porphyroblasts of mm to 1 cm large anhedral garnet. Grt surrounded by crd, qtz and plag.
	H12-G	foliation defined by bt-rich zones with spl and light coloured zones with qtz and fds. Porphyroblast of anhedral pinkish garnet. Bt shows two main orientations: remnant of crenulation cleavage.
	H19-H	foliation defined by sil-spl bands and light coloured qtz-plag bands. Porphyroblasts of fragmented garnet.
	H20-C	foliated and relative large poikiloblastic garnet porphyroblasts. Grt has reaction rim of crd. Remnants of qtz within crd. Sillimanite shows two preferred orientations which is possibly a remnant of crenulation cleavage.
	H17-C	foliation defined by dark spl-rich zones and lighter qtz-bearing zones, both overgrown by oxidized mineral(s) (probably due to weathering), pinkish garnet porphyroblasts. Whole sample has undergone weathering, indicated by a reddish brown weathering product that fills cracks and has overgrown all the minerals. Therefore the sample is not useful for analysis.
Kırşehir massif	***K4***	Relatively fine grained. Foliation defined by bt-rich zones and qtz-fds zones with porphyroblasts of garnet (few mm large). Foliation seems to be slightly folded and bt minerals show two preferred orientations with a small angle, presenting relics of crenulation cleavage.
	K11	Relatively fine grained. Foliation defined by bt-rich bands and cpx-rich cm-scale zones. In the biotite-rich bands, biotite minerals bend around porphyroblasts of clinopyroxene. Both plagioclase and quartz minerals are coarser grained in cpx-rich zones.
	K12	Relatively fine grained. Foliation defined by cm-scale bt-rich zones and cpx-rich bands. Biotite minerals show a shape-preferred orientation and bends around larger grains of plagioclase and clinopyroxene.
	K13	Relatively fine grained. Foliation defined by cm-scale bt-rich bands and cpx-rich zones. In the bt-rich zone some remnants of garnet porphyroblasts are found.
	K21	Relatively fine grained. Foliation defined by bt-rich bands and cpx-rich zones. Biotite minerals show two main shape preferred orientations which possibly indicate an old crenulation cleavage. Plagioclase minerals in the cpx-rich band have exsolution lamellae

Table 3. *Microstructural remarks on the studied samples.*

Sample K4 (Kırşehir):

1. garnet + biotite + plagioclase + sillimanite (slightly younger)
2. K-feldspar + quartz
3. Chlorite + muscovite (retrograde)

Sample K13 (Kırşehir):

1. Biotite + quartz + K-feldspar + clinopyroxene (with biotite and clinopyroxene in separate zones)
2. Clinopyroxene (as reaction rim around biotite) + plagioclase + quartz (intergrowth plagioclase+ quartz)

The textural and chemical characteristics of the minerals used for thermobarometry are outlined below. Representative mineral analyses (compositions) are given in Appendix 8.

3.3.2 Microstructure of the samples

Sample H12-G shows a foliation defined by biotite-rich dark bands including spinel and in smaller amounts fibrolite, that separates light coloured zones with coarse grained quartz and feldspar that almost show a foam texture. The spinel grows over the sillimanite needles and is therefore younger than the sillimanite, and the spinel seems to overgrow the biotite as well. The dark biotite-rich bands bend around garnet porphyroblasts as well as around porphyroblasts of microperthite.

Sample H19-H shows a similar structure, but the dark coloured zones that define the foliation are dominated by spinel and sillimanite in which spinel replaces both sillimanite and biotite.

In sample H20-C, the matrix is dominated by quartz and cordierite with relatively large garnet porphyroblasts. The garnets are surrounded by cordierite that close to the garnet rim shows a symplectitic intergrowth with quartz. At the boundary between garnet and cordierite and also at inclusion sites where cordierite is incorporated in the garnet, well developed crystal faces have formed. The garnet grains are idioblastic. The foliation is mainly defined by aggregates of fibrous sillimanite and ilmenite. Quartz minerals in the matrix show undulose extinction.

In sample K4 the foliation is defined by dark-coloured bands of aluminosilicates (biotite, spinel and sillimanite) with K-feldspar, quartz and relatively small amounts of plagioclase in light coloured zones in between. Garnets are relatively small (0.5-1.5 mm in diameter). The biotite minerals show two preferred orientations that might be a relic of crenulation cleavage.

Sample K13 shows a banded structure of ca. 1 cm wide calc-silicate zones alternated with zones rich in biotite with in between bands that are rich in clinopyroxene. For PT analysis only the pelitic biotite-rich band and the clinopyroxene-rich band are taken into account, because they are expected

to preserve peak metamorphic conditions best. In the biotite-rich zones some remnants of garnet porphyroblasts are found, but they are rare and could not be analysed.

3.3.3 Petrography of key minerals

In the following section, the texture and chemistry is described of minerals that are useful for thermobarometric calculations. These minerals are garnet, spinel, sillimanite, biotite, feldspar and cordierite.

Garnet - Texture

Hırkadağ samples

The garnet grains in the metapelitic rock samples from the Hırkadağ massif are mm-scale and some 1 cm large idioblastic to xenoblastic porphyroblasts that show a poikiloblastic to skeletal structure. The mm-scale garnets are less poikiloblastic and are often cut by cracks. Most garnets are surrounded by a reaction rim of bt, spl, fds and smaller amounts of sil.

The garnet grains have inclusions of qtz ± plag ± bt ± wh mica ± sil ± Kfs ± spl.

Aside garnet porphyroblasts, samples H12-G and H19-H contain pseudomorphs (figure 7) of garnet, in which the former garnet blast shape can be recognized in the orientation of the replacing minerals spinel, biotite and plagioclase.

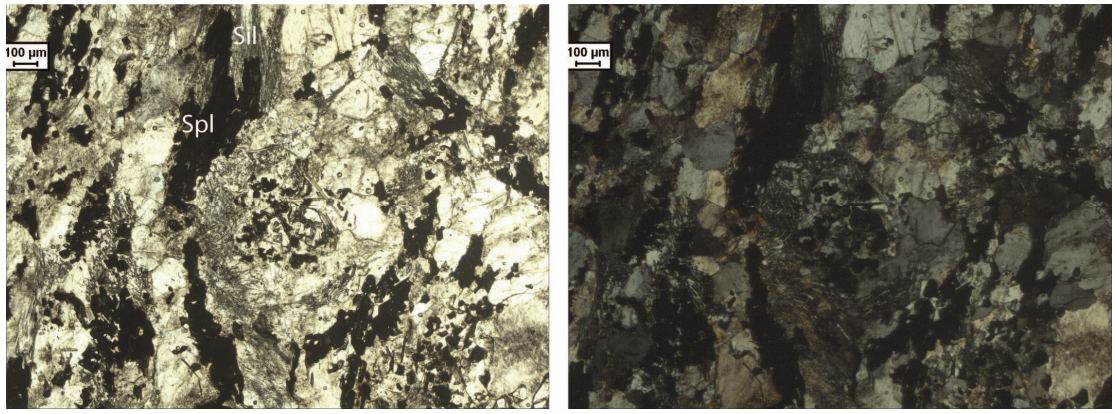

Figure 7. *Photomicrograph of a pseudomorph of garnet (left PPL, right XPL). The garnet has been replaced by spinel, biotite and plagioclase. Spinel in the centre of the pseudomorph shows a symplectitic structure*

Sample H20-C shows relatively large, fractured garnet grains (up to 1 cm) with a reaction rim of cordierite and remnants of quartz in which the boundary between garnet and cordierite is a perfect crystal face, suggesting the presence of a melt phase. The mm-scale garnet grains in sample H20-C are more fragmented with a skeletal structure and a reaction rim consisting of biotite, plagioclase, spinel and small amounts of sillimanite. Sample H17-C1 shows a similar reaction texture of garnet

replaced by cordierite with relatively small quatz minerals inside the cordierite, but because the sample is strongly weathered, it has not been used for analyses.

Kırşehir samples

The garnet grains in the samples from the Kırşehir massif occur as relatively fine grained porphyroblasts, 0.5-1.5 mm in diameter. The grains are more equidimensional than the garnets in the Hırkadağ massif, but are also fractured, showing a skeletal structure. The garnets are less abundant than in the Hırkadağ metapelitic rocks, making up less than 5% of the rocks volume and are only found in few samples, of which sample K4 has been analyzed. Inclusions in garnet consist of plagioclase, quartz and biotite.

Garnet - Mineral chemistry

Garnet compositions are fairly similar for all analysed samples (figure 8). The garnets analysed range from $Alm_{75-86}Grs_{4-11}Pyr_{6-21}Spess_1$ for both the Hırkadağ and Kırşehir massifs. Sample H12-G, situated east of sample H19-H and west of H20-C shows a slight depletion in iron content and enrichment of X_{Mg}, which could indicate higher temperatures.

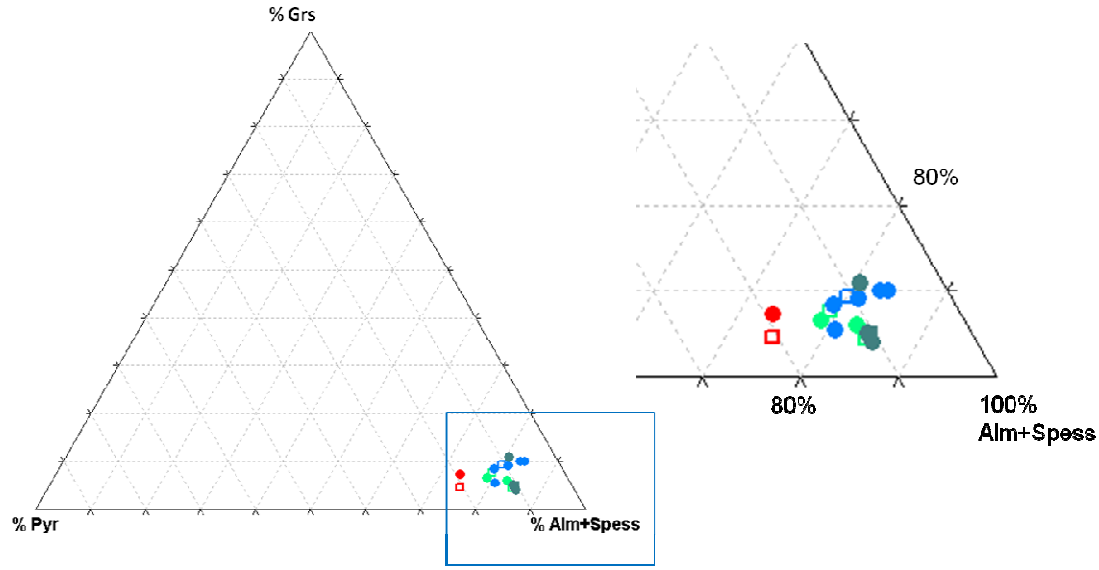

***Figure 8**. Ternary plot of garnet compositions. H12-G: red, H19-H: blue, H20-C: light green, K4: dark green. Circles refer to core compositions and boxes to rim compositions.*

The zoning patterns, resulting from linescans through garnet minerals, show more variety. The zoning in garnets results from slow diffusion in the garnet lattice, so that it is possible to record differences in chemical composition. Two types of zoning can be distinguished: growth or normal zoning and zoning as the result of fast diffusion at elevated temperatures.

Growth zoning can be viewed as the addition of successive shells of material whose composition reflect equilibrium at the time of growth. This so called growth zoning is the result of a fractionation

process and is found in garnets which have formed at temperatures below ~650 °C (Waters, personal website). As with most dehydration reactions in the KFMASH system, the Fe end member reaction occurs at a lower temperature than the Mg end member reaction (Spear, 1993). This implies that a decrease of the Fe/(Fe+Mg) ratio in the garnet indicates an increase in the metamorphic temperature. Assuming that temperatures increase during garnet growth, growth zoning is characterized by Fe and Mg (almandine and pyrope, respectively) concentrations that increase from core to rim, while the Ca and Mn concentrations (grossular and spessartine respectively) decrease from core to rim.

At high grade the diffusion will become faster and the garnet may reflect a homogeneous equilibrium composition. This means that the garnet composition is modified by exchange of material with the rock matrix (Waters, personal website) and the extensive diffusion of cations within the garnet probably eliminates the originally normally zoned cores (Dempster, 1985). The usual result is a garnet with no zoning in the core and a depletion in Mg, and commonly also an enrichment in Mn, at the rim of the garnet, resulting in a reverse zoned rim that formed after the peak of metamorphism. This type of zoning pattern is found in garnets which have experienced temperatures above about 600°C.

Thus, garnet porphyroblasts show systematic changes in zoning profiles with metamorphic grade, relating to increased diffusion rates. Growth zoning seen in the lowest grades (up to a formation temperature of ~650°C), is followed by an area showing modified growth zoning and finally by garnets with unzoned cores at high grades (Dempster, 1985).

The garnets in sample H12-G show different zoning patterns (figure 9). The most massive garnet, with a small amount of inclusions and only a few cracks, H12-G3A, shows a zonation pattern indicative for changing compositions during garnet growth. Garnet H12-G3B contains more inclusions and cracks and show no zonation pattern. This is probably the result of homogenisation of the composition by diffusion at high temperatures by which homogenisation is accelerated by the presence of cracks and inclusions. Garnet H12-G1A shows an up-and downgoing profile for the elements iron and magnesium. The rough trend shows a decrease of Fe/(Fe+Mg) ratio towards the rims, which corresponds to an increase in temperature during garnet growth. The wobbling trend in the X_{Fe} and X_{Mg} could be the result of the beginning of homogenisation at elevated temperatures at spots where diffusion is accelerated by the presence of cracks or inclusion sites, for example. Nearby spot position 8-9 in the garnet zoning graph as well as spot position 13-14 and 17, X_{Fe} is relatively low and X_{Mg} is relatively high, assuming a normal growth zoning profile. This supports the

explanation of homogenisation in this garnet mineral. However, since cracks are not abundant in this garnet, the inclusions could be the only sites where diffusion is accelerated.

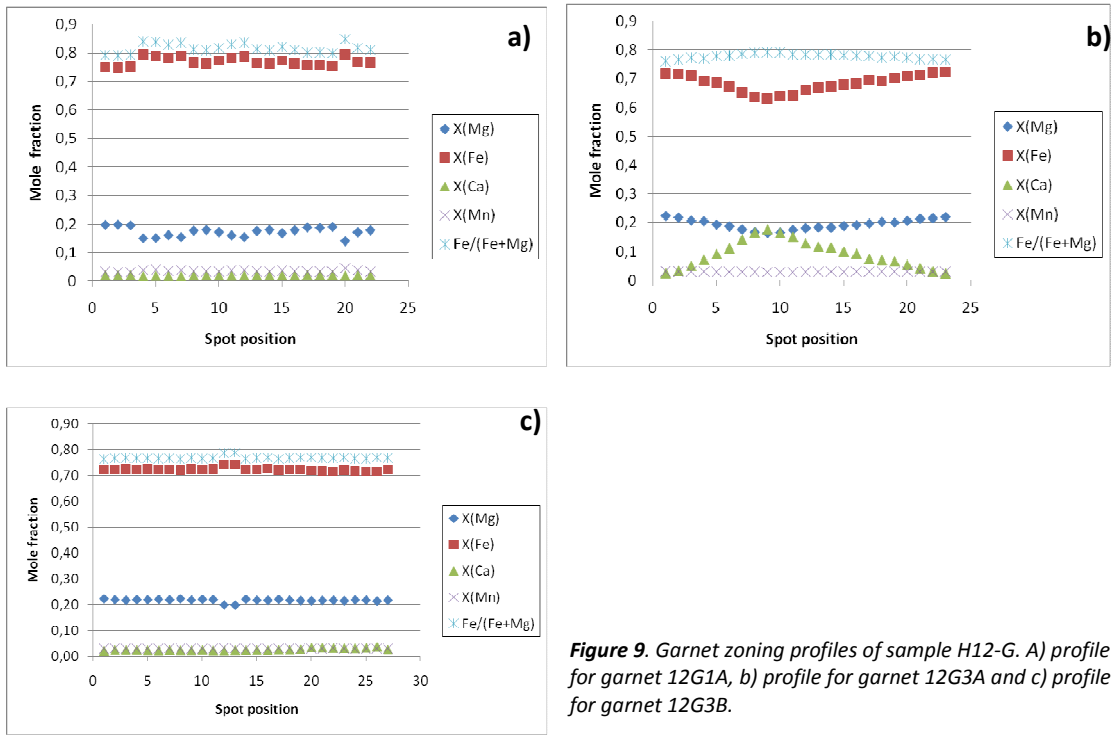

***Figure 9**. Garnet zoning profiles of sample H12-G. A) profile for garnet 12G1A, b) profile for garnet 12G3A and c) profile for garnet 12G3B.*

Sample H19-H contains one large elongated garnet mineral (~1 cm in diameter) and some smaller (1-3 mm in diameter) garnets. The large garnet shows a growth zoning profile (figure 10) with a decrease of Fe/(Fe+Mg) towards the rim, indicating a temperature increase during garnet growth (e.g. Spear, 1993). This is confirmed by two profiles, one through the shorter side (H19-G1A) and one through the longer side (H19-G1C) of the elongated crystal. The rim of H19-G1A show only a slightly reversed pattern of the iron concentration, while the other elements are normally zoned. One of the smaller garnets shows a zoning profile that probably reflects growth zoning. Since the garnet shows reaction products including much biotite at the right hand side of the garnet, which are situated inside the reaction rim of sill+plag that borders the garnet at the left hand side, the profile H19-G12A (figure 10c) does not show a rim-core-rim profile, but only a rim-core profile where the right hand side rim is missing because it has been replaced by bi. Assuming that only the right hand side rim and the core are reflected by this profile, the elements in this profile show a slight zoning pattern that corresponds to growth zoning (Fe/(Fe+Mg) increases towards the core).

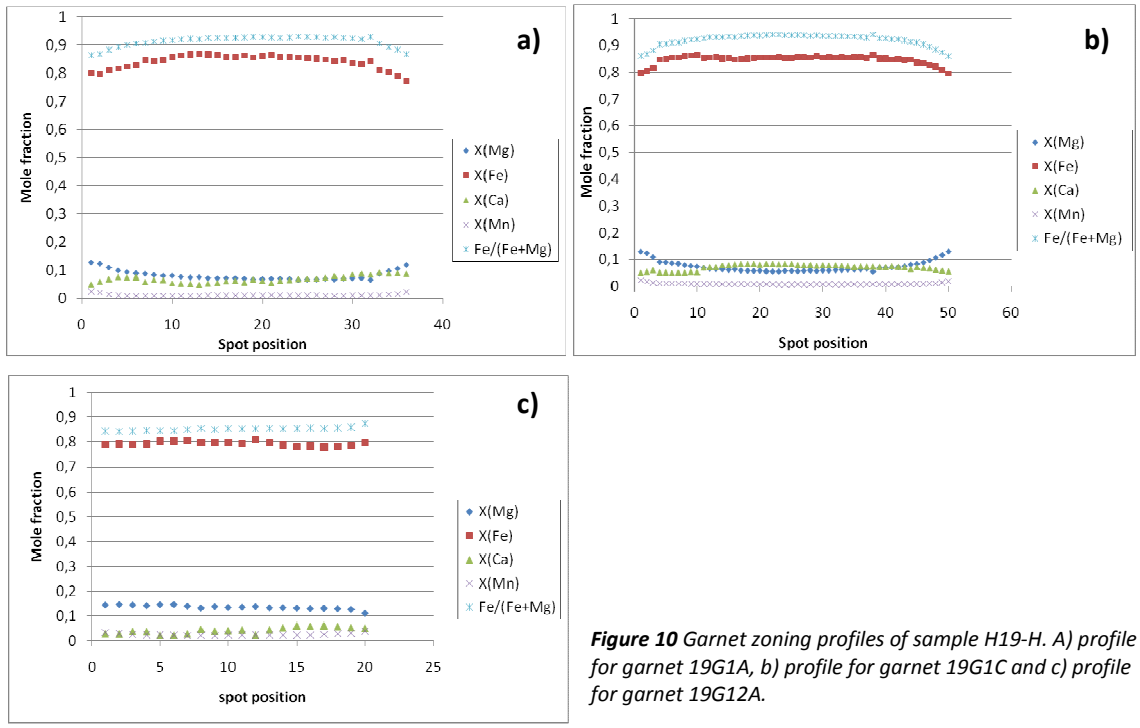

Figure 10 *Garnet zoning profiles of sample H19-H. A) profile for garnet 19G1A, b) profile for garnet 19G1C and c) profile for garnet 19G12A.*

The 1 cm large garnet in sample H20-C show a retrograde zoning pattern (figure 11). The Fe/(Fe+Mg) ratio shows an increase towards the garnet rim, which implies a decrease in temperature. The presence of cordierite and the newly grown crystal faces at the boundary between cordierite and garnet imply temperatures higher than 700 °C and it is therefore likely that the garnet has been homogenized before cooling. If this is the case, the core composition of this garnet reflects near-peak temperatures and the rim shows retrograde conditions. The zoning profile of H20-G1A in particular shows a few heterogeneities. The position of these heterogeneities corresponds to a band consisting of a heavier mineral than garnet (darker grey at BSE image). This band could be a kind of exsolution lamella, since the temperature in this band is slightly lower than of the surrounding garnet as indicated by a slightly increased Fe/(Fe+Mg) ratio. In profile H20-G1B the heterogeneity of this band can also be recognized.

The garnets from the Kırşehir massif, represented by sample K4, are slightly zoned (figure 12). The garnet in profile K4G1A shows a higher Ca concentration in the core, the Mn concentration is also slightly increased in the core, while both the Fe and Mg concentrations are slightly higher in the rim all

indicating growth zoning, suggesting that the metamorphic temperature increased during garnet growth. The garnet profile shows a deviating value at the right hand side of the core in the graph, which corresponds to a crack that cuts through the entire garnet mineral. The values nearby the crack

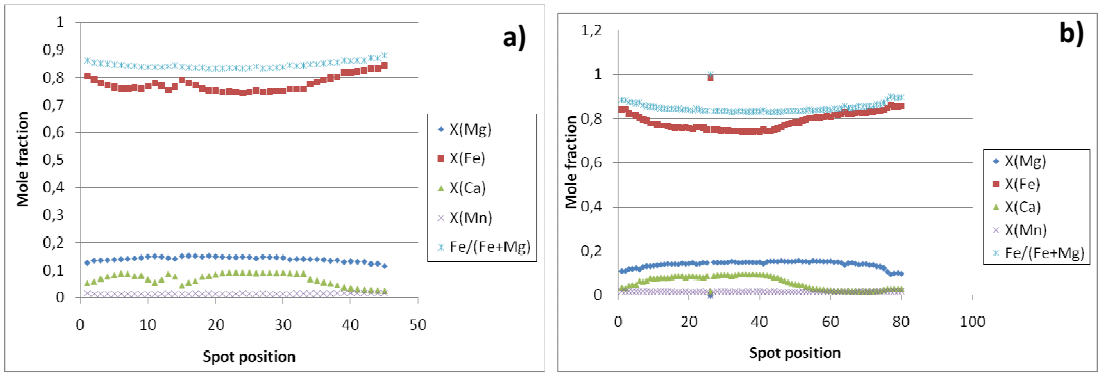

Figure 11. *Garnet zoning profiles of sample H20-C. A) profile through the short side of the cm-scale garnet and b) profile through the long side of the same garnet.*

show an anomalous high Fe/(Fe+Mg) ratio and Fe concentration while the Ca and Mg concentration are lower than would be expected in a normal growth zoning profile. This could indicate a retrograde effect: the temperature is lower than expected close to the core. Especially at the right hand side rim, the Fe/(Fe+Mg) ratio increases, indicating a retrogression in temperature and providing data for the retrograde part of the PT-path.

The garnet profile K4G2A shows growth zoning with a retrograde rim, as implied by a higher Fe/(Fe+Mg) ratio at the core and Ca and Mn concentrations that decrease towards the rim. The retrograde rim is indicated by an increase in Fe/(Fe+Mg) near the rim as well as a decrease in Mg and an increase in Mn near the rim. Close to the core, some elements reflect the effect of the presence of a large crack in the garnet. At the location of the crack the inferred temperature is lower, which is probably the result of retrograde conditions. The Mn concentration is not affected by this retrogression. Profile K4G2A through another mm-scale garnet of the Kırşehir massif also shows growth zoning with a retrograde rim. The Fe/(Fe+Mg) ratio in general decreases towards the rim, indicating a temperature increase during garnet growth, with a small increase in the rim which implies an decrease in temperature. In the range from spot position 6 to about 10, especially the Ca composition suddenly decreases in the core, but since this anomaly is not favoured by the other elements and is not found in the other garnets in this region, it is interpreted as a local effect, possibly caused by the presence or absence of Ca-bearing phases during garnet growth.

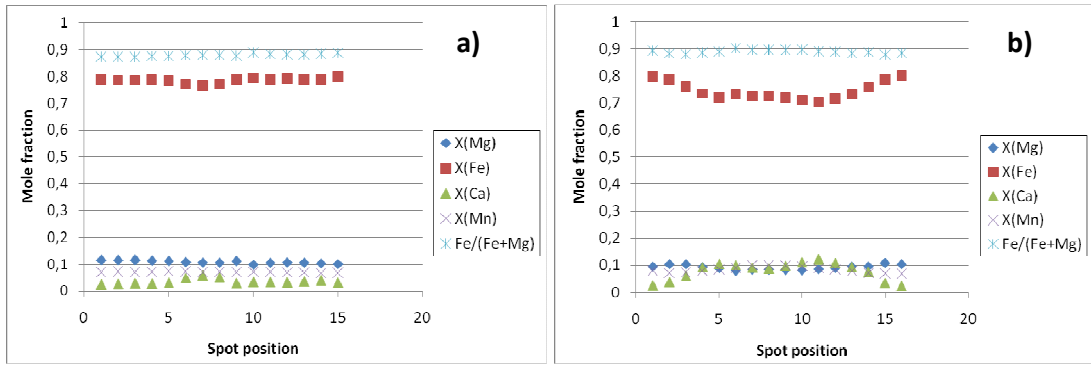

Figure 12. *Garnet zoning profiles of sample K4. A) profile for garnet K4G1A, b) profile for garnet K4G2.*

Spinel - Texture

The spinels in the samples from the Hırkadağ massif are (dark) green coloured, indicating a high metamorphic grade. In sample H12-G spinel occurs both in the bi-rich zones that define the foliation as in the form of an inclusion in garnet. The spinel grains that occur as inclusions are not in direct contact with the garnet, but are surrounded by quartz or feldspar and in smaller amounts white mica, while the spinel in the matrix shows direct contacts with the garnet. In sample H19-H, sillimanite and spinel are the most important minerals in the darker coloured zones and spinel has overgrown both sillimanite and biotite (figure 13a). The spinels occurring as inclusions and near the garnet rims show relatively small grain sizes and often have a symplectitic structure (figure 7), while the spinel in the dark coloured bands have larger grain sizes. Spinel is also found at reaction rims of garnet and in pseudomorphs of garnets, replacing the garnet together with plagioclase, biotite, K-feldspar and in smaller amounts corundum.

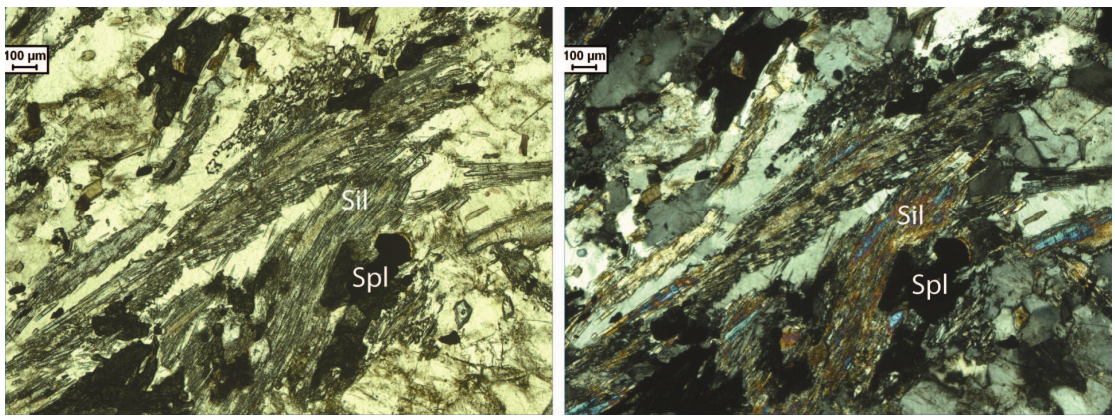

Figure 13. *Spinel replacing fibrous sillimanite (left PPL, right XPL).*

In sample H20-C spinel only occurs as a minor phase as inclusion in garnet. In this case, the symplectitic spinel is surrounded by cordierite, and does not show direct contact with the garnet. The foliation in this sample is mainly defined by aggregates of fibrous sillimanite and ilmenite, where the sillimanite is not replaced by spinel and biotite is only found in the surroundings of garnet.

In the Kırşehir massif, spinel is only found in sample K12 which is not used here for microprobe analyses. The spinel occurs in biotite-rich bands, is relatively fine grained and has a dark green colour.

Spinel - Mineral chemistry

Spinel in the Hırkadağ samples is rich in (ferrous) iron and is therefore better called hercynite ($FeAl_2O_4$), although the spinel contains small amounts of magnesium (2.5-4.5 wt% MgO) and, in sample H20-C, Zn (3.4 wt% ZnO) as shown in Appendix 8 (representative mineral analyses).

Biotite - Texture

In the Hırkadağ samples the biotite occurs mainly in zones, defining the foliation (gneissic banding) of the metapelitic rocks, with the exception of sample H20-C in which the biotite is associated with garnet grains and only occurs as a minor phase away from garnets. Biotite also occurs as inclusions in garnet. The biotites are pleochroic and have a brown colour which is often darker at the centres of the grains. Biotite is one of the minerals that replaces garnet. In sample H12-G biotite shows two main orientations that can be interpreted as the remnant of a crenulation cleavage (figure 14).

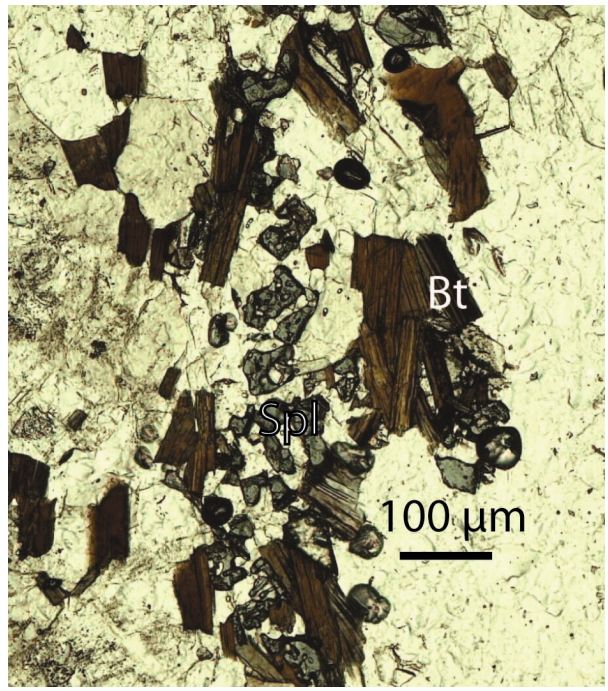

Figure 14. *The angular relation between biotite grains, PPL.*

The biotite in the Kırşehir samples is relatively fine grained and more abundant than in the metapelitic rocks of the Hırkadağ massif. Biotite occurs in zones of a few mm to cm wide, alternating with light coloured zones (quartz + feldspar-rich for sample K4 and rich in clinopyroxene for the other samples), defining the banded structure of the rock. In this massif, the biotite is partly

replaced by chlorite during retrogression and is often darker brown in the centres of the grains. The biotite shows a shape preferred orientation in which sometimes two main directions can be recognized, probably inherited from an earlier crenulation cleavage.

Biotite - Mineral chemistry

The Fe and Mg content of biotite in the Hırkadağ samples varies from $0.41<X_{Mg}<0.50$, except for biotite inclusions in sample H19-H which has a Mg content of $X_{Mg}=0.23$. The Mg content of biotite in the Kırşehir massif is slightly lower with $0.33< X_{Mg}<0.37$ and $X_{Mg}=0.46$ for sample K13.

Sillimanite - Texture

In the metapelitic rocks of the Hırkadağ massif and in sample K4 from the Kırşehir massif, fibrous sillimanite (fibrolite; figure 15) is found and minor amounts of prismatic sillimanite. The darker coloured zones rich in biotite and often also in spinel contain the most sillimanite needles. In these zones, sillimanite occurs together with biotite and is replaced by spinel and in sample H20-C the foliation is mainly defined by aggregates of fibrous sillimanite and ilmenite, where the sillimanite is not replaced by spinel. In samples H17-C and H19-H besides fibrolite also massive sillimanite is found. In addition, sillimanite is also found as small fibres enclosed in quartz. The interference colours that can be seen with the optical microscope using cross polarized light are of a higher order in the centre of a sillimanite aggregate. In sample H12-C sillimanite is replaced by a yellowish fine grained reaction product that most likely consists of cordierite but that is hard to identify in light microscopy. No indications for former kyanite have been found in the analyses with the optical microscope and the electron microprobe.

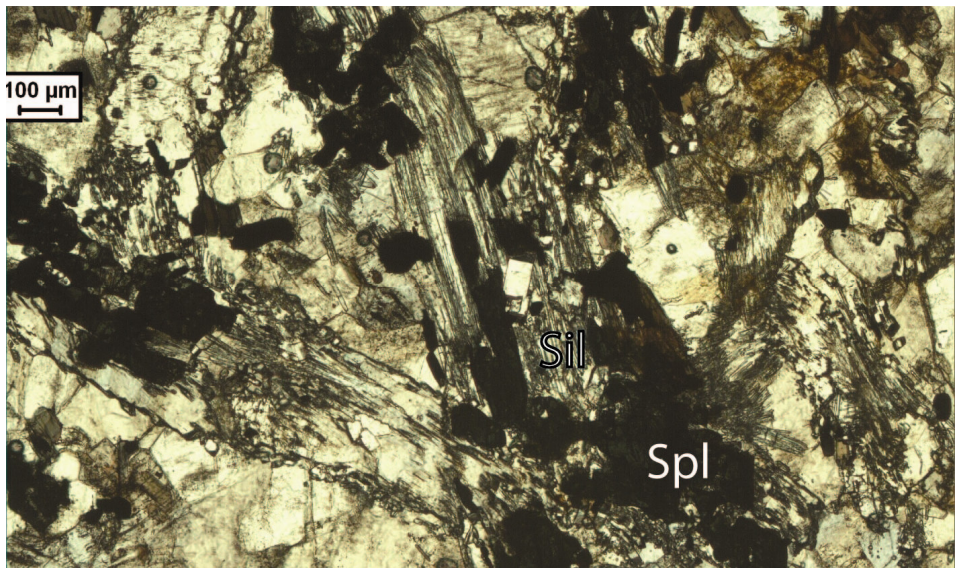

Figure 15. *Photomicrograph of fibrous and prismatic sillimanite associated with biotite (not shown in this picture) and spinel, PPL.*

Feldspar - Texture

Feldspars are most abundant in the light coloured zones, often together with quartz. The main feldspar in these light coloured bands is K-feldspar, especially in sample H19-H. Sample H12-G contains more equal amounts of plagioclase and K-feldspar in the matrix and sample H20-C on the other hand contains only very small amounts of K-feldspar in the light coloured zones that mainly consist of cordierite with minor amounts of quartz and plagioclase. At reaction rims around garnets as well as in pseudomorphs of garnet, plagioclase is found as a reaction product together with spinel, quartz, biotite and in smaller amounts K-feldspar and sillimanite. Both plagioclase and K-feldspar occur as inclusions in garnet, in some cases surrounding other included minerals like sillimanite and spinel.

The feldspars are twinned and some altered grains show exsolution lamellae concentrated in the centre of the grain, though with the optical microscope the exsolution product is not identifiable. Some highly altered grains show relics of cross-hatched twinning, indicating the existence of a former microcline (K-feldspar) that has been altered to a microperthite (plagioclase). This microperthite coexists with non-altered plagioclase. Some grains show undulose extinction as well as the quartz grains, which implies deformation. Another indication for a (multistage) deformation event is deformation twins in two different directions within plagioclase. According to Mora and Valley (1985), perthitic exsolution is common in slowly cooled, high-grade metamorphic rocks.

The feldspars in the metapelitic rocks of the Kırşehir massif show similar microstructures. In sample K4 K-feldspar and smaller amounts of plagioclase are found in the matrix of the lighter coloured zones, as well as near biotite in the bi-rich zones. In the cpx-rich samples K11 and K13, plagioclase and K-feldspar are found in more equal amounts where in the biotite-rich zones the feldspar grains are relatively small. Sample K13 shows an intergrowth of quartz and plagioclase (myrmekite; figure 16) often in contact with K-feldspar. Some K-feldspars in this sample are zoned. This zoning is visible at the BSE image made with the electron microprobe, where the core is darker coloured than the rim, indicating elements with a higher mass at the rim of the grain.

Feldspar - Mineral chemistry

Both plagioclase and K-feldspar occurs in the analysed metapelitic samples. Ternary plots of plagioclase and K-feldspar compositions are shown in figure B. The composition of plagioclase differs between the Hırkadağ and the Kırşehir massifs, while in the Kırşehir massif the composition is most diverse. The Hırkadağ metapelitic rocks show general compositions of $Ab_{56-77}An_{22-43}Or_{0-2}$ for plagioclase and $Ab_{13-20}An_{0-1}Or_{79-86}$ for K-feldspar (figure 17).

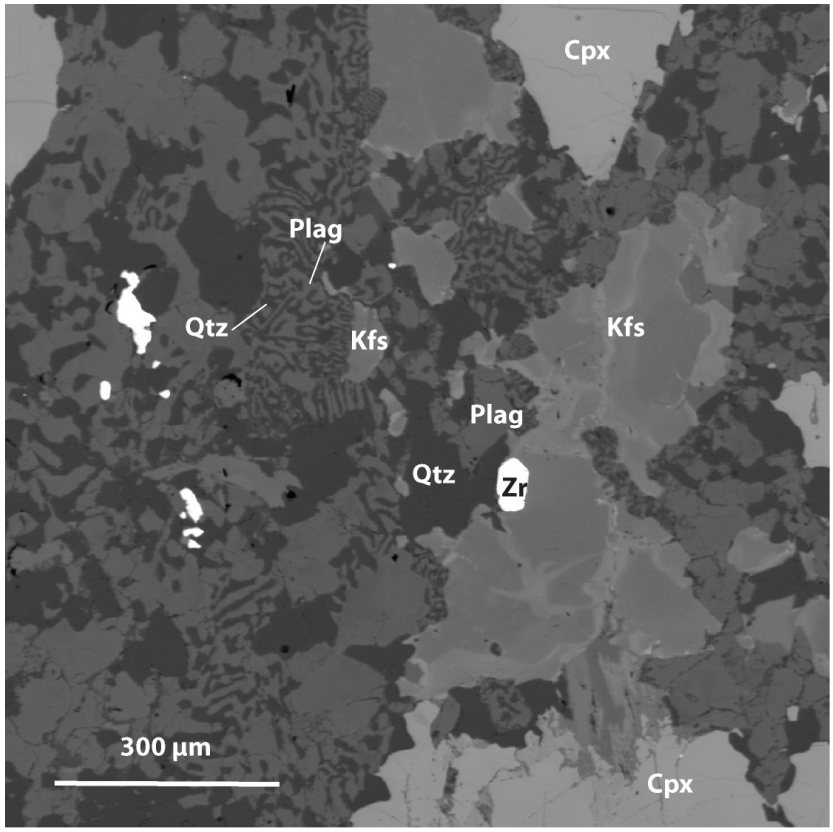

Figure 16. *Intergrowth of quartz and plagioclase (myrmekite) in sample K13 (Kırşehir).*

The composition of the garnet-bearing metapelitic sample of the Kırşehir massif is close to the albite end member ($Ab_{88-90}An_{10-11}Or_{0.5}$), while the clinopyroxene-bearing samples K11 and K13 contain a higher amount of anorthite ($Ab_{42-52}An_{46-57}Or_{1}$) than K4 or the Hırkadağ samples . K-feldspar in the metapelitic rocks of the Kırşehir massif has a composition of $Ab_{9-11}An_{0}Or_{89-91}$ (figure17X).

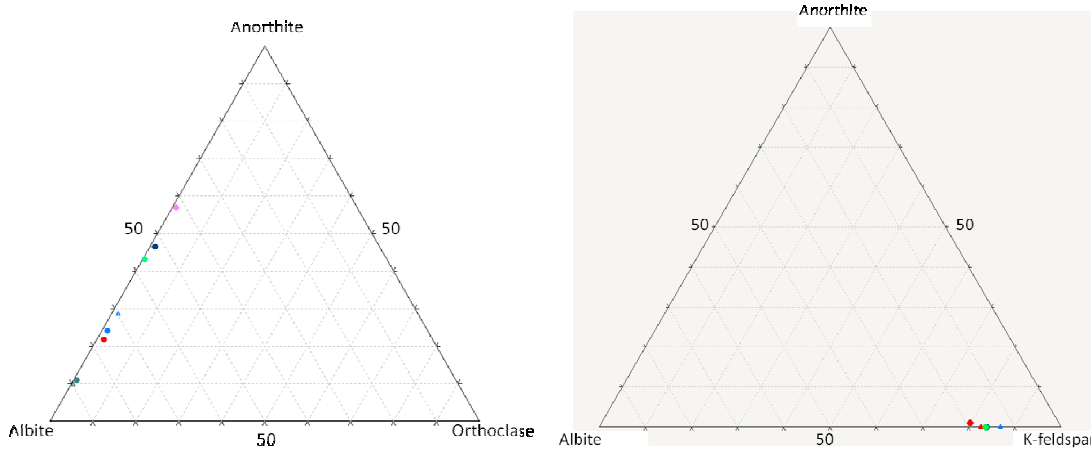

Figure 17. *Ternary plot of plagioclase (left) and K-feldspar (right) compositions. (H12-G: red, H19-H: blue, H20-C: light green, K4: dark green, K11: dark blue, K13: purple. Circles are matrix compositions, triangles are inclusions.)*

Clinopyroxene

Clinopyroxene is only found in samples from the Kırşehir massif, where it occurs in zones interlayered with biotite-rich zones defining the foliation. The grains are idioblastic to xenoblastic with some cracks and are mainly surrounded by K-feldspar, plagioclase and quartz.

The composition of the pyroxenes in the Kırşehir samples is shown in the ternary diagram of figure 18. The nomenclature used for sodic-calcic pyroxenes is adapted from Morimoto et al. (1988).

The pyroxene formula $M2M1T_2O_6$ contains six oxygens and four cations: two in the tetrahedral sites and one each in M1 and M2 (Waters, personal website). The site preference is as follows:

T (tetrahedral): Si, Al

M1 (small octahedron): Al, Cr, Fe^{3+}, Ti, Fe^{2+}, Mg.

M2 (larger cation site): Ca, Na, Mn, Fe^{2+}, Mg.

Although aluminium is commonly present only in small amounts in the pyroxene structure, it can occur both in the tetrahedral and octahedral coordination. High temperatures and relatively low pressures favour tetrahedral coordination for Al. Granulite-facies pyroxenes, therefore, tend to have tetrahedral Al equal to or greater than octahedral Al, and their Al content can be expressed in terms of the Tschermak's molecule end members (Waters, personal website).

The representative analyses of pyroxenes, as given in Appendix 8, show a greater amount of tetrahedral Al than octahedral Al for pyroxenes from samples K11 and K13. The composition of the pyroxenes in the Kırşehir samples is $Hd_{50-59}Di_{41-50}$Al-Tsch$_{0-0.5}$ for sample K13 and $Hd_{50}Di_{49}$Al-Tsch$_{0.5}$ for sample K11.

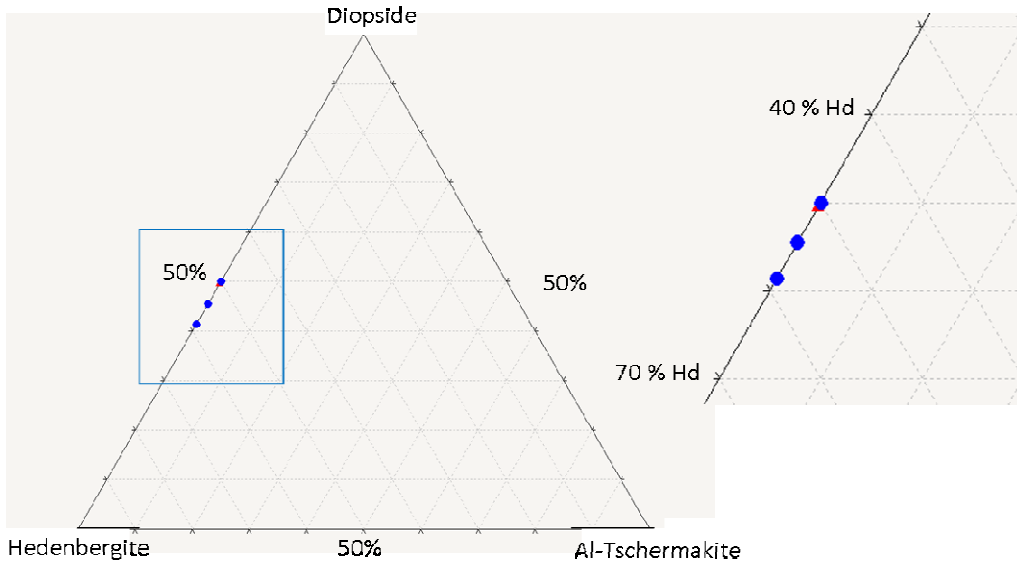

Figure 18. *Ternary plot of pyroxene compositions. Red triangle refers to sample K11, blue circles to pyroxene compositions of sample K13.*

Cordierite

Cordierite is only found in the samples from the Hırkadağ massif and could only be analysed in sample H20-C, since the other analysed samples do not contain cordierite or were highly altered or weathered so that electron microprobe analyses would not provide reliable data. In sample H20-C the cordierite comprises a relatively large part of the matrix and is also found as a reaction product surrounding garnet, showing well developed crystal faces at the boundary with garnet (figure 19).

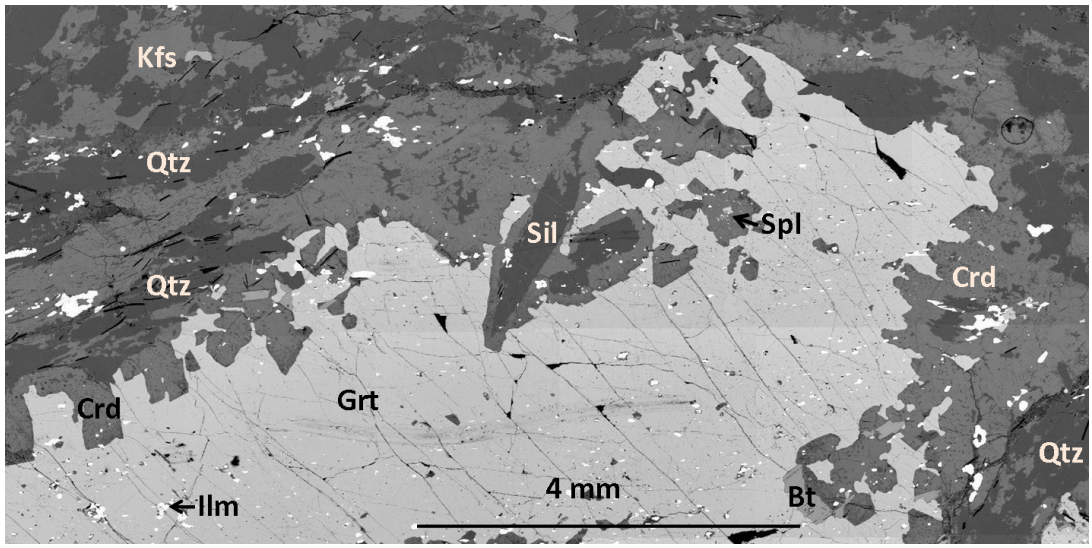

Figure 19*. BSE image of a part of the cm-scale garnet in sample H20-C, showing the reaction rim of cordierite surrounding the garnet with well developed crystal faces.*

Representative compositions of both cordierite in the matrix and inclusions in garnet are given in Appendix 8. The analytical totals are less than 100%, indicating the presence of volatile components such as CO_2 and H_2O. The X_{Mg} ($Mg/Mg+Fe^{2+}$) ratios in cordierite range from 0.44 to 0.53.

3.4 Partial melting

3.4.1 In theory

The melt produced by prograde metamorphism of pelitic mica schists is close to the composition of a granite. Small amounts of melt will not migrate over long distances and will be preserved as leucocratic quartzo-feldspathic bands. The light Qtz-Fds material in gneisses representing the anatectic melt phase (leucosome) typically shows randomly oriented minerals and fabrics typical for igneous rocks. The restite material from which the 'granitic' melt has been extracted has a high modal proportion of mafic minerals (mainly aluminosilicates, e.g.sillimanite, biotite and garnet) and has a dark gneissic appearance (melanosome) (Bucher and Frey, 2002). These anatectic gneisses are commonly termed migmatites (after Bucher and Frey, 2002).

3.4.2 Partial melting in metapelitic samples?

The metapelitic samples show mineral assemblages that indicate high temperature, low pressure metamorphism. KFMASH petrogenic grids show that these mineral assemblages are stable in the upper amphibolites or granulite facies field and that they have passed the melting curve or liquidus. That implies that the rocks possibly have partially been molten during metamorphism. Some features of the rocks indicate high temperature metamorphism and could suggest the occurrence of a (partially extracted) melt:

The presence of perthites (K-feldspar with plagioclase lamellae: a re-equilibration of older intermediate feldspar) does not prove the presence of a melt phase, but at least suggests that the rock experienced high temperatures.

Sample H12-G shows quartz and K-feldspar grains with lobate crystal faces that indicate quick mineral growth (see Appendix 5). This relatively fast growth rate indicate high temperatures and possibly the presence of melt. The occurrence of quartz and K-feldspar in zones alternated with alumino-silicate rich zones (sillimanite, biotite and garnet) could indicate a microstructure of leucosomes and restites that are typical for migmatites. However, this gneissic banding should be interpreted with great care, since the light coloured (quartz and feldspar) and dark coloured (aluminosilicates) zones could also be the result of deformation and recrystallisation. Possibly we are dealing with a gneiss that is close to the transition to a migmatite due to high temperature metamorphism.

Another indication for the formation of a melt is the occurrence of well developed crystal faces at the boundary between garnet (primary) and cordierite (secondary) in sample H20-C from the Hırkadağ massif (figure 19). In metamorphic rocks, crystals with well-developed crystal faces are presumed to have grown in an environment consisting mainly of solids but with a fluid phase in the interstices (MacKenzie and Adams, 2003). In this case, that interstitial fluid could be a melt phase.

3.5 Possible HP Al_2SiO_5 polymorph

As outlined in section 3.3.3 (petrography of key minerals), sillimanite occurs both as fibrolite and prismatic crystals. Especially the prismatic sillimanite aggregates seem to be pseudomorphs. XRD analyses have been carried out on sillimanite to investigate if relicts of kyanite or maybe andalusite are present. The presence of a Al_2SiO_5 polymorph would include important additional information for the construction of a PT path.

However, the diffraction patterns that result from the XRD analyses do not show evidence for the presence of former kyanite. It should be noted that this not implicitly means that no kyanite was present, because the powder analysed with XRD was no pure sillimanite, but a mixture of sillimanite

with minor amounts of other minerals present in the metapelitic schist. In an X-ray diffractogram of a mixture, the peaks of the different minerals could not always be visible due to overlapping peaks of other minerals. Results for samples from the Hırkadağ massif are shown in figure 20.

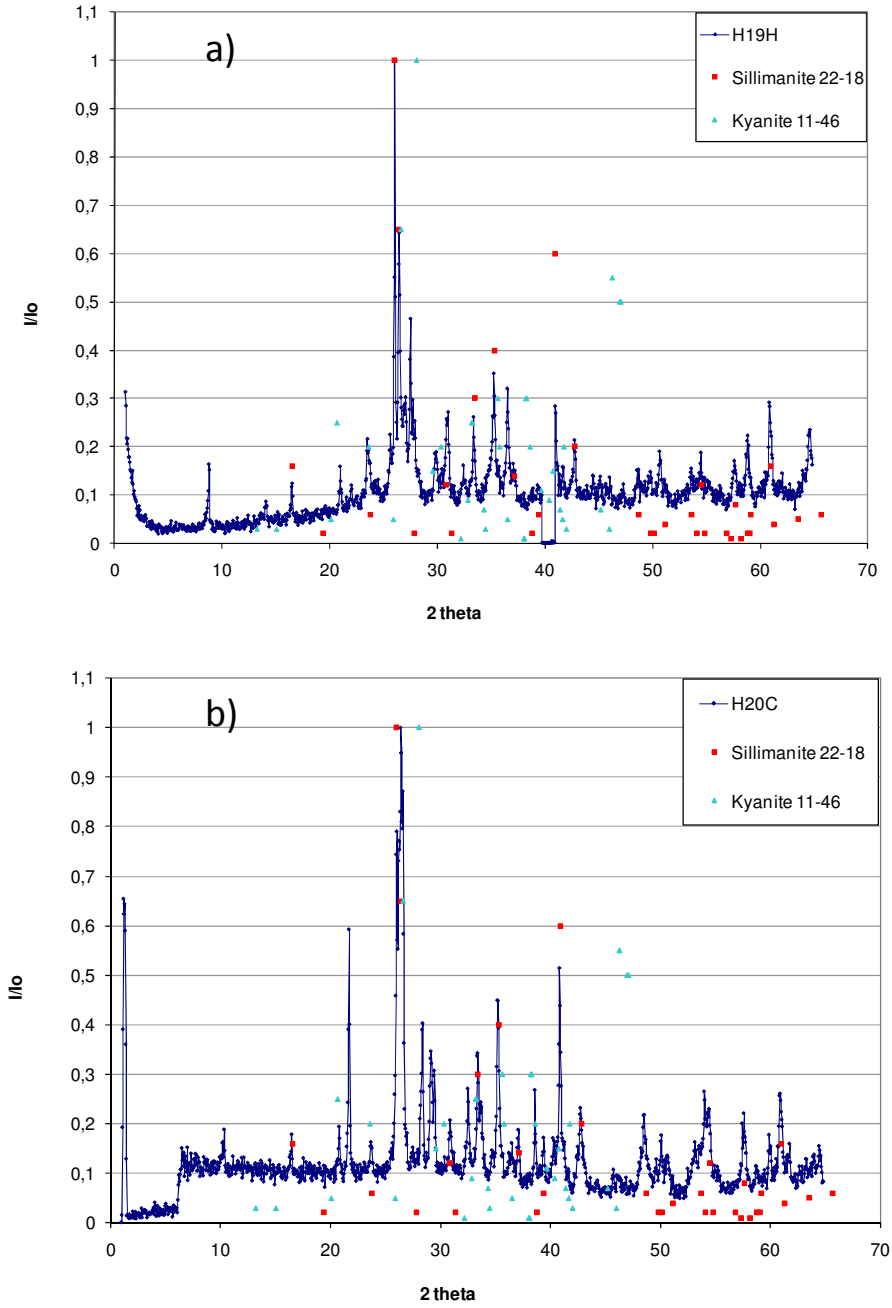

Figure 20. *X-ray diffractograms of samples a) H19-H and b) H20-C. Diffraction angles (2 theta) for sillimanite (red) and kyanite (light blue) are given for comparison with the diffraction pattern obtained with XRD.*

3.6 Geothermobarometry

The pressure (P) and temperature (T) conditions under which a rock formed, provide information about the origin of the rock as well as its metamorphic evolution (if time is constrained) and some tectonic processes the rock experienced (Blatt et al., 2006).

In this study, the thermobarometric conditions are determined first by the interpretation of the mineral assemblages and textures of the rock sample, followed by a quantitative estimate based on the chemical composition of minerals in a stable assemblage.

The first order interpretation of pressure and temperature conditions is based on groups of minerals that reflect equilibrium and can be located in a petrogenic grid. This method gives a range of the P-T conditions in which an assemblage was stable, but do not provide exact numbers.

In order to obtain information about the thermal evolution of the rock, including prograde-, peak- and retrograde conditions, more than one (meta)stable mineral assemblage in one rock is defined if possible.

3.6.1 First order interpretation of mineral assemblages

To obtain a rough indication of the pressure and temperature conditions experienced by Hırkadağ and Kırşehir samples, the metastable mineral assemblages as given in section 3.3.1 (mineral assemblages) are plotted on a petrogenic grid for pelitic rocks in the KF(M)ASH system (figure 21 and 22; Bucher and Frey, 2002; Spear and Cheney, unpublished). It is worth noting that the metapelitic rocks from both massifs also contain the elements Mg, Ca, Na, Mn and Ti. The petrogenic grid therefore represents a simplified system and the stability fields in which the defined mineral assemblages are stable only an approximate of the PT conditions experienced by the samples studied.

The petrogenic grid based on the thermodynamic dataset of Spear and Cheney (unpublished) for the KFMASH system shows that the assemblage garnet + sillimanite + biotite is stable at temperatures higher than 600 °C and pressures between ~3 and 8 kbar. The stability field for this assemblage is limited at the low-temperature side by the staurolite-in reaction, at the high-pressure side by the occurrence of kyanite (at pressures >8-10 kbar) and at the low-pressure side by the formation of secondary cordierite. When cordierite becomes stable (in the second assemblage in sample H20-C), this implies a decrease in pressure to values lower than ~3 kbar.

The petrogenic grid for LP, HT reactions in metapelites in the KFASH system (Bucher and Frey, 2002) shows higher temperatures: T ≥ 775 °C for the occurrence of spinel. According to this petrogenic grid, assemblages in which garnet + sillimanite are stable reflect equilibrium temperatures higher than 550 °C (at lower temperatures staurolite becomes stable).

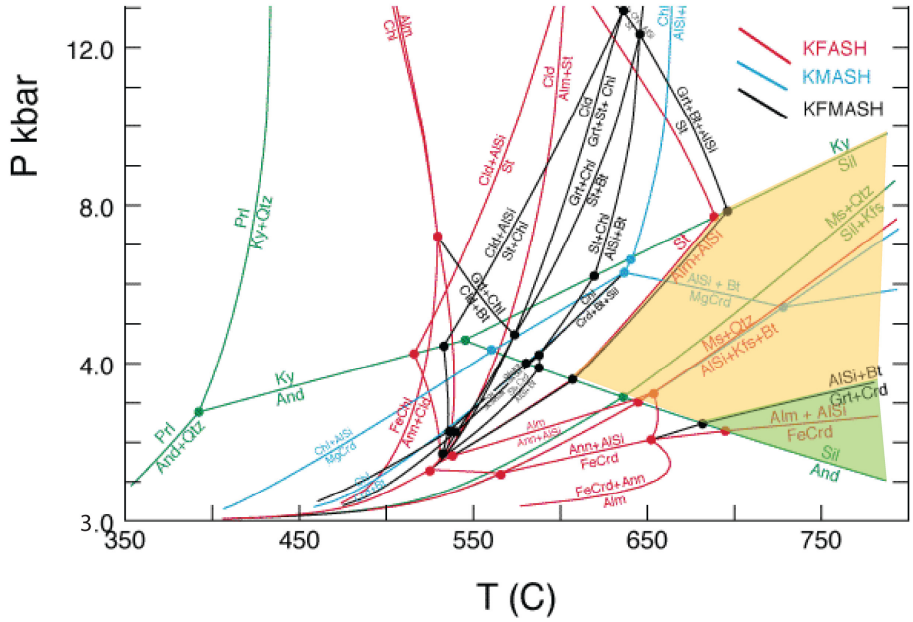

Figure 21. *Petrogenic grid for modified from Spear and Cheney (unpublished). The mineral reactions in the KFMASH system are given in black and used to define the stability field for the assemblage garnet + sillimanite + biotite(given in yellow). The stability field for secondary cordierite is given in green.*

Similar to the petrogenic grid based on Spear and Cheney, the occurrence of cordierite in the petrogenic grid of Bucher and Frey (2002) implies a decompression to at least 2.5 kbar.

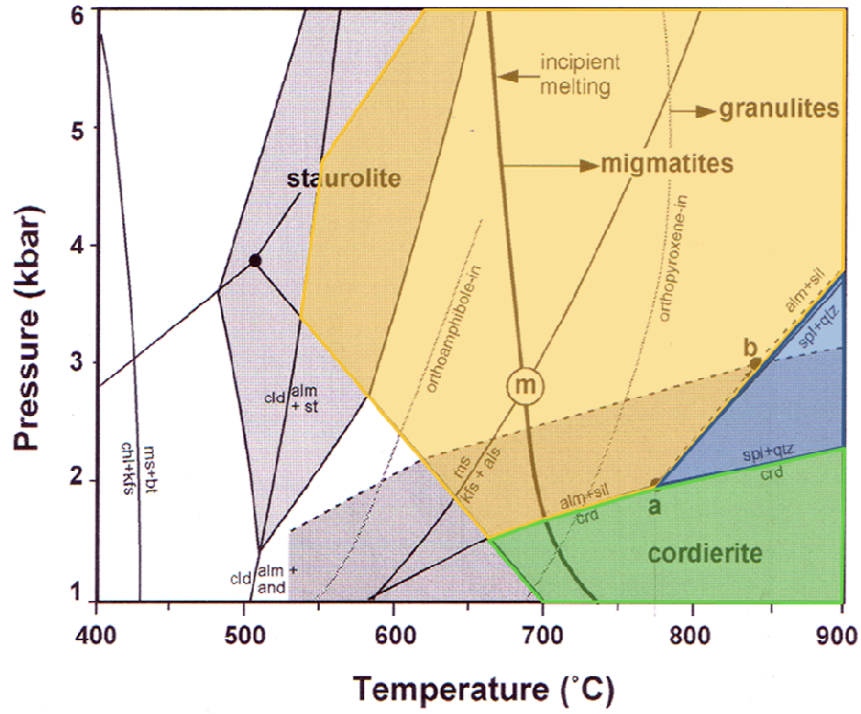

Figure 22. *Petrogenic grid showing low-pressure high-temperature reactions in metapelitic rocks in the KFASH system (modified from Bucher and Frey, 2002). The stability fields of the assemblage garnet + sillimanite is given in yellow, the field in which spinel + quartz are stable is given in blue and the stability field for cordierite is given in green.*

3.6.2 Geothermobarometers

A quantitative way to determine the peak metamorphic conditions involves calculation of equilibrium pressure(s) and temperature(s) based on the measured distribution of elements between coexisting mineral phases (Winter, 2001). If good experimental and theoretical data of both the minerals and the reactions between them are available, it is possible to locate a reaction in P-T-X space and constrain the conditions under which the metamorphic rock has been formed. However, there are some pitfalls in this approach as outlined in paragraph 3.1.2. Representative mineral pairs, especially those including metastable assemblages, should be chosen carefully by examination of the microstructure and chemical zoning.

In this study, thermometers and barometers are used to obtain a first quantitative estimate of the pressure and temperature conditions of the metamorphism of the metapelitic rocks. The results are compared with the pseudosections calculated with the computer programme TheriakDomino. For temperature estimates (1) garnet-biotite (Bhattacharya et al., 1992) exchange thermometer and (2) the saturation content of Ti in biotite (TIB; Henry et al., 2005) thermometer are used:

Almandine + phlogopite = pyrope + annite (1)

The garnet-cordierite thermometer (Bhattacharya et al., 1988) is not used, since cordierite replaces garnet in sample H20-C and therefore this mineral pair cannot be assumed to be in equilibrium.

Pressure is calculated with the GASP (3) and the GPMB-Fe (4) and GPMB-Mg (5) net transfer barometers:

Grossular + 2 sillimanite + quartz = 3 anorthite (3)

Grossular + almandine + muscovite = 3 anorthite + annite (4)

Grossular + pyrope + muscovite = 3 anorthite + phlogopite (5)

It should be noted that the garnet analyses used as input for the barometers yield a relatively low Ca content, which makes the barometers less precise (Todd, 1998).

The estimated values for temperature and pressure conditions are given below in table 4.

The above described thermometers and barometers yield temperatures and pressures shown in figure 23.

For the samples from the Hırkadağ massif, equilibrium conditions for peak metamorphism are 624-742 °C and 2.7-8.0 kbar for garnet-biotite thermometer in combination with the average pressure of the GASP, GPMB-Fe and GPMB-Mg barometers. Samples from the Kırşehir massif equilibrated at peak metamorphic conditions of 623 °C and 6.0 kbar for the garnet-biotite thermometer and the average of GASP, GPMB-Fe and GPMB-Mg barometers and 620 °C at the assumed pressure of 6.0 kbar for the Ti-in-biotite thermometer.

Table 4. *Results from PT calculation with garnet-biotite and Ti-in-biotite thermometers and garnet-sillimanite-plagioclase-quartz and garnet-plagioclase-muscovite-biotite barometers.*

Sample	Prograde/ peak/retrograde	Garnet-Biotite (℃)	Ti in biotite (℃)	GASP (kbar)	GPMB-Fe (kbar)	GPMB-Mg (kbar)	Average P (kbar)
H12-G	peak	729		2.67			2.67
H19-H	prograde	526		3.63	5.01	3.54	4.06
H19-H	peak	624		7.84	9.08	7.04	7.98
H20-C	peak	742		7.99	9.45	6.91	8.12
H20-C	retrograde	520					ca. 3
K4	prograde	585		11.74			11.74
K4	peak	623		7.03	6.49	4.47	6.00
K13	peak		620				ca.6

Figure 23. *PT points calculated with garnet-biotite thermometer or Ti-in-biotite thermometer (only sample K13) and the average pressure given in table 4 for the garnet-sillimanite schists from the Hırkadağ and Kırşehir massifs.*

In general, the GSAP barometer yields pressures that are 6-36% higher than the pressures estimated with the GPMB-Mg barometer, while the GPMB-Fe gives relatively high pressures (18-38% higher than GASP), except for sample K4 that shows a lower pressure than GASP for the GPMB-Fe barometer.

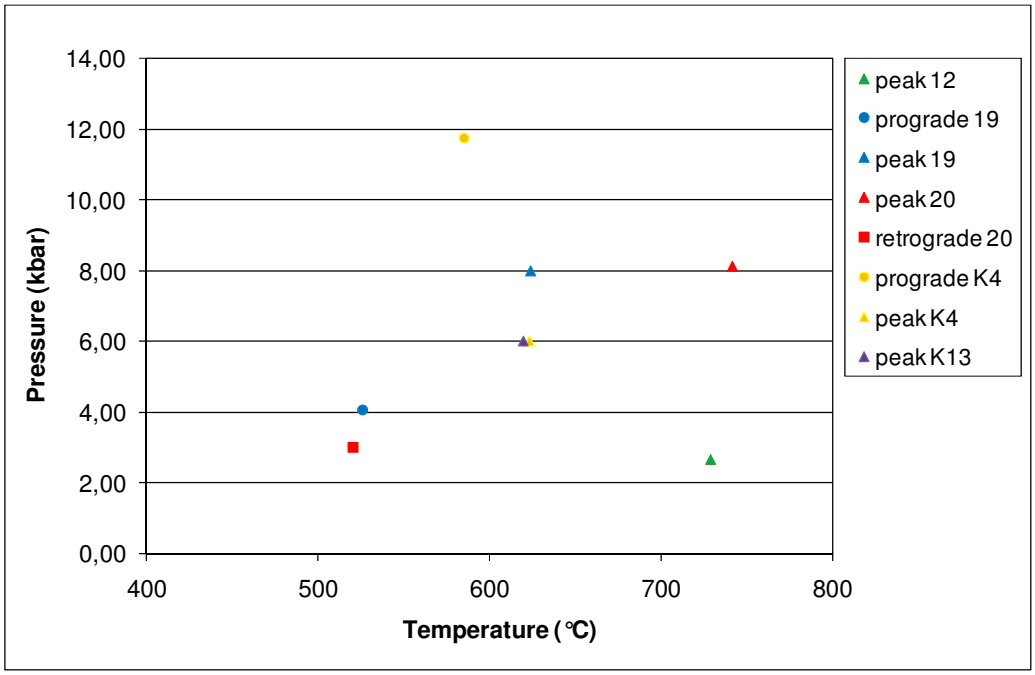

3.6.3 Construction of the PT path

Petrography and rock major element analyses are used to calculate and interpret TheriakDomino PT-pseudosections or equilibrium phase diagrams for specific bulk rock compositions in the CNKFMASH system.

A pseudosection is a phase diagram that explicitly shows the assemblage in a system of specified bulk composition as a function of two independent variables (in this study pressure and temperature) (after Dave Waters, personal website). The difference with a petrogenic grid is that a petrogenic grid shows all minerals reactions that will occur in a model system, while the mineral reactions that will occur in a pseudosection are limited to a specific bulk composition.

The thermobarometric calculations with TheriakDomino result in the interpretation of stable mineral assemblages and the construction of a pressure-temperature path for the five representative samples outlined in the previous chapter. These PT paths are combined to show the metamorphic evolutions of the Hırkadağ block and the Kırşehir massif, and to assess possible overlaps in the metamorphic history of both massifs.

The amount of water added to the system (as part of the calculation with Domino) influences the size of the fields in which particular minerals are stable, e.g. at what conditions and if mineral reactions occur. In this study, for most samples a surplus amount of water is added, to make sure that micas (biotite) and other H_2O-bearing phases like cordierite can form. However, a varying amount of water will change the stability fields of (some) minerals. E.g. the stability field of sillimanite becomes smaller when a surplus amount of water is added to the system (especially for sample H12-G). For that reason in sample H12-H a slightly smaller amount of water is added, to make sure that the sillimanite stability field is representative (showing an overlap with the garnet stability field) for the mineral assemblages observed in thin section.

Hırkadağ

Sample H12-G

Figure 24 shows the pseudosection calculated with Domino for sample H12-G. The PT pseudosection shows the stability fields of all stable mineral assemblages, separated by lines that represent mineral reactions. Areas where key minerals are stable are coloured and labelled and the inferred PT path is shown in red.

As outlined in the Petrology chapter, three metastable mineral assemblages are defined:

1. Sillimanite + plagioclase + garnet + biotite ± quartz
2. Spinel (as reaction product of sillimanite)

3. K-feldspar + plagioclase + quartz (in light-coloured zones in between the foliation that is formed by sil, bt, sp and fine grained plag and qtz)

The PT conditions of assemblage 1 and 2 are restricted by isolines of pyrope in the garnet stability field and hercynite in the stability field of spinel, respectively. The upper boundary of assemblage 1 and thereby the start of the PT path is formed by the kyanite-in reaction line, since no kyanite has been found in this rock. Two generations of garnets have been recognized in thin section: an older xenoblastic garnet that is relatively small (up to 8 mm) and a younger generation with more idioblastic and relatively garnet grains. The younger garnets seem to replace biotite and have inclusions of sillimanite, so these garnets are younger than biotite and sillimanite.
The part of the PT path from assemblage 1 to the formation of spinel is characterised by more or less isothermal decompression from 9.5 kbar to about 4 kbar at 800°C. At this stage, the main deformation event (Dm, isoclinal folding; Wehrens, 2008) took place, forming a main foliation that is defined by dark coloured biotite + sillimanite and post-dates garnet growth.
After the formation of spinel, the rock starts to cool. At this stage, the pressure does not drop below 3kbar, otherwise cordierite would have been formed. The end of the PT path in this figure is marked by the stability fields of quartz (with some sillimanite inclusions), K-feldspar and muscovite. These minerals are relatively late. Quartz and K-feldspar form large grains with lobate grain boundaries, occurring in separate domains together with plagioclase, possibly indicating a melt phase. The rock was most likely brought to the surface from this point, indicating a geothermal gradient of about 60°C/km.

Sample H19-H

Figure 25 shows the PT pseudosection for sample H19-H is shown. This sample belongs to a different geological formation (the Kaleboynu formation, Wehrens, 2008) than sample H12-G and H20-C (Gümüşler formation, Wehrens, 2008), but is also a grt-sil schist. In this pseudosection the areas where key minerals are stable are coloured and metastable mineral assemblages are labelled. In this sample the following metastable assemblages are recognised:

1. garnet + K-feldspar + sillimanite (fibrolite in foliation) ± muscovite ± quartz + ilmenite

2a. sillimanite (in plagioclase) + biotite + plagioclase + spinel (in domain around garnet)

2b. Spinel (as the reaction product of fibrolitic sillimanite)

The isopleths of pyrope and hercynite are plotted, to indicate in which part of the garnet field and the spinel field the mineral assemblage was stable.

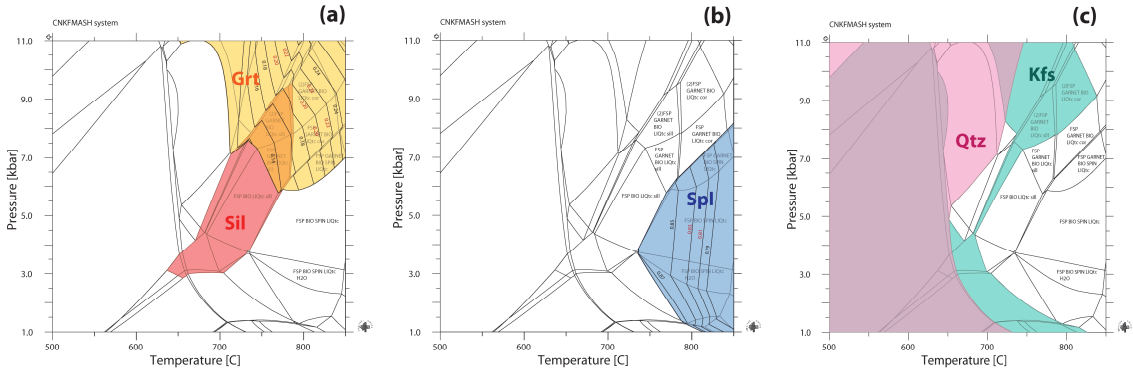

Figure 24a. CNKFMASH pseudosections calculated with DOMINO for the bulk rock composition of sample H12-G (Hırkadağ), with water added. (a) Stability fields of minerals of assemblage 1: sillimanite + garnet + biotite + plagioclase ± quartz. Biotite and plagioclase are stable almost throughout the given PT-range. Isopleths for pyrope are shown with measured values given in red. (b) Stability field of assemblage 2: spinel. Isopleths for hercynite are shown with values measured in this sample in red. (c) Stability fields of K-feldspar and quartz, that are together with plagioclase the stable minerals of assemblage 3. Plagioclase is stable for almost all pressures and temperatures given.
The mineral assemblages in the most important stability fields are listed. Abbreviations are given in Appendix 6. The relative proportion of the elements used as input for DOMINO calculations for sample H12-G: SI(1027)AL(381)FE(80)MG(34)CA(20)K(129)NA(114)H(800)O(?).

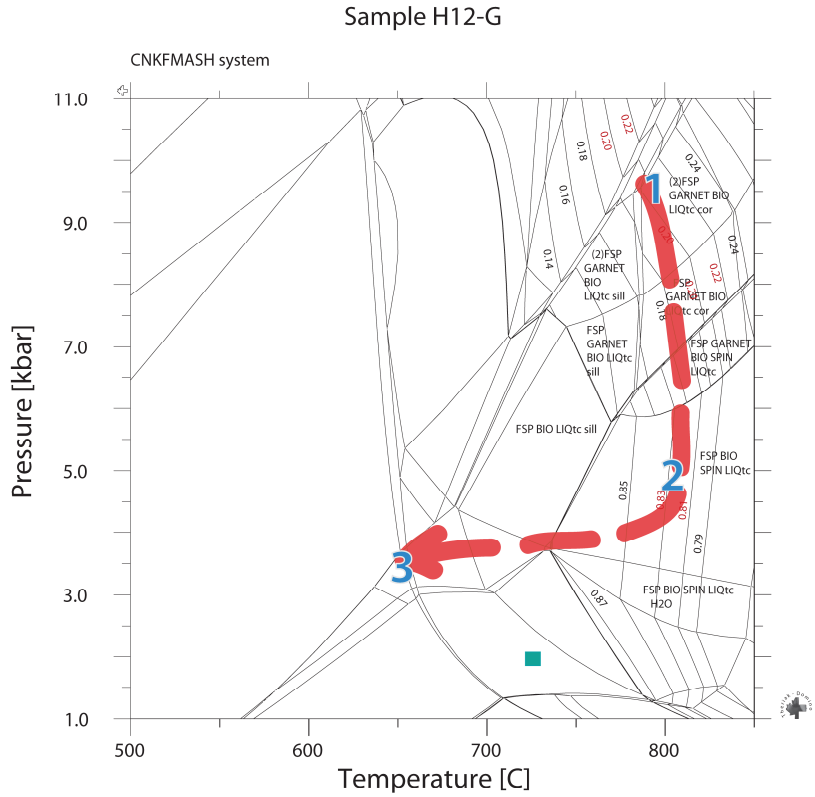

Figure 24d. CNKFMASH pseudosection calculated with DOMINO for the bulk rock composition of sample H12-G (Hırkadağ), with water added. The inferred PT path is indicated with a red arrow. Stability fields of the key minerals of the 3 assemblages are numbered, according to figures 24a-c (above). The mineral assemblages in the most important stability fields are listed. Abbreviations are given in Appendix 6. Isopleths are shown of pyrope in the garnet stability field and hercynite in the spinel stability field, with values found in this sample in red. The relative proportion of the elements used as input for DOMINO calculations for sample H12-G: SI(1027)AL(381)FE(80)MG(34)CA(20)K(129)NA(114)H(800)O(?). The PT point calculated with the garnet-biotite thermometer and the average of the GASP and GPMB barometers is shown as a green box for the peak of metamorphism.

The kyanite-in reaction line again is taken as the upper boundary, since no kyanite has been found in thin section. The isopleths of pyrope show that garnet was stable close to this reaction line. The isopleths of pyrope in garnet are also visible at lower pressures (and slightly higher temperatures) close to the reaction-in line of spinel. It is therefore possible that the PT path in this figure started at lower pressure (the isopleth outside the Kfs stability field is ignored, since textural relationships show that garnet and K-feldspar where stable together). I have chosen the higher pressure-start of the PT path for the following reasons: (1) white mica (muscovite) is found as inclusions in garnet and remnants of grains in the matrix. The stability field of white mica shows an overlap with the K-feldspar and the garnet fields close to the kyanite-in reaction line; (2) sillimanite and biotite have grown after garnet was formed but before the formation of spinel. In case of the lower pressure-start there are hardly no changes in the PT conditions for sillimanite to grow before it has been partly replaced by spinel.

The location of the PT path leads to some difficulties with sillimanite as a stable mineral in assemblage 1. The PT pseudosection shows a relatively small stability field for sillimanite that only has a small overlap with the garnet stability field. According to the PT calculations with Domino, sillimanite is not stable on the proposed PT path. This could be the result of an incorrect amount of water that is added to the system. The sillimanite field will become larger when the system is not saturated with water at each point in the PT pseudosection. Another possibility is that another Al-rich phase is overestimated by Domino on (at the expense of) the presence of sillimanite. This is supported by the relatively large amount of stable corundum (Al_2O_3). The amount of corundum at the location of the star (see figure
25) is 14 vol%, whereas only very small amounts (<1%) are observed in thin section. Corundum could be replaced by spinel, but textural relationships show that spinel is mainly replacing sillimanite. Other options for model results that do not fit the textural observations are an incorrect bulk analysis (e.g. due to the escape of a melt phase) or the presence of more end-members than calculated with Domino. E.g., the system is simplified, ignoring elements that are difficult to model, in this case Mn and Ti. If, for example, garnet contains a significant amount of Mn or if Ti is present in biotite, this would influence the reliability of the results calculated with Domino.

Besides the option that calculations with Domino do not represent the real chemistry of the rock, it is possible that the minerals in the rock did not internally equilibrate. Thin sections show corona-textures around garnet porphyroblasts. These textures often form due to differences in the rate of

transport between elements during metamorphism. Principally the transport of Al is generally

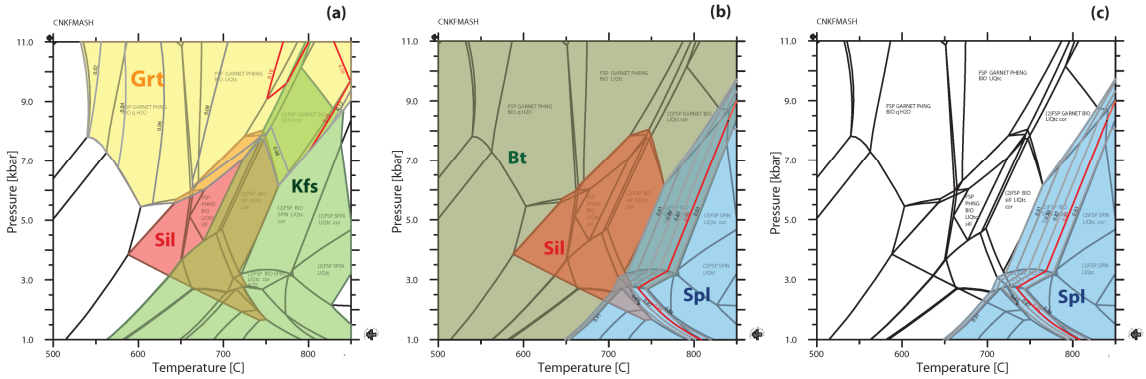

Figure 25 a-c. CNKFMASH pseudosections calculated with DOMINO for the bulk rock composition of sample H19-H (Hırkadağ), with water added. (a) Stability fields of minerals of assemblage 1: garnet + K-feldspar + sillimanite ± phengite (muscovite) ± quartz + ilmenite. Only the main minerals are shown. Ilmenite is not part of the calculation, since the system has been symplified leaving out Ti. Isopleths for pyrope in garnet are shown with measured values given in red. (b) Stability field of assemblage 2a: sillimanite + biotite + plagioclase + spinel (in small amounts). Plagioclase is stable for almost all pressures and temperatures. (c) Stability field of spinel, forming the stable 'assemblage' 2b (replacing fibrous sillimanite). Isopleths for hercynite in spinel are shown with values measured in this sample given in red.
The mineral assemblages in the most important stability fields are listed. Abbreviations are given in Appendix 6. The relative proportion of the elements used as input for DOMINO calculations for sample H19-H: SI(829)AL(573)FE(116)MG(25)CA(12)K(152)NA(86)H(500)O(?)

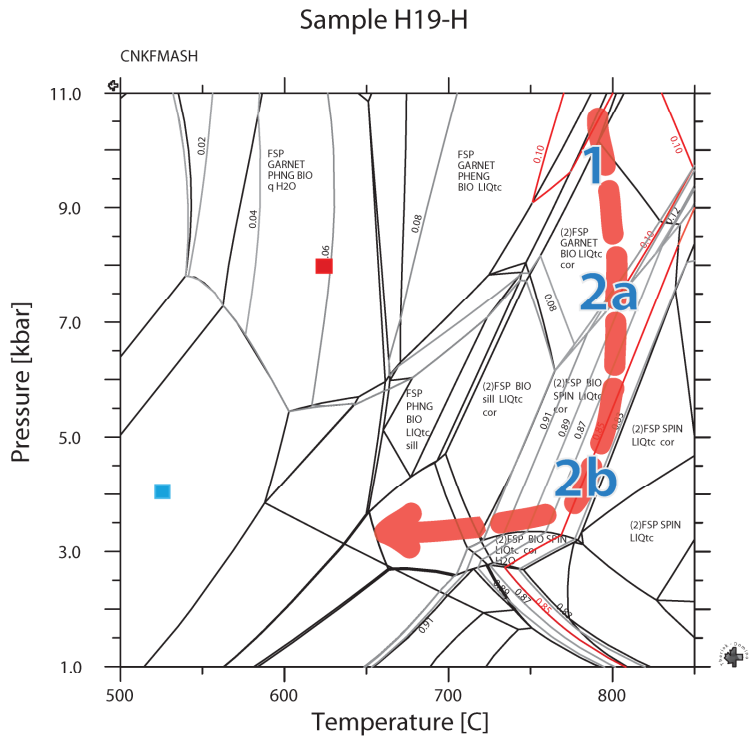

Figure 25d. CNKFMASH pseudosection calculated with DOMINO for the bulk rock composition of sample H19-H (Hırkadağ), with water added. The inferred PT path is indicated with a red arrow. Stability fields of the key minerals of the 2 assemblages are numbered, according to figures 25a-c (above). The mineral assemblages in the most important stability fields are listed. Isopleths are shown of pyrope in the garnet stability field and hercynite in the spinel stability field, with values found in this sample in red. The relative proportion of the elements used as input for DOMINO calculations for sample H19-H: SI(829)AL(573)FE(116)MG(25)CA(12)K(152)NA(86)H(500)O(?). The PT points calculated with the garnet-biotite thermometer and the average of the GASP and GPMB barometers are given in a red box for the peak and in a blue box for the prograde metamorphism.

assumed to be slower than necessary for the rock to equilibrate (Kelsey et al., 2003). Since this rock is rich in Al-bearing minerals, this could explain difficulties with the construction of a PT path that is based on the stability fields of rock forming minerals.

From the first assemblage to the formation of spinel, the rock has undergone isothermal decompression from about 10 kbar to 8 kbar (spinel-in reaction line) and down to 4 kbar at temperatures of 800°C. Within the spinel stability field the rock starts to cool, but is not uplifted to lower pressures than about 3 kbar, otherwise the rock would have entered the cordierite stability field and cordierite would probably have been formed.
The PT path ends before the quartz stability field is entered at a pressure of about 3.5 kbar and a temperature of 680°C. Quartz is found as a minor and relatively early phase, as rare inclusions in garnet and no newly crystallised quartz grains are observed. Obviously, the rock has gone through the quartz stability field when it was brought to the surface, but in this pseudosection only the part of the PT path is shown that is represented by the mineral assemblages in this rock sample.

Sample H20-C
Figure 26 shows the pseudosection calculated with Domino for sample H20-C. The PT pseudosection shows the stability fields of all stable mineral assemblages, separated by lines that represent mineral reactions. Areas where key minerals are stable are coloured and the metastable assemblages are labelled. The inferred PT path is given in red. The metastable assemblages that are recognised in this rock are:

1. garnet + biotite + sillimanite + quartz ± plagioclase + ilmenite
2. cordierite + spinel + quartz + K-feldspar

The location of the first assemblage is defined by the isopleths of pyrope in garnet, albite in plagioclase and the lack of kyanite. Therefore, the PT path starts at about 7.5 kbar and 690 °C. There is no strong petrological evidence for the relative timing of the growth of K-feldspar. K-feldspar occurs in zones together with quartz, showing irregular crystal phases. This could indicate that K-feldspar recrystallised or that K-feldspar grew relatively late. The stability field of K-feldspar is limited to relatively low pressures (<2.5 kbar) and a limited temperature range (~600-750°C). This supports the idea that K-feldspar is a relatively young mineral, forming at lower pressures and temperatures than the minerals that represent peak metamorphic conditions. The rock shows a decompression to about 4.0 kbar for the replacement of garnet by cordierite. The growth of spinel (hercynite) indicates

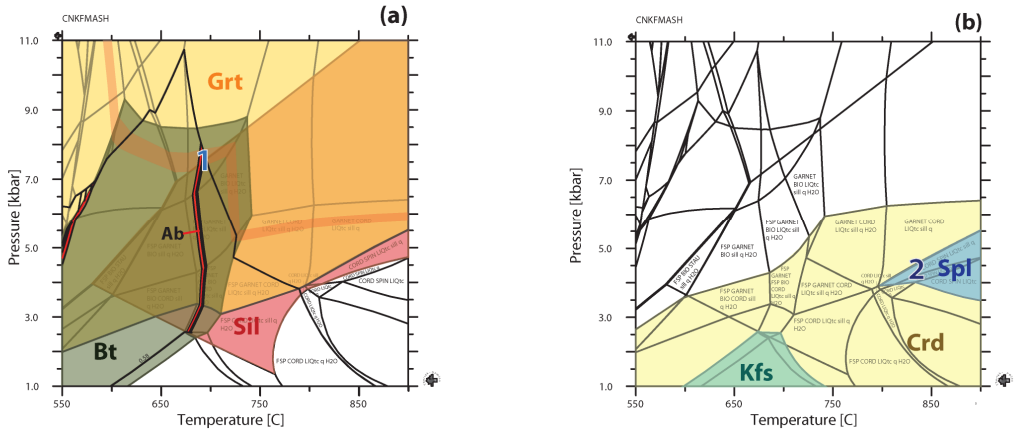

Figure 26 a, b. CNKFMASH pseudosections calculated with DOMINO for the bulk rock composition of sample H20-C (Hırkadağ), with water added. (a) Stability fields of minerals of assemblage 1: garnet + biotite + sillimanite + quartz ± plagioclase + ilmenite. Isopleths of pyrope in garnet are indicated with the thick orange line in the garnet stability field. The isopleths of albite in plagioclase are shown, with the measured value (0.56 Ab) in red. The stability field of plagioclase is not coloured. Ilmenite is not part of the calculation, since the system has been symplified leaving out Ti. The location where assemblage 1 is assumed to be stable is numbered.
(b) Stability fields of cordierite, K-feldspar and spinel, that together with quartz form the second (meta)stable assemblage. The stability field of quartz covers almost the total PT range given in this figure and is therefore not indicated. The assumed location for assemblage 2 is numbered. The mineral assemblages in the most important stability fields are listed. Abbreviations are given in Appendix 6. The relative proportion of the elements used as input for DOMINO calculations for sample H20-C: SI(1047)AL(431)FE(128)MG(32)CA(10)K(41)NA(17)H(500)O(?) .

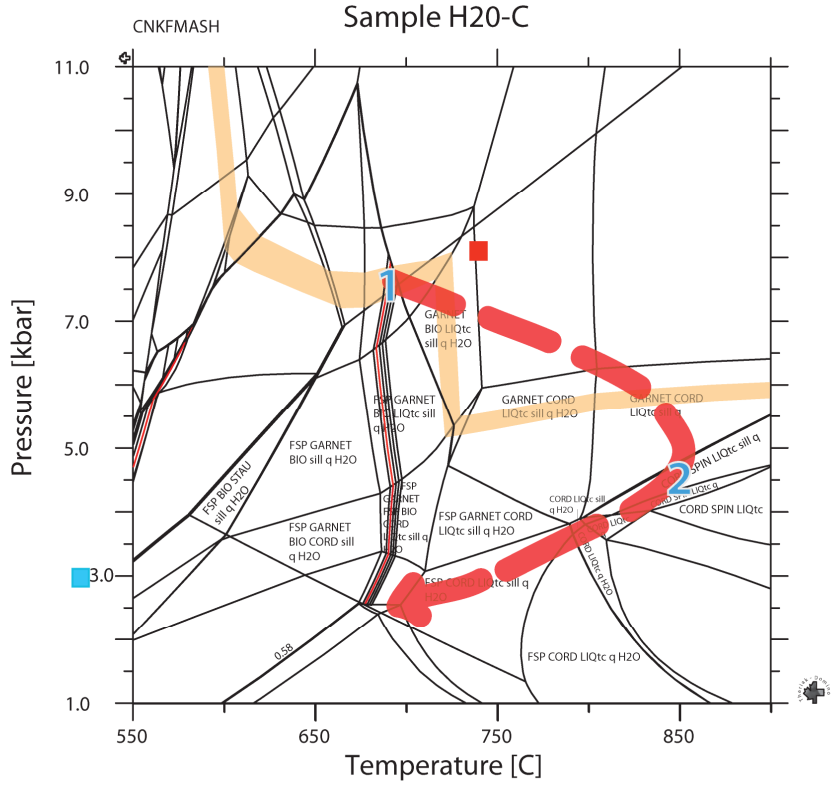

Figure 26c. CNKFMASH pseudosection calculated with DOMINO for the bulk rock composition of sample H20-C (Hırkadağ), with water added. The inferred PT path is shown as a red arrow. The locations where the described assemblages are assumed to be stable, are numbered according to figure 26 a, b (above). The mineral assemblages in the most important stability fields are listed. Isopleths are shown of pyrope in the garnet stability field (thick orange line) and albite with values found in this sample in red. The relative proportion of the elements used as input for DOMINO calculations for sample H20-C: SI(1047)AL(431)FE(128)MG(32)CA(10)K(41)NA(17)H(500)O(?) . The PT point calculated with the garnet-biotite thermometer and the average of the GASP and GPMB barometers is given in a red box for the peak- and in a blue box for the retrograde metamorphic conditions.

heating to at least 800°C. Microstructural relationships show that the first assemblage is partly replaced by the second assemblage (grt → crd + qtz; sil → spl) and hence the two assemblages can be linked in a clockwise PT path. Secondary biotite and muscovite grow in randomly oriented patches, either indicating a retrograde phase or a melanosome. The well developed crystal faces of cordierite and the quartzofeldspathic layers might indicate the presence of a melt. The calculations with Domino also indicate the presence of a liquid phase, a melt in this case, that is rich in feldspar and quartz.The PT path ends at the Kfs-in reaction line. If K-feldspar is indeed relatively late, the rock would have entered this field at about 2.5 kbar and a temperature of 700 °C.

Kırşehir

Sample K4

Figure 27 shows the pseudosection calculated with Domino for sample K4 from the Kırşehir massif. As in the other pseudosections, the stability fields of calculated stable mineral assemblages are shown and areas where key minerals are stable are coloured. The metastable mineral assemblages as given below are labelled and the inferred PT path is given in red. In this metapelitic sample from the Kırşehir massif, the following metastable mineral assemblages are defined:

1. garnet + biotite + sillimanite + feldspar (sillimanite seems to be slightly younger than garnet)
2. K-feldspar + quartz ± plagioclase
3. retrograde chlorite + muscovite

The PT conditions of the first assemblage are restricted by the isopleths of pyrope in the garnet stability field and the relatively small stability field of sillimanite. The PT path starts at the isopleths of $pyrope_{0.10}$ in garnet. Since no evidence for high pressure conditions is found, the upper boundary of assemblage 1 is chosen at the low-pressure end of the $pyrope_{0.10}$ isopleth, at about 8.5 kbar. The overlap between the garnet- and the sillimanite stability fields is relatively small, so the PT path is limited to this overlap at about 710 °C and shows a decrease in pressure from the start of the path to the stability field of sillimanite at 7.5 kbar. Biotite and feldspar are stable over a large range of PT conditions and do therefore not constrain the location of assemblage 1. The occurrence of microperthite indicates the presence of a former intermediate feldspar that was stable at relatively high temperatures and that now shows exsolution lamellae due to cooling.

The second metastable mineral assemblage that consists of zones rich in K-feldspar, quartz and a minor amount of plagioclase and plagioclase rims around garnet is controlled by temperature rather than pressure as shown by the stability fields. The inferred PT path shows a decrease in temperature from assemblage 1 to assemblage 2 in order to enter the field in which K-feldspar, quartz and plagioclase are stable together.

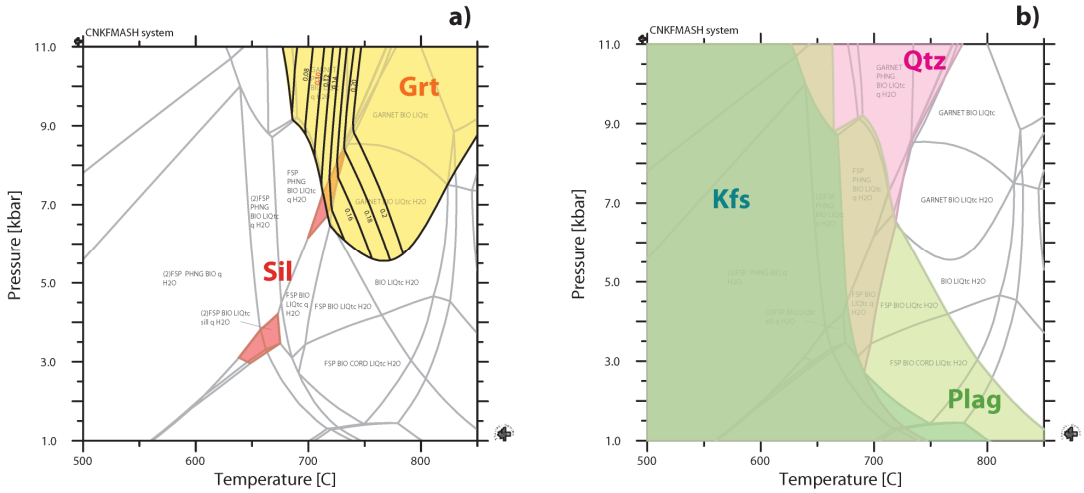

Figure 27a, b. CNKFMASH pseudosections calculated with DOMINO for the bulk rock composition of sample K4 (Kırşehir), with water added. (a) Stability fields of minerals of assemblage 1: garnet + biotite + sillimanite + feldspar. Biotite is stable at temperatures below 800 °C. Isopleths of pyrope in garnet are indicated in the garnet stability field with measured values given in red. (b) Stability fields of quartz, K-feldspar and plagioclase, that together form the second (meta)stable assemblage. The mineral assemblages in the most important stability fields are listed. Abbreviations are given in Appendix 6. The relative proportion of the elements used as input for DOMINO calculations for sample K4: SI(1160)AL(289)FE(62)MG(34)CA(14)K(143) NA(56)H(1300)O(?).

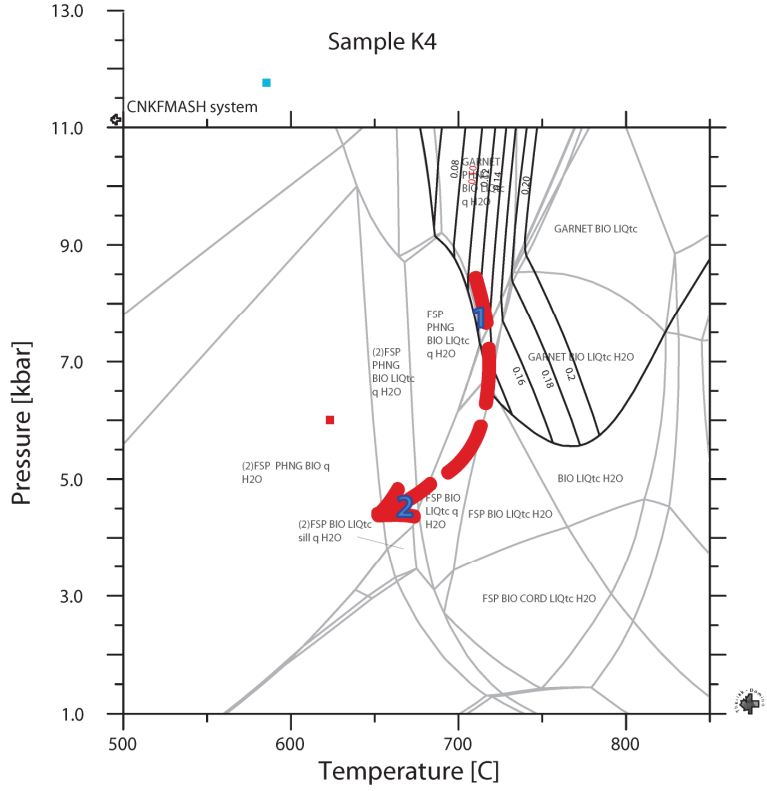

Figure 27c. CNKFMASH pseudosection calculated with DOMINO for the bulk rock composition of sample K4 (Kırşehir), with water added. The inferred PT path is given as a red arrow. The locations where the described assemblages are assumed to be stable, are numbered according to figures 27a, b (above). The mineral assemblages in the most important stability fields are listed. Isopleths are shown of pyrope in the garnet stability field with values found in this sample in red. The relative proportion of the elements used as input for DOMINO calculations for sample K4: SI(1160)AL(289)FE(62)MG(34) CA(14)K(143)NA(56) H(1300)O(?). The PT points calculated with the garnet-biotite thermometer and the average of the GASP and GPMB barometers are shown as a red box for the peak- and as a blue box for the prograde metamorphic conditions.

There are no indications for a decrease in pressure from the first to the second assemblage, however. Most likely, the pressure did not drop below 3.5 kbar, because the rock then would have entered the cordierite stability field and no cordierite is found in this sample. Assuming that the rock has been brought to the surface from this point, favoured by the occurrence of retrograde chlorite and muscovite, the PT path shows a slight decrease in pressure when temperature decreases from 710 °C for assemblage 1 to a maximum of 670 °C for assemblage 2.

3.8.5 Sample K13

Figure 28 shows the PT pseudosection calculated with Domino for sample K13 from the Kırşehir massif. This rock consists of an alteration of pelitic biotite-rich bands and calc-silicate bands with in between bands that are rich in clinopyroxene. For PT analysis only the pelitic biotite-rich band and the clinopyroxene-rich band are taken into account, because they are expected to preserve peak metamorphic conditions best and the modelling of calc-silicates is more complicated due to the presence of CO_2 in the bulk rock composition.

The pseudosection shows the stability fields of stable mineral assemblages with areas where key minerals are stable in colour. In the stability field of plagioclase isopleths of anorthite are given with the value measured in this sample given in red. The metastable mineral assemblages defined in this sample are

1. Biotite + quartz + K-feldspar + clinopyroxene (with biotite and clinopyroxene in separate zones)
2. Clinopyroxene (as reaction rim around biotite) + plagioclase + quartz (intergrowth plagioclase+ quartz: myrmekite)

The stability fields of the minerals of assemblage 1 do not give a good indication of especially the pressure and in minor amounts temperature conditions in which this assemblage was stable. The fields in which biotite and quartz are stable together show that the temperature did not exceed 725 °C for assemblage 1. At temperatures >725°C, quartz is not stable and in addition orthopyroxene is stable in this PT zone and no orthopyroxene is observed in sample K13. K-feldspar is stable at temperatures below 675 °C as calculated with Domino. This would imply that the first assemblage

was stable at a temperature <680°C. However, microstructural relationships show that plagioclase is a secondary mineral that together with quartz forms a myrmekite. Assuming that the myrmekite formed by exsolution due to cooling of primary K-feldspar (HT orthoclase that contains dissolved Na and Ca)in which K-feldspar releases Na and Ca (Collins, 1997), K-feldspar was stable at a higher temperature than plagioclase. The isopleths of $anorthite_{0.57}$ in plagioclase gives a temperature of about 675°C.

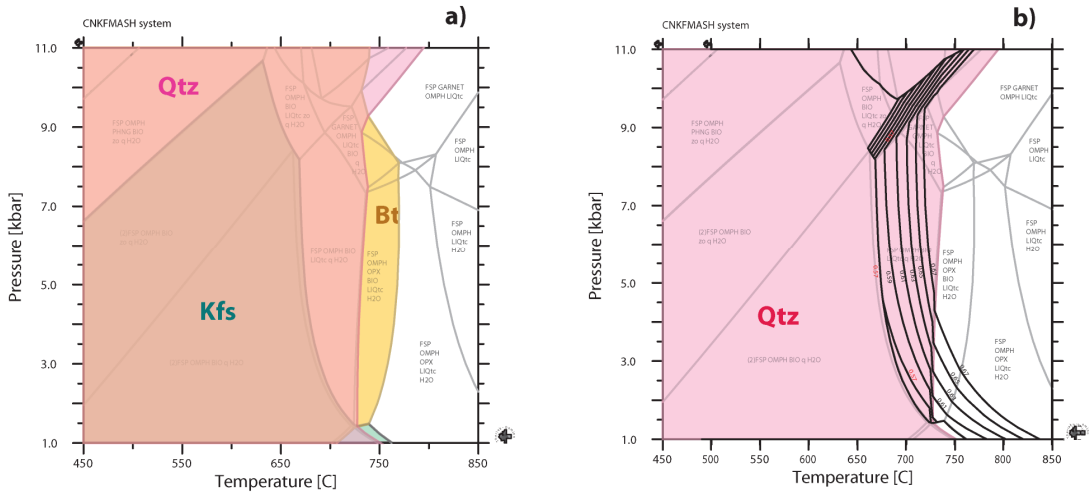

Figure 28a, b. CNKFMASH pseudosections calculated with DOMINO for the bulk rock composition of sample K13 (Kırşehir), with water added. (a) Stability fields of minerals of assemblage 1: biotite + quartz + K-feldspar + clinopyroxene. Clinopyroxene is stable over the given PT range and is therefore not coloured. (b) Stability fields of quartz, plagioclase and clinopyroxene that together form the second (meta)stable assemblage. The stability field of clinopyroxene is not coloured, since clinopyroxene is stable throughout the given PT range. For plagioclase only the isopleths of anorthite are shown with the values measured in this sample given in red. The mineral assemblages in the most important stability fields are listed. Abbreviations are given in Appendix 6. The relative proportion of the elements used as input for DOMINO calculations for sample K13: SI(1048)AL(282)FE(81)MG(63)CA(142) K(66)NA(75)H(900)O(?).

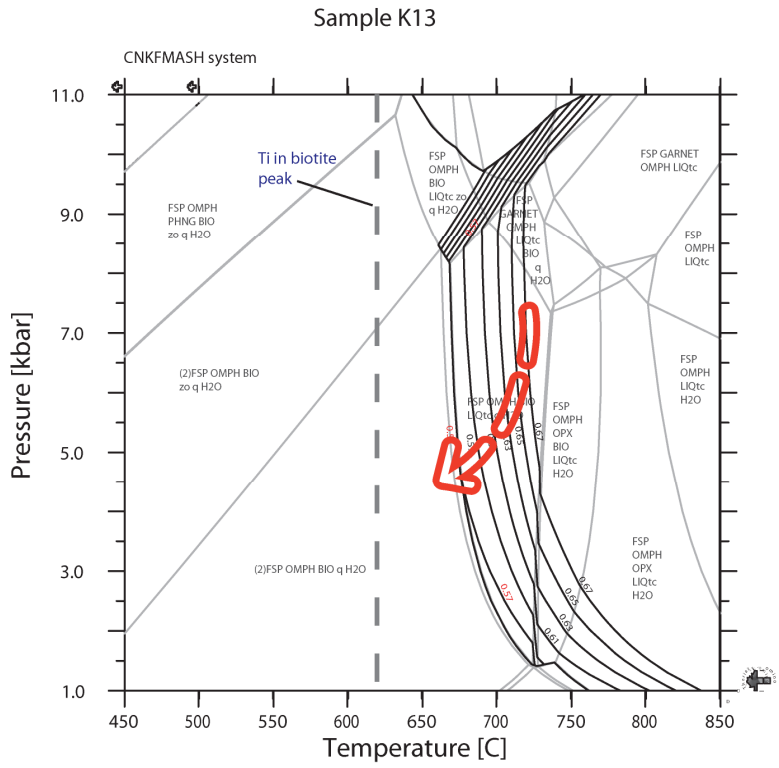

Figure 28c. CNKFMASH pseudosection calculated with DOMINO for the bulk rock composition of sample K13 (Kırşehir), with water added. The inferred PT path is given as a red dotted arrow. The mineral assemblages in the most important stability fields are listed. Isopleths are shown of pyrope in the garnet stability field with values found in this sample in red. The relative proportion of the elements used as input for DOMINO calculations for sample K13: SI(1048)AL(282)FE(81)MG(63)CA(142)K(66)NA(75) H(900)O(?). The temperature calculated with the Ti-in-biotite thermometer is shown as a grey dotted line.

According to the assumption that K-feldspar is a primary mineral, the first assemblage has been stable at temperatures >675°C, which is supported by the stability fields of quartz and biotite. So, the first assemblage was stable at temperatures between 675 °C and 725 °C and the second assemblage was stable at 675 °C. The formation of myrmekite has changed the composition of K-feldspar, which could explain the relatively low temperature of the K-feldspar stability field in the pseudosection. Clinopyroxene is stable for all PT conditions in this figure and do therefore not restrict the equilibrium PT conditions of both assemblage 1 and 2.

The stability fields of the minerals in assemblage 1 and 2 do not give good indications for the pressure conditions of both assemblages. In the temperature range given for the first assemblage (675-725 °C) the upper pressure limit is given by the stability field of garnet at 7.5-8.5 kbar. Garnet is found in this rock in very low amounts and no garnet could be analysed in thin section. The PT path given in figure XX is an approach of the real PT path the rock experienced, due to the lack of indications for pressure. The inferred PT path shows a decrease in temperature from the first to the second assemblage and decompression is assumed based on the PT path of sample K4 .

The inferred PT paths of the Hırkadağ massif and Kırşehir massif are plotted together in figure 29, respectively. The peak temperatures are the highest for sample H20-C in which cordierite replaces garnet. The samples from the Kırşehir massif show lower peak temperatures (~700 °C) than the estimated peak metamorphic conditions of the Hırkadağ massif (800 °C). Both massifs have experienced approximately isothermal decompression.

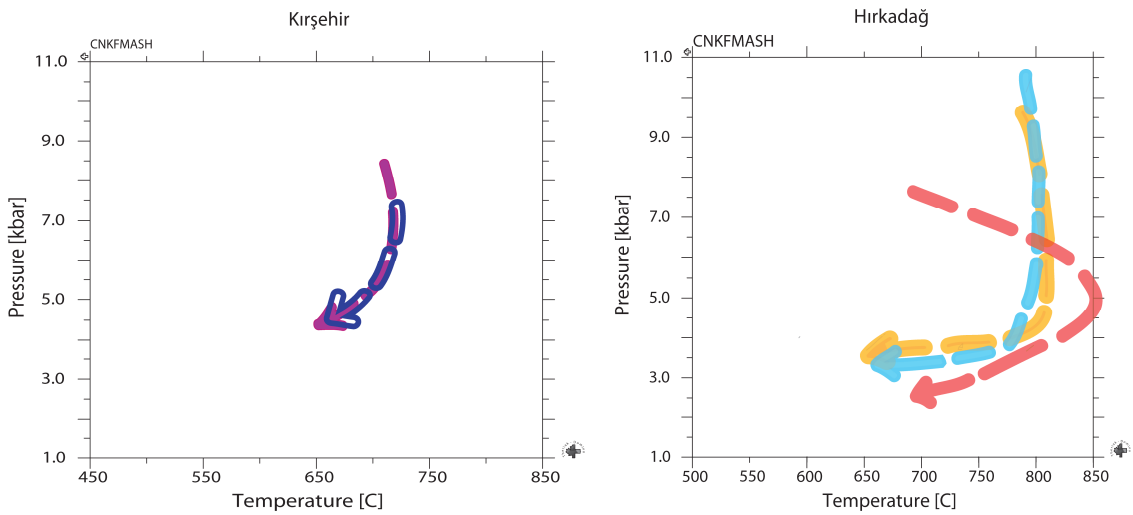

Figure 29. *The inferred PT paths for a) samples K4 (purple) and K13 (blue) from the Kırşehir massif and b) for samples H12-G (yellow), H19-H (light blue) and H20-C (red) from the Hırkadağ massif, calculated with Domino for the CNKFMASH system.*

4. Discussion

The compilation of PT paths based on the pseudosections calculated with Domino yields some questions. Subjects related to these problems are discussed below, followed by a comparison of the thermobarometric results of the garnet-biotite, Ti-in-biotite thermometers and GASP and GPMB barometers with the TheriakDomino calculations, and some general remarks on the metamorphic evolution of the studied samples.

4.1 Bulk rock composition

For PT calculations with Domino, the bulk rock composition is used as input. As for all computer models, the results of TheriakDomino are strongly dependent on the quality of the input. Although the parts of the rocks used for bulk rock analyses are carefully chosen, they might not represent an adequate bulk composition. The garnet sillimanite schists show mineral assemblages that are incompletely consumed by coronal or symplectitic mineral assemblages, dividing the rock in domains with different compositions. This diffusion-controlled growth typically occurs under fluid-absent conditions (Keller et al., 2004) and characterize granulite facies rocks (Kelsey et al., 2003). The corona textures in sample H19-H necessitate a careful interpretation of the PT pseudosection, bearing in mind that the calculated stability fields only partly represent this rock (Clarke and Powell described similar coronas, 1991). In case the bulk composition is not representative for the rock, the different domains/zones could be investigated separately if possible. In addition, if there was a melt phase extracted from the rock, the bulk rock analyses that we measure today do not represent the original bulk rock compositions. This results in PT calculations that do not fully represent the metamorphic evolution of the rock.

Other factors that influence the quality of the results calculated with Domino and associated with bulk rock composition are the amount of water in the chemical system, the presence of ferric iron (Fe^{3+}), the formation and possible escape of a melt, and chemical simplification of the system.

4.2 Water content

The amount of water added to the system plays an important role. In this study, a surplus amount of water is added for all samples excluding sample H12-G, to ensure that micas (biotite) and other H_2O-bearing phases like cordierite can form. Theriak is used to calculate the amount of water needed to saturate the system. A varying amount of water will change the stability fields of both hydrous and anhydrous minerals. The stability field of sillimanite, for example, is very sensitive to the addition of water. It becomes much smaller when a surplus amount of water is added to the system. The presence of a hydrous fluid also influences the production of a melt. For example, these rocks would

melt at lower temperatures at saturated conditions. So, if the rock was not saturated, it would probably melt at higher temperatures (that even might not have been reached during metamorphism). However, calculations with Domino do not show a significant shift in the liquidus curve when the amount of water added to the system is decreased.

4.3 Formation of melt

Petrological analyses show that the metapelitic rocks from the Hırkadağ and Kırşehir massifs record high-grade metamorphic conditions and that they are stable in the upper amphibolite and granulite facies fields. According to KFMASH petrogenic grids and pseudosections calculated with Domino, these rocks have passed the liquidus, suggesting that if metasomatic hydrous fluids moved through the rocks at these temperatures, anatexis should have taken place (Collins, 1997). In section 3.4.2 some features are described that justify the occurrence of melt, like the separation of K-feldspar + quartz (± plagioclase)-rich zones and zones rich in aluminosilicates, the well developed crystal faces at the boundary between primary garnet and secondary cordierite and the occurrence of myrmekite (plagioclase and quartz intergrowth).

The formation of myrmekite can be explained by different processes: (1) the replacement of K-feldspar by Ca- and Na-bearing fluids forming myrmekite (Collins, 1997). This indicates metasomatism and thereby an open system in which (hydrothermal) fluids (e.g. a melt) can enter the system. In this case the PT conditions are hard to determine, since the bulk composition changed in time. (2) Exsolution during cooling of primary high-temperature Na- and Ca-bearing K-feldspar, forming microcline with subsequent exsolution of Na and Ca at the rims forming myrmekite (Collins, 1997). Although I do not know which mechanism formed the myrmekite in sample K13, the infiltration of a Na- and Ca-bearing fluid phase would not only explain the formation of myrmekite, but also the occurrence of secondary plagioclase in other samples (e.g. sample H19-H) where no other Na-bearing minerals are initially present. Nevertheless, myrmekite indicates the restricted diffusion range of Al and Si, that is supported by the development of symplectitic spinel (Ashworth, 1986). These slow diffusion rates of mainly Al and Si cause the development of zones that are chemically not in equilibrium (e.g. the corona textures in sample H19-H) and that should be investigated separately for representative PT analyses.
In order to calculate the best pseudosections as possible with TheriakDomino for the high-grade metapelitic rocks, a Holland and Powell's based database (tcdb55c2d) is used that can deal with melting.

Whitney and Dilek (2001) suggested that some of the quartzofeldspathic layers may represent anatectic leucosomes, but that the origin of the K-feldspar + quartz and plagioclase + biotite + sillimanite layers is not well known. The regions that contain biotite + sillimanite + plagioclase + quartz + garnet may represent migmatic isolated zones modified by deformation (creating the gneissose structure) and recrystallised during the late HT, LP metamorphic event (Whitney and Dilek, 2001).

4.4 Simplification of the chemical system

For calculations with Domino, the most complicated system is used that can be calculated using a modern PC, since this will be closest to the real chemical system of the rock. The more complicated the system, the smaller the spaces in which stable assemblages are defined. In this study, the chemical system is simplified leaving out the elements Ti and Mn. The garnet end members used for calculating isopleths with Domino are recalculated ignoring spessartine. Spessartine makes up 1-3% of the garnet composition. Ilmenite can not be incorporated in the PT calculations when Ti is ignored. Besides ilmenite, Ti is also measured in biotite with values of 1.91-4.88 wt% TiO_2. Simplification of the chemical system will therefore influence the reliability of the results calculated with TheriakDomino.

4.5 Ferric versus ferrous iron

As stated in the Methods section, the relative proportion of ferric (trivalent) and ferrous (divalent) iron cannot be determined directly by microprobe analyses or by XRF analyses. In this study only the ferric iron content of garnet and clinopyroxene is estimated according to the analysis of Schumacher (1991) and used for end-member calculations. The other minerals have been assumed to contain ferrous iron only. In calculations with TheriakDomino all iron is assumed to be ferrous iron (Fe^{2+}), since the bulk rock composition is used as input and no difference can be made for separate minerals. In the input file for TheriakDomino, the notation O(?) is used, which means that the amount of oxygen is not given, but the programme will use the amount of oxygen that is required to charge balance the oxides that are incorporated in the calculation, assuming that $Fe_{total} = Fe^{2+}$.

4.6 Prograde – peak – retrograde path

In this study I tried to distinguish between different stages in the metamorphic evolution of the metapelitic rocks, to obtain as much information as possible about the metamorphic history of the Hırkadağ and Kırşehir massifs rather than only calculating the peak metamorphic conditions.

For PT calculations with geothermo- and geobarometers, I used groups of EMP point analyses that are assumed to reflect single stages of the metamorphic history. If garnet shows growth zoning (samples H12-G, H19-H, K4), point analyses of the garnet core in combination with inclusions of useful minerals (e.g. biotite, plagioclase) in the garnet core record prograde metamorphic conditions, while the garnet rim combined with matrix minerals provide information about peak metamorphism. Note that if the garnet has a retrograde rim (sample K4), the rim of the garnet combined with matrix minerals near the garnet rim give retrograde PT estimates and that for peak metamorphic conditions the "inner rim" (with lowest values for Fe/(Fe+Mg)) in combination with matrix minerals further away from the garnet reflect peak metamorphic conditions. In case the garnet has a homogeneous composition presumably due to high diffusion rates at elevated temperatures (sample H20-C), the mineral pairs should be chosen differently: the homogeneous core combined with matrix minerals away from the garnet (or other Fe and Mg bearing phases) give peak metamorphic conditions (peak temperatures). If the garnet has a retrograde rim (sample H20-C), this can be combined with adjacent matrix mineral analyses to obtain retrograde PT estimates. It is worth noting that for high grade rocks it is hard to suggest a prograde PT path, since the diffusion rates are high at elevated temperatures and information about the prograde part of the path is often overprinted.

In the calculation of pseudosections with TheriakDomino the differentiation between stages in metamorphism is more difficult, since the bulk rock analyses are the input for the programme and no distinction can be made between core and rim compositions. The metastable mineral assemblages that are distinguished within one sample are plotted in the pseudosection to define the area in PT space where each assemblage is stable, resulting in different areas reflecting different stages in the metamorphic history. For most samples this method worked well, but for sample K13 from the Kırşehir massif the mineral stability fields show a large overlap so no good estimates for especially pressure could have been made.

Besides, end members of key minerals can be used to limit the area in which a mineral assemblage is stable. For zoned minerals, the end members calculated for different zones within the mineral and plotted in the pseudosection as isopleths, show the change in PT conditions related to these different compositions.

4.7 Comparison of the geothermobarometers and TheriakDomino pseudosections

The pressure-temperature estimates obtained with geothermometers and geobarometers are plotted in the pseudosections calculated with Domino (figures 24-28). In general, the garnet-biotite and Ti in biotite thermometers give lower temperatures than the stability fields in the

pseudosections of Domino suggest, ranging from 60-180°C difference in peak temperatures. Sample H19-H shows the largest difference in PT results: the PT path inferred from Domino mineral stability fields shows isothermal decompression from 10 to 4 kbar at 800 °C followed by cooling to at least 680 °C. The prograde and peak PT conditions estimated with use of the garnet-biotite thermometer and GASP, GPMB-Fe and –Mg barometers show a prograde path through which the rock is heated and compressed from 526 °C at 4.1 kbar to a peak of 624 °C at 8.0 kbar. This large difference can not easily be explained. The results from Domino calculations could be interpreted in a wrong way: it is possible that the rock started at lower pressure and temperature and was heated and compressed. However, that would suggest that the metamorphic evolution of this sample is different from the other samples from the Hırkadağ massif, which is not very likely since the Hırkadağ block is relatively small and the sample locations are not separated by large fault zones. Another way to explain the differences is that sample H19-H shows relatively large corona structures with Al as the main immobile element, suggesting that the rock did not reach internal equilibrium. A pseudosection based on a bulk rock analysis without distinguishing between these different chemical zones would provide results that are not representative.

Sample K4 shows the same decompressional PT path for both the PT point calculations and the Domino pseudosection, with the difference that the path inferred from the PT points calculated with geothermobarometers is about 110 °C lower.

For samples H12-G and H20-C the points calculated with the garnet-biotite thermometer and average pressures given by GASP, GPMB-Fe and GPMB-Mg give lower temperatures, but are plotted near the PT path inferred from Domino calculations. For sample H20-C the peak temperature of >800°C inferred from the Domino pseudosection is based on the occurrence of spinel and cordierite, while these minerals are not incorporated in calculations with geothermobarometers. This yields one of the differences between the two geothermobarometric calculations: they are based on different mineral equilibria, which could explain the differences in estimated temperatures and pressures and at the same time the location of the PT points close to the inferred PT path from Domino.

The advantage of using geothermobarometers for PT calculations is that the chemical compositions determined with the electron microprobe can be used as input, providing a way to distinguish between prograde-, peak- and/or retrograde conditions. The bulk rock analyses used as input for TheriakDomino thereby form a good start for homogeneous rocks. In the case of layered or heterogeneous rocks, one should try to separate these zones to obtain different bulk compositions. This could, however, be technically impossible.

In future research the PT point calculations could be used as reference points in calculating a pseudosection with Domino, bearing in mind that the PT point calculations are based on certain mineral equilibria (e.g. the garnet-biotite mineral pair) and therefore do possibly not cover the total PT path of the rock (e.g. if cordierite and spinel suggest a higher temperature peak than garnet-biotite). One could vary the amount of water and, for example, the amount of ferric iron to obtain a pseudosection that fits best the results calculated with thermo- and barometers, remembering that the pseudosection should in the first place be consistent with the microstructural observations.

4.8 Structural/geodynamic implications

The peak assemblages of the Hırkadağ massif are associated with the main foliation that is consistent with horizontal shortening in the Dm phase (Wehrens, 2008). The retrograde conditions are most likely related to the Dm+1 phase; a phase of presumably horizontal extension (Wehrens, 2008).

The cause of the high temperature low pressure metamorphism is not well understood.

A magmatic origin of the HT LP metamorphism is debated by several authors (Whitney and Dilek, 2001). There is no clear evidence for a contact aureole in the rocks surrounding the granodiorite body in the Hırkadağ massif (Wehrens, 2008). Field relations and studies on the timing of the metamorphism indicate that magmatic events (Late Cretaceous) largely post-dated the Cretaceous peak of metamorphism (Whitney and Dilek, 2001; Köksal and Göncüoğlu, 1997; Köksal et al., 2004). It is suggested that the granodiorite intruded at high temperatures similar to the peak temperatures in the metamorphic rocks, so no contact aureole or evidence for contact metamorphism developed (Wehrens, 2008).

All samples from the Hırkadağ block and sample K4 of the Kırşehir block show (part of) a clockwise PT path. In general, a clockwise PT path is an indication of continental collision, while anticlockwise PT paths may result from magmatic heating (Vernon and Clarke, 2008). This supports the idea that peak metamorphism was related to horizontal shortening rather than lithospheric extension or the intrusion of granodiorite bodies.

A major compressional event in the evolution of the CACC was the subduction of the Neo-Tethyan Ocean in the Cretaceous. This convergence has lead to continental collision (the CACC is a continental fragment) after subduction of the oceanic crust. The continental crust could have been subducted due to drag forces exerted by the subducted dense oceanic lithosphere of the Neo-Tethys (Lin and Roecker, 1998). If the continental material of the CACC was subducted to depths of more than 100 km, the temperatures described for the Hırkadağ high grade rocks could have been reached. However, this implies high temperature high pressure metamorphism and despite a careful

search, no petrological evidence is found to show that the Hırkadağ block was ever subjected to (ultra)high pressure metamorphism, nor is there any evidence for such metamorphism documented in other parts of the CACC.

An alternative to the above described scenario is the detachment of the subducted slab. In this case, the drag of the high density oceanic subducted lithosphere on the continental crust of the CACC with a lower density might cause the downgoing slab to break off (Wortel and Spakman, 1992, 2000; Davies and Von Blanckenburg, 1995). This would cause hot buoyant asthenospheric material to fill the gap in lithosphere, metamorphosing the overlying continental crust at HT LP, still maintaining compression.

Another hypothesis for the origin of HT LP metamorphism in a compressional setting is crustal thickening of the continental crust due to collision and subsequent removal of the lithospheric root. The presence of a lithospheric root in combination with convection cells in the asthenosphere is suggested to result in the detachment of the lithospheric root by convective removal (Platt and England, 1993; Platt and Vissers, 1989). The gap in the lithosphere is filled with rising hot asthenospheric material creating conditions for high temperature low pressure metamorphism of the overlying crust.

Similar to the Hırkadağ and Kırşehir massifs, LP-HT effects are recorded elsewhere in the CACC: in the Akdağ massif, throughout the Aksaray block and in the high grade rocks of the Niğde core complex (Whitney and Dilek, 2001; Whitney et al., 2001; Whitney and Dilek, 2000). This calls for a regional cause of the HT LP metamorphic event rather than local heating of the two massifs studied here. A conceivable hypothesis for the common origin of HT LP metamorphism based on structural data of Wehrens (2008) and discussions with Lefebvre (PhD, Utrecht University) is that the different metamorphic massifs as seen today possibly have been one large scale metamorphic core complex, later separated by fault zones that displaced and rotated the different complexes. The overall structure and geometry of the different metamorphic massifs are similar: the cores of the massifs are made up of metamorphic rocks, whilst magmatic or volcanic rocks (granite, syenite) occur at the side(s). Ophiolites are found in between the metamorphic and volcanic rocks, often associated with the igneous rocks. In the Hırkadağ massif evidence is found for the existence of a detachment fault (low angle extensional fault with both brittle and ductile deformation at the contact between the metamorphic rocks and the sediments) along which the metamorphic rock could have been brought to the surface. The occurrence of a metamorphic core complex in the CACC has been earlier described. Whitney and Dilek (1997 and 1998) identified the Niğde massif in the south of the CACC as a metamorphic core complex that developed during Alpine collision and subsequent extension in the hanging wall of a north-dipping subduction zone. Paleomagnetic studies are currently carried

out by Lefebvre (PhD, Utrecht University) and these could provide more information about the original setting of the metamorphic massifs in the CACC and a possible shared metamorphic evolution and cause of HT LP metamorphism.

5. Geochronology

At the onset of this research, it was planned to study the geochronology of the metapelitic rocks by monazite U-Th-Pb age dating. Monazite can be present in both igneous, metamorphic and sedimentary rocks. Monazites in metamorphic rocks form at temperatures exceeding 680 °C (Williams et al., 2007). Diffusion rates of many elements in monazites are slow, implying that the monazite can retain a record of previous geologic conditions (Williams et al., 2007). The basic assumption for monazite dating is that all lead (Pb) in the monazite is the result of radioactive decay of uranium (^{238}U, ^{235}U) and thorium (^{232}Th) and that there is no loss of Pb to other minerals. The crystals typically contain separate compositional domains that represent successive generations of monazite, which can be used to distinguish between different stages in the geological history.
The monazite U-Pb ages were expected to reflect the time that the monazites and metamorphic minerals grew or crystallized (given by the cooling age; Pyle and Spear, 2003). Some of the monazites in the samples from the Hırkadağ and Kırşehir massifs are zoned (figure 30) due to polyphase metamorphism and could therefore possibly provide ages of different metamorphic stages.
However, detection limits of the electron microprobe at Utrecht University precludes to measure significant amounts of Pb. This may be due to the age of the high-temperature event. Normally, ages can be determined with the monazite U-Pb method for rocks older than 100 million years. It follows that no ages could be determined for the metamorphism in the Hırkadağ and Kırşehir massifs, as the metapelitic rocks were metamorphosed in Cretaceous times (<100 Ma).

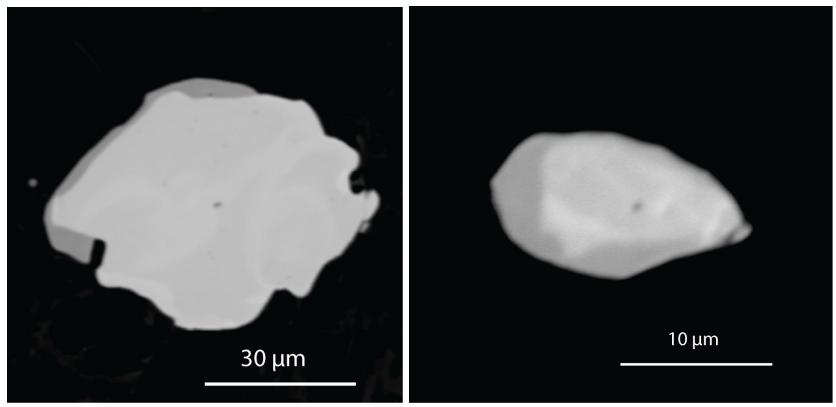

Figure 30. *BSE images of zoned monazites from a) sample H19-H from the Hırkadağ massif and b) sample K4 from the Kırşehir massif.*

6. Conclusions

The garnet-sillimanite schists from both the Hırkadağ and Kırşehir massifs preserved peak temperature conditions and remnants of the prograde metamorphic conditions. We distinguish two metastable mineral assemblages: (1) garnet + biotite + sillimanite ± quartz + feldspar + ilmenite and (2) spinel ±cordierite + feldspar + quartz + ilmenite. Microstructural relationships show that the first assemblage is replaced by the second assemblage (grt → crd; sil → spl). The two assemblages can be linked in a clockwise PT path. The peak temperature conditions are less well preserved in the biotite-clinopyroxene schists without garnet from the northeastern part of the Kırşehir massif.

The inferred PT paths calculated with TheriakDomino for the Hırkadağ and Kırşehir samples show peak temperatures of 800 °C for the Hırkadağ massif and lower peak temperatures (~700 °C) for the Kırşehir massif. The peak metamorphic conditions calculated with the garnet-biotite and Ti-in-biotite thermometers and GASP and GPMB barometers show lower peak temperatures: 620-740 °C at about 8 kbar for the Hırkadağ massif and 620 °C at 6 kbar for the Kırşehir massif. The estimated peak metamorphic conditions are the highest in cordierite-bearing samples.

Both massifs have experienced approximately isothermal decompression. The samples from the Hırkadağ massif show decompression from ~9.5 kbar to 4 kbar and even 3 kbar (for the replacement of garnet by cordierite) at temperatures of 800 °C. The Kırşehir massif experienced decompression from about 8 kbar down to 5 kbar at 700 °C. The imprint of high-temperature, low pressure metamorphism is most clearly visible in the Hırkadağ massif.

The presence of a melt as inferred by the high-temperature low-pressure metamorphic conditions and shown in TheriakDomino pseudosections is supported by microstructural relationships.

No ages could be determined with monazite U-Pb dating for the metamorphism in the Hırkadağ and Kırşehir massifs, as the metapelitic rocks were metamorphosed in Cretaceous times (<100 Ma), i.e. too recent to yield significant amounts of radiogenic Pb could be measured.

The inferred HT/LP history calls for an anomalous hot thermal state of the pertinent crust. This may be consistent with lithospheric models in which hot asthenosphere can reach lower crustal levels, such as slab breakoff or the removal of a gravitationally unstable thickened lithospheric root.

Acknowledgements

Dear Côme (C.J.C. Lefebvre)! Thank you very much for the good discussions about metamorphism, the teamwork during programming and stimulation when times seemed hard. Your advise when I had to prepare a presentation or poster was very useful. Thanks also for introducing me in the field and to the Turkish people. You really helped me finishing this thesis!

Reinoud (Prof. Dr. R.L.M.) Vissers, I would like to thank you for the opportunity to do this challenging MSc project! It feels like an honour to do part of the metamorphic work in this large scale project. Thanks for your supervision. Your work in and knowledge and very good teaching about orogens inspired me to specialise in this field of geology.

Thanks also to Douwe (Dr. D.J.J.) van Hinsbergen for making this project possible.

Philip (P.C. Wehrens), thank you for the teamwork during the last years of my MSc study and providing the samples from the Hırkadağ area! It was nice to discuss the deformation and metamorphism of the area and helping each other with our final projects.

Fraukje (Dr. F.M. Brouwer) thank you very much for your indispensable and crucial advise about the PT calculations with TheriakDomino! I am surprised and very grateful that you always found time for discussions, helpful answers about my questions and your enthusiasm!

I would also like to thank:

Herman van Roermund for his introduction to and help with the microprobe.

Tilly Bouten for her technical support with the microprobe analyses.

Hans de Bresser for reviewing the thesis.

Molengraaff fonds for the financial support.

Auke Barnhoorn for his stimulation and practical help and my roommates Veronique, Annelies, Yvonne, Maartje, Renske and Karen for the pleasant time and tea!

Dear Sander, thank you for your never ending support!

References

Akiman, O., Erler, A., Göncüoğlu, M.C., Gülec, N., Geven, A., Türeli, T.K. and Kadioğlu, Y.K., 1993. Geochemical characteristics of granitoids along the western margin of the Central Anatolian Crystalline Complex and their tectonic implications. Geological Journa; , vol. 28, p. 371-382.

Ashworth, J.R., 1986. Myrmekite replacing albite in prograde metamorphism. American Mineralogist, vol. 71, p. 895-899.

Berman, R.G., 1988. Internally-consistent thermodynamic data for minerals in the system Na2O – K2O – TiO2 – H2O – CO2. Journal of Petrology, vol. 29, p. 445-522.

Bohlen, S.R. and J.J. Liotta, 1986. A barometer for garnet amphibolites and garnet granulites. J.Petrol., vol. 27, p. 1025-1034.

Bhattacharya, A., Mazumdar, A.C. and Sen, S.K., 1988 Fe-Mg mixing in cordierite: constraints from natural data and implications for cordierite-garnet thermometry in granulites. American Mineralogist, vol. 73, p. 338-344.

Bhattacharya, A., Mohanty, L., Maji, A., Sen, S.K. and Raith, M., 1992. Non-ideal mixing of the phlogopite-annite binary; constraints from experimental data on Mg-Fe partitioning and a reformulation of the biotite-garnet geothermometer. Contrib. Mineral. Petrol., vol. 111, p. 87-93.

Blatt, H., Tracy, R.J., and Owens, B.E., 2006, Petrology Igneous, Sedimentary, and Metamorphic: New York, W.H. Freeman and Company, 530 p.

Brandelik, A., Massonne, H.-J., 2004. PTGIBBS-an EXCEL^{TM} Visual basic program for computing and visualizing thermodynamic functions and equilibria of rock-forming minerals. Computer and Geosciences, vol. 30, p. 909-923.

Brouwer, F.M., 2000. Thermal evolution of high-pressure metamorphic rocks in the Alps. Geologica Ultraiectina, Mededelingen van de Faculteit Aardwetenschappen, Universiteit Utrecht, No. 199, *proefschrift*.

Bucher, K. and Frey, M., 2002. Petrogenesis of metamorphic rocks. Springer-Verlag, Berlin, Germany.

Clarke, G.L. and Powell, R., 1991. Decompressional coronas and symplectites in granulites of the Musgrave Complex, central Australia. Journal of Metamorphic Geology, vol. 9, 441-450.

DeCapitani, C., 1994. Gleichgewichts-Phasendiagramme: theorie und Software. Eur. J. Mineral., vol. 6.

Davies, J.H. and Von Blanckenburg, F., 1995. Slab breakoff: a model of lithosphere detachment and its test in the magmatism and deformation of collisional orogens. Earth and Planetary Science Letters, vol. 129, p. 85-102.

Dempster, T.J., 1985. Garnet zoning and metamorphism of the Barrovian type area, Scotland. Contrib. Mineral Petrol., vol. 89, p. 30-38.

Dilek, Y., Whitney, D.L. and Tekeli, O., 1999. Links between neotectonic processes and landscape evolution in an Alpine collision zone, south-central Turkey. Geomorphology, vol. 118, p. 147-164.

Droop, G.T.R., 1987. A general equation for estimating Fe^{3+} concentrations in ferromagnesian silicates and oxides from microprobe analyses, using stoichiometric criteria.

England, P. and Thompson, A.B., 1984. Pressure-temperature time paths of regional metamorphism I. Heat transfer during the evolution of regions of thickened continental crust. Journal of Petrology, vol. 25, p. 894-928.

Fayon, A.K., Whitney, D.L., Teyssier, C., Garver, J.I. and Dilek, Y., 2001. Effects of plate convergence obliquity on timing and mechanisms of exhumation of a mid-crustal terrain, the Central Anatolian Crystalline Complex. Earth and Planetary science letters, vol., 192, p. 191-205.

Gautier, P.E., Bozkurt, E., Bosse, V., Hallot, E. And Dirik, K., 2008. Coeval extensional shearing and lateral underflow during Late Cretaceous core complex development in the Niğde Massif, Central Anatolia, Turkey. Tectonics, vol, 27.

Göncüoğlu, M.C., 1977. Geologie des westlichen Niğde massives. PhD thesis, University of Bonn, Germany [unpublished].
Henry, D. J., Guidotti, C. V. and Thomson, J. A., 2005. The Ti-saturation surface for low-to-medium pressure metapelitic biotite: Implications for Geothermometry and Ti-substitution Mechanisms. American Mineralogist, vol. 90, p. 316-328.
Holland, T.J.B. and Powell, R., 1998. An internally-consistent thermodynamic dataset for phases of petrological interest. Journal of Metamorphic Geology, vol. 16, p. 309-344.
Keller, L.M., Abart, R., Stünitz, H. and De Capitani, C., 2004. Deformation, mass transfer and mineral reactions in an eclogite facies shear zone in a polymetamorphic metapelite (Monte Rosa nappe, western Alps). Journal of Petrology, vol. 22, p. 97-118.
Kelsey, D.E., Powell, R., Wilson, C.J.L. and Steele, D.A., 2003. (Th-U)-Pb monazite ages from Al-Mg-rich metapelites, Rauer group, east Antarctica. Contrib. Mineral. Petrol., vol. 146, p. 326-340.
Köksal, S. and Göncüoğlu, M.C., 1997. Geology of the Ĭdış Dağı – Avanos area (Nevşehir – Central Anatolia). Mineral Resource Exploration Bulletin, vol. 119, p. 41-58.
Köksal, S., Romer, R.L., Göncüoğlu, M.C. and Toksoy-Köksal, F., 2004. Timing of post-collisional H-type to A-type granitic magmatism: U-Pb titanite ages from the Alpine central Anatolian granitoids (Turkey). International Journal of Earth Sciences, vol. 93, p. 974-989.
Kretz, R., 1983. Symbols for rock-forming minerals. Am. Mineral., vol. 68, p. 277-279.
Lin, C.H. and Roecker, S.W., 1998. Active crustal subduction and exhumation in Taiwan when continents collide: geodynamics and geochemistry of ultrahigh-pressure rocks.
Okay, A.I. and Tüysüz, O., 1999. Eastern Mediterranean Tethyan sutures of northern Turkey. Geological society, vol., 156, p. 475-515.
MacKenzie, W.S., Adams, A.E., 2003. A colour atlas of rocks and minerals in thin section. Manson Publishing Ltd, London.
Mora, C.I. and Valley, J.W., 1985. Ternary feldspar thermometry in granulites from the Oaxacan Complex, Mexico. Contrib Mineral Petrol., vol. 89, p. 215-225.
Morimoto, N., Fabries, J., Ferguson, A.K., Ginzburg, I.V., Ross, M., Seifert, F.A. and Zussman, J., 1988. Nomenclature of pyroxenes. American Mineralogist, vol. 73, p. 1123-1133.
Patiño Douce et al., 1993. Octahedral excess mixing properties in biotite: A working model with applications to geobarometry and geothermometry. American Mineralogist, vol. 78, p. 113-131.
Platt, J.P., and Vissers, R.L.M., 1989. Extensional collapse of thickened continental lithosphere: a working hypothesis for the Alboran Sea and Gibraltar Arc. Geology, vol. 17, p. 540-543.
Platt, J.P. and England, P.C., 1993. Convective removal of lithosphere beneath mountain belts: thermal and mechanical consequences. American Journal of Science, vol. 293, p. 307-336.
Pyle, J.M., Spear, F.S., 2003. Four generations of accessory-phase growth in low-pressure migmatites from SW New Hampshire. Am. Mineral., vol. 88, p. 338–51.
Schumacher, J.C., 1991. Empirical ferric iron corrections: necessity, assumptions and effects on selected geothermobarometers. Mineral. Mag., vol. 55, p. 3-18.
Seymen, I., 1981. Stratigraphy and metamorphism of the Kırşehir massif around Kaman (Kırşehir – Turkey). M.T.A. Bulletin, vol. 24, p. 7-14.
Shulters, J.C. and Bohlen, S.R., 1989. The atability of hercynite and hercynite-gahnite spinels in corundum- or quartz-bearing assemblages. J. Petrol., vol. 22, p. 41-84.
Spear, F.S. and Peacock, S.M., 1989. Metamorphic Pressure-Temperature-time paths. Short course presented at the 28th International Geological Congress Washington, USA.
Spear, F.S., 1993. Metamorphic phase equilibria and pressure-temperature-time paths. Mineralogical Society of America, Washington, D.C.
Teklehaimanot, L.T., 1993. Geology and petrography of Gülşehir area, Nevşehir, Turkey. MSc thesis, Middle East Technical University, Ankara, Turkey [unpublished].
Todd, C.S., 1998. Limits on the precision of geobarometry at low grossular and anorthite content. Am. Mineral., vol. 83, p. 1161-1167.

Vernon, R.H. and Clarke, G.C., 2008. Principles of Metamorphic Petrology. Cambridge University Press, UK.
Wehrens, P.C., 2008. Structural evolution of the Hırkadağ massif, Central Anatolian Crystalline Complex, Turkey. MSc thesis, University of Utrecht, The Netherlands [unpublished].
White, R.W., Powell, R., Holland, J.B., 2007. Progress relating to calculation of partial melting equilibria for metapelites. J. metamorphic Geology, vol. 25, p. 511-527.
Whitney, D.L. and Dilek, Y., 1997. Core complex development in central Anatolia. Geology, vol. 25, p. 1023-1026.
Whitney, D.L., and Dilek, Y., 1998. Metamorphism during Alpine crustal thickening and extension in Central Anatolia, Turkey: the Niğde Metamorphic core complex. Journal of Petrology, vol. 39, p. 1385-1403.
Whitney, D.L. and Dilek, Y., 2000. Andalusite – sillimanite – quartz veins as indicators of low-pressure – high-temperature deformation during late-stage unroofing of an metamorphic core complex, Turkey. Journal of Metamorphic Geology, vol. 18, p. 59-66.
Whitney, D.L. and Dilek, Y., 2001. Metamorphic and tectonic evolution of the Hırkadağ block, Central Anatolian Crystalline Complex. Turkish Journal of Earth Sciences, vol. 10, p. 1-15.
Whitney, D.L., Dilek, Y. and Fayon, A.K., 2001. Metamorphism of the Central Anatolian Crystalline Complex, Turkey: influence of orogen-normal collision vs. wrench-dominated tectonics on P-T-t paths. Journal of the Geological Society, vol., 19, p. 411-432.
Whitney, D.L., Teyssier, C., Fayon, A.K., Hamilton, M.A. and Heizler, M.H., 2003. Tectonic controls on metamorphism, partial melting, and intrusion: timing and duration of regional metamorphism and magmatism in the Niğde Massif, Turkey. Tectonophysics, vol., 376, p. 37-60.
Whitney, D.L. and M.A. Hamilton, 2004. Timing of high-grade metamorphism in central Turkey and the assembly of Anatolia. Journal of the Geological Society, vol. 161, p. 823-828.
Williams, M.L., Jercinovic, M.J., Hetherington, C.J., 2007. Microprobe monazite geochronology: understanding geologic processes by integrating composition and chronology. Annual Review of Earth and Planetary Sciences, vol. 35, p. 137-175.
Winter, J.D., 2001. An introduction to igneous and metamorphic petrology. Prentice-Hall Inc., Upper Saddle River, New Jersey, USA.
Wortel, M.J.R. and Spakman, W., 1992. Structure and dynamics of subducted lithosphere in the Mediterranean region: Proceedings. Koninklijke Nederlandse Academie van Wetenschappen, vol. 95, p. 325-347.
Wortel, M.J.R. and Spakman, W., 2000. Subduction and slab detachment in the Mediterranean-Carpathian region. Science, vol. 290, p. 1910-1917.

Internet

- Personal site of Dave Waters
  www.earth.ox.ac.uk/~davewa/pt/index.html
- Dex Perkins, University of North Dakota; Andrea Koziol, University of Dayton; and Dave Mogk, Montana State University Webpage for integrating research and education. Teaching phase equilibria. Based on personal site of Dave Waters (mentioned above) and Spear, 1993.
  http://serc.carleton.edu/research_education/equilibria/index.html
- Personal site of Collins (1997)
  http://www.csun.edu/~vcgeo005

Appendices

1. UTM coordinates of the Kırşehir samples
2. Activity models
3. Introduction to the practical aspects of TheriakDomino
4. Overview pictures of thin sections
5. BSE images of analysis spots
6. Mineral abbreviations
7. Hand specimen of samples selected for PT analyses
8. Representative mineral analyses

APPENDIX 1

UTM coordinates of sample locations in the Kırşehir massif.

Sample	UTM longitude	UTM latitude	Altitude (m)
K4	3650577439	4349420	1538
K11, K12, K13	3650600712	4373190	1097
K21	3650578004	4353264	1257

APPENDIX 2.

Activity models

The calculation of mineral equilibria in order to determine pressure and temperature conditions requires an understanding not only of the end member properties of the minerals of interest, but also of the activity-composition (a-X) relationships for every phase involved (White et al., 2007). The thermodynamic properties of the end members of many minerals are relatively well constrained, especially those that are stable in their pure form, the a-X relationships on the other hand are less well known.

For most types of thermodynamic calculation it is useful to define a standard state in a way that the thermodynamic quantity chemical potential of a phase (μ_i) (the reactive energy) can be divided into two parts: the standard state part and a "real" part. The chemical potential is expressed by the formula:

$$\mu_i=\mu^o{}_i+RT\ln a_i^j$$

The "real" part of the chemical potential depends on the activity (a_i^j) of the component i in the phase j. The activity is a value that describes how reactive a particular end member component is for a given mineral composition (Perkins, Koziol and Mogk, 2007). If a mineral is pure, the corresponding activity is 1. The activity of an end member in an impure phase is always smaller than 1 and will be related to its mole fraction and can be thought of as the composition correction to the free energy (Waters, updated 2004). Activity depends not only on composition, but also on pressure and temperature.

The formulation of the activity of a component in a phase requires a model for the behaviour of the real material, a so called activity model (Spear, 1993). In order to make any thermodynamic calculations it is necessary to have an activity model that relates the composition of the phase (which is a measurable quantity) to its thermodynamic quantities.

Activity models can be subdivided into molecular models in which mixing occur between entire formula units and ionic models that assume that cations mix over individual crystallographic sites in a mineral structure (Spear, 1993). For the following, ionic mixing models are described.

Besides, a distinction should be made between ideal and non-ideal behaviour of minerals. Although some mineral solutions have close to ideal activities, most minerals exhibit non-ideal mixing because of interactions between elements in different crystallographic sites that affect the ability of the components to react in the system (Perkins, Koziol and Mogk, 2007).

Ideal activity models

Ideal mixing can be described as there is no enthalpy of mixing, and the free energy of mixing is determined only by the configurational entropy of mixing. In an ideal solution with mixing on one site only, the activity is simply equal to the mole fraction: $a_i^j = X_i^j$.

Besides mixing on one site, there are crystalline solids with two distinct crystallographic sites on which mixing occurs. Assuming that the mixing on each site is random and independent of the occupancy in the other type of site, a mineral can be considered with the general formula $(A,B)_\alpha(Y,Z)_\beta$ (in this case there are four possible end members) for which the activity of the end member $A_\alpha Y_\beta$ is given by:

$$a_{A\alpha Y\beta}=(X_A)^\alpha(X_Y)^\beta$$

where X_A and X_Y are the mole fractions of cations A and B on respectively the first and second site. An example for this mixing model is garnet with the general formula $(Mg,Fe,Mn,Ca)_3(Al,Fe^{3+})_2Si_3O_{12}$. The activity of the end member pyrope $Mg_3Al_2Si_3O_{12}$ is given by:

$$a_{prp}=(X_{Mg})^3(X_{Al})^2$$

The models discussed above assume that cation mixing is random on all sites. However, in some minerals cation exchanges are coupled. This coupling occurs in order to maintain local charge balance. For example, the substitution of an Al^{3+} atom for a Mg^{2+} atom creates a local charge excess

of 1. This can be compensated by substitution of an Al^{3+} atom for a Si^{4+} atom (the so called tschermak's substitution). In this study, activity models are available for minerals with coupled cation exchange. For details about this method the reader is referred to Spear, 1993.

Non-ideal activity models

In the case of non-ideal mixing, the non-ideal behaviour should be corrected by applying an activity coefficient γ_i in the way that $a_i = \gamma_i X_i$ (mixing on one site) where X_i^j is the mole fraction of component i in phase j (Spear, 1993; Water, 2004; Perkins, Koziol and Mogk, 2007). The activity coefficient γ_i is a function of pressure and temperature as well as composition. Generally, γ_i approaches 1 (ideal mixing) at increasing temperatures and decreasing pressures and as the mole fraction X_i is close to 1. For mixing on more than one crystallographic site, there is an activity coefficient for each site and the coefficient is raised to the power of the site multiplicity, i.e. for the generalized mineral with formula $(A,B)_\alpha(Y,Z)_\beta$ (Spear, 1993):

$$a_{A\alpha Y\beta}=(X_A\gamma_A)^\alpha(X_Y\gamma_Y)^\beta$$

In the case of non-ideal mixing, an appropriate functional relation for γ should be found. The most common approach is to consider that a non-ideal solution has a non-ideal Gibbs free energy (G), involving an ideal and a non-ideal or excess part:

$$G_{solid\ solution} = G_{ideal} + G_{excess}$$

where the excess part is calculated using an activity model.

A relatively simple activity model is to assume that the excess energy is distributed symmetrically. In this case the excess energy can be calculated with

$$G_{excess} = W_G X_1(1-X_1)$$

where X_1 is the mole fraction of one of the end members and W_G (J/mol) is the interchange energy or the Margules parameter (Perkins, Koziol and Mogk, 2007). For a single site crystal, the activity coefficient can be expressed by:

$$\gamma_i=\exp[((1-X_i)^2W_G)/\alpha RT(K)]$$

where X_i is the mole fraction of cation I, W_G is the Margules parameter, α is the site multiplicity and R is the gas constant.

However, for many geological materials, the symmetric model does not adequately represent the free energy of the solution, and an asymmetric model is used instead:

$$G_{excess} = X_1X_2(W_{G1}X_2 + W_{G2}X_1) \quad \text{(binary solution with components 1 and 2)}$$

The activity coefficients can be determined with:

$$\gamma_1=[(X_2^2[W_{G12}+2(W_{G21}-W_{G12})X_1])/(\alpha RT)]$$

$$\gamma_2=[(X_1^2[W_{G21}+2(W_{G12}-W_{G21})X_2])/(\alpha RT)]$$

In this study, ideal mixing behaviour is assumed for (almost) pure phases like sillimanite and ilmenite and a symmetric non-ideal activity model has been used for the minerals spinel and cordierite in order to obtain a more realistic activity. For the other minerals that are important for the calculation of pressure and temperature conditions, solid solution models are incorporated in the PT-program package PTGIBBS (Brandelik and Massonne, 2004).

Although the models used are simplified (e.g. no asymmetrical activity models are used), they are expected to extrapolate better than the more complicated models. Natural minerals are more complex than experimentally investigated equivalents and errors within the extrapolation process are avoided by using simplified models.

APPENDIX 3

How to use Domino and Theriak for your bulk rock (XRF) to obtain constraints about PT conditions?
Based on a meeting with Fraukje Brouwer and Côme Lefebvre 3/2/2010 at the VU

- Define the (stable **mineral assemblage(s)** of your rock. Which elements do you really need? Use the most complicated system that can be calculated with your computer, since this is the closest to the real chemical system of your rock. The more complicated the system, the smaller the spaces in which stable assemblages are defined.
- Recalculate the **wt% of oxides to cations** (you can use both cation proportions and cations p.f.u., since the proportions remain the same). Cations can be multiplied by 1000 to make them more legible. Use values without decimals (so simplify).
- When you simplify the system by taking out some elements (e.g. Mn), you do not have to **renormalize** the remaining oxides to 100% (proportions are the same).
- Check in the **database** which end members and solution models (the way end members interact) are incorporated for your minerals. E.g. most databases do not have a Mn-end member for garnet (spessartine). That is no problem as long as you know that the amount of Mn in your garnet is not significant (see EMP analyses). Another example: the programme might put all the Ti that is given in titanite and ignores that that this element can also be present in biotite. Again: if the amount of Ti in other minerals is low, this is no problem. Note that your results are restricted by the database you use.
- In the input file THERIN.txt: use the notation **O(?)** instead of a value for the amount of oxygen. This is done, because the amount of Fe2+ and Fe3+ is hard to identify. XRF analyses (and analyses with the EMP) cannot distinguish between ferric (3+) and ferrous (2+) iron. The Fe2+ and Fe3+ ratio can be calculated, for example based on charge balance, but in this case the charge balance could also be affected by other elements than Fe only. The notation O(?) means that the programme will take the amount of oxygen that is required to "complete" the oxides that are incorporated in the calculation, assuming that all iron is Fe2+.
- Note: it is possible that the XRF analyses are given in **Fe_2O_3**. The apparatus measures the element Fe2+, but then it is recalculated to an oxide, in this case Fe_2O_3. That does not mean that $Fe_{tot}=Fe^{3+}$, actually $Fe_{tot}=Fe^{2+}$. So you have to recalculate the wt% of Fe_2O_3 to wt% of FeO (use the steps for calculating cation proportions, but in reversed order).
- Decide how much **water** you would add to the your system. Almost all systems have an excess of water. Try different amounts of water and look how much of a hydrous phase is formed (with Theriak) and compare that to your thin section. E.g. you have an amount of 5 vol% biotite in your thin section, use Theriak (that also gives vol% of all minerals that are stable at a given P and T) to find the amount of water you need to produce 5 vol% of biotite. If free water is produced, you know for sure that the equilibrium area of the hydrous mineral is not affected by the water you added to the system any more. (To define the prograde part of the path, use an excess of water. For the retrograde part this is more complicated, because it is possible that no water entered the system when it was on its retrograde path.) It is also possible to calculate a T-X(H_2O) diagram with use of Domino.
- **Equilibrium area** that you choose in the pseudosection calculated with Domino is primarily based on textural observations. Always go back to your rock/thin section to find the calculated solution that is most consistent with reality.
- To distinguish between different **stages in the metamorphic evolution** of your rock, use the end members of minerals that belong to the equilibrium assemblages (e.g. take garnet core with inclusions for prograde path and garnet rim with matrix minerals for peak T) and plot isolines in your pseudosection. With help of these isopleths, you are possibly able to find the location in an equilibrium area that corresponds to a certain part of your PT path. Note that if you have simplified the system by omitting one or more elements (e.g. Mn), you have to recalculate the end members from the EMP analyses by ignoring the same elements. E.g. if Mn isignored, than you have to recalculate the end members of garnet to 100% by leaving out spessartine.
- **Notation** for a system: often TiCNKFMASH. No strict rules for the order of the elements.

APPENDIX 4

Overview of thin sections and analyses spots

Sample H12-G

Photograph of thin section of sample H12-G. Locations of EMP analyses on garnets are indicated with blue boxes.

Sample H19-H

Photograph of thin section of sample H19-H. Locations of EMP analyses on garnets (19G1 and 19G2) and on the garnet polymorph (19P) are indicated with blue boxes.

Sample H20-C100

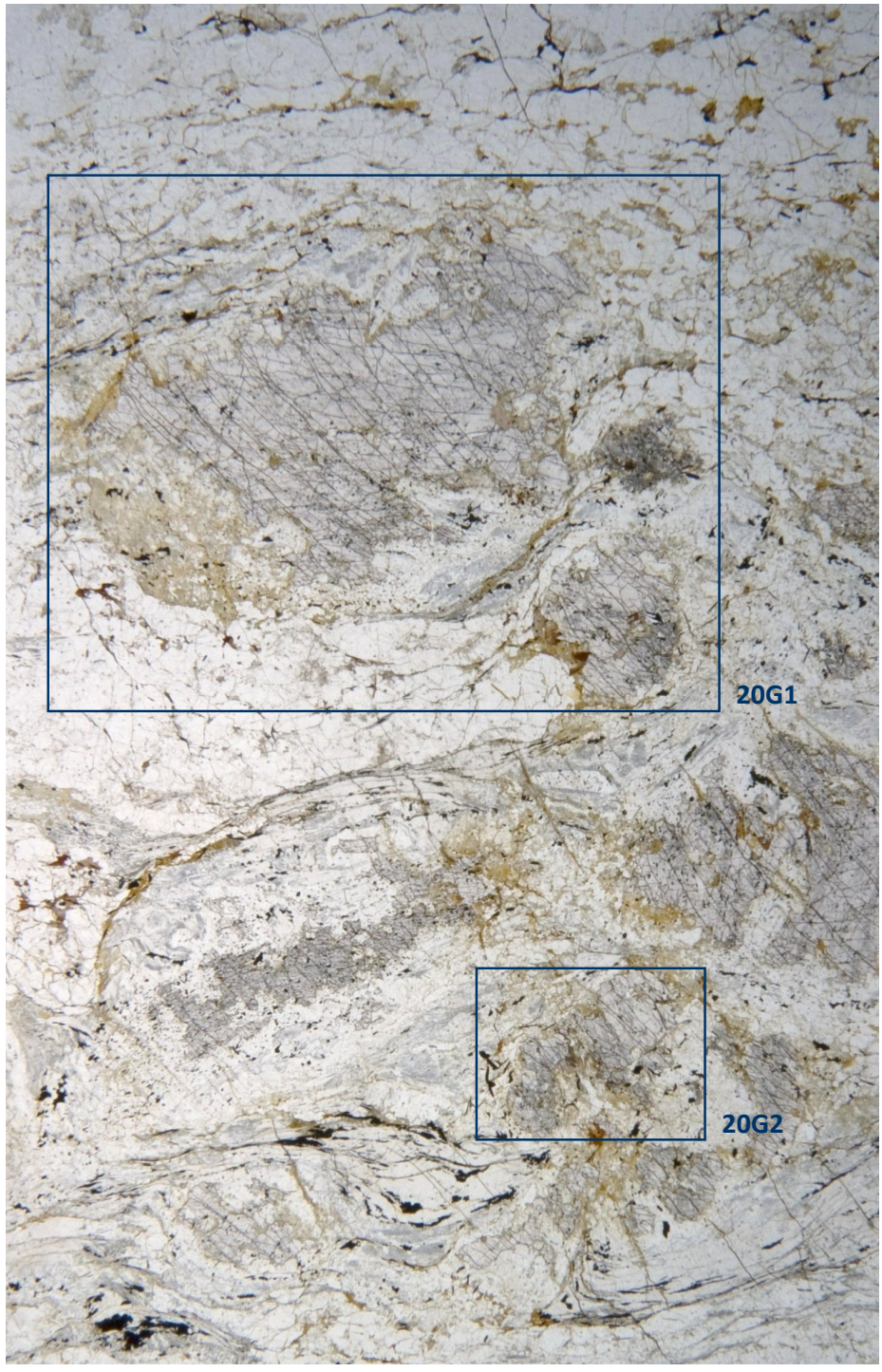

Photograph of thin section of sample H20-C. Locations of EMP analyses on garnets are indicated with blue boxes.

Sample K4

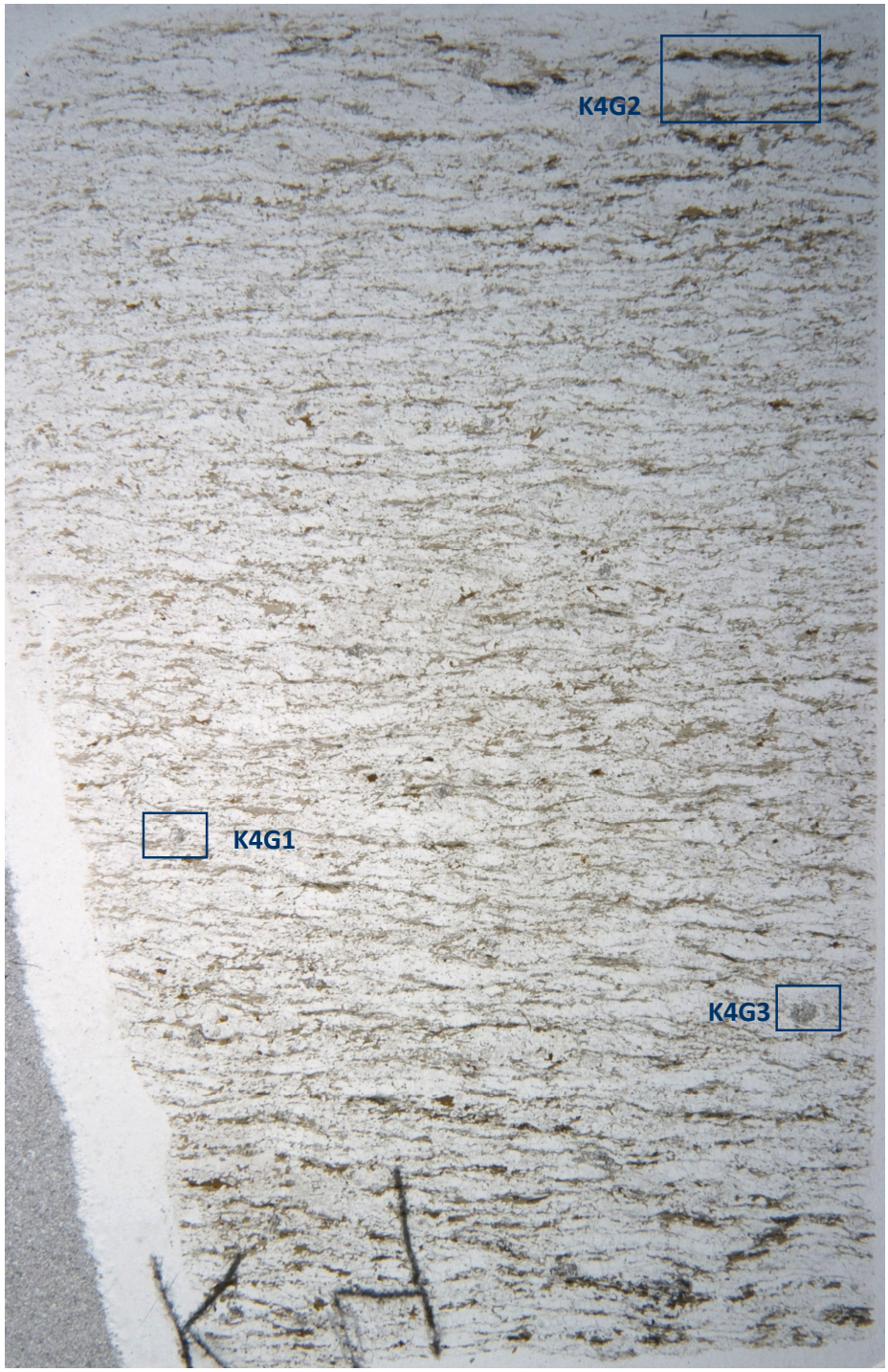

Photograph of thin section of sample K4. Locations of EMP analyses on garnets are indicated with blue boxes.

Sample K13

Photograph of thin section of sample K13. Locations of EMP analyses on clinopyroxeen-rich zones (cpx1), biotite-rich zones (bt1 and -2) and K-feldspar + myrmekite (Kfs 1 and 2) are indicated with blue boxes.

APPENDIX 5

BSE images of the locations of garnet zoning profiles

Sample H12-G

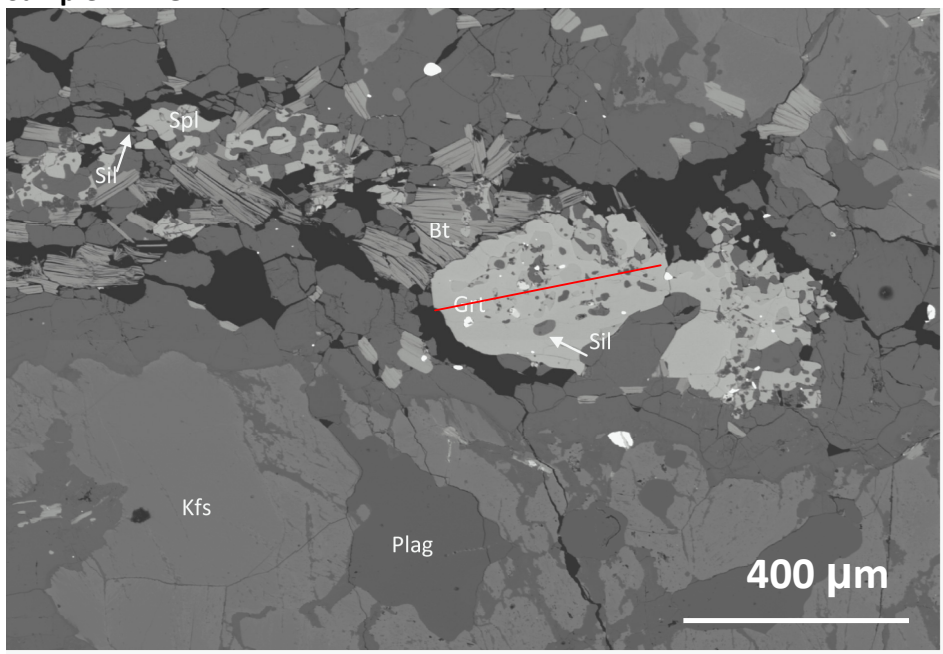

Backscattered electron (BSE) image of location **12G1** in sample H12-G. The position of the zoning profile through garnet is indicated with a red line.

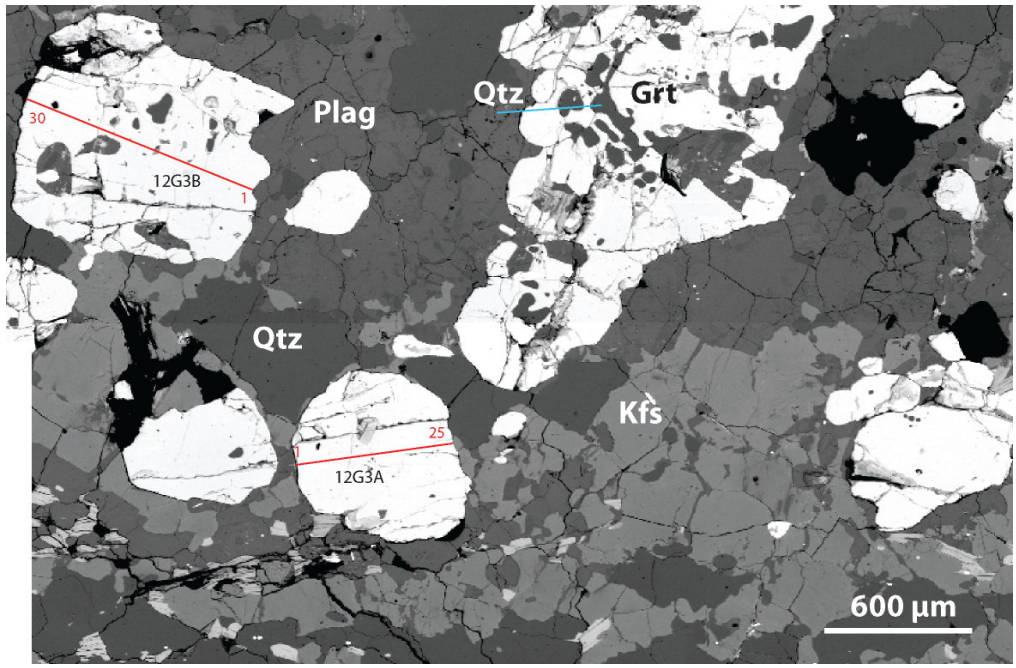

BSE image of location **12G3** in sample H12-G. The position of the zoning profiles through garnet are indicated with red lines.

Sample H19-H

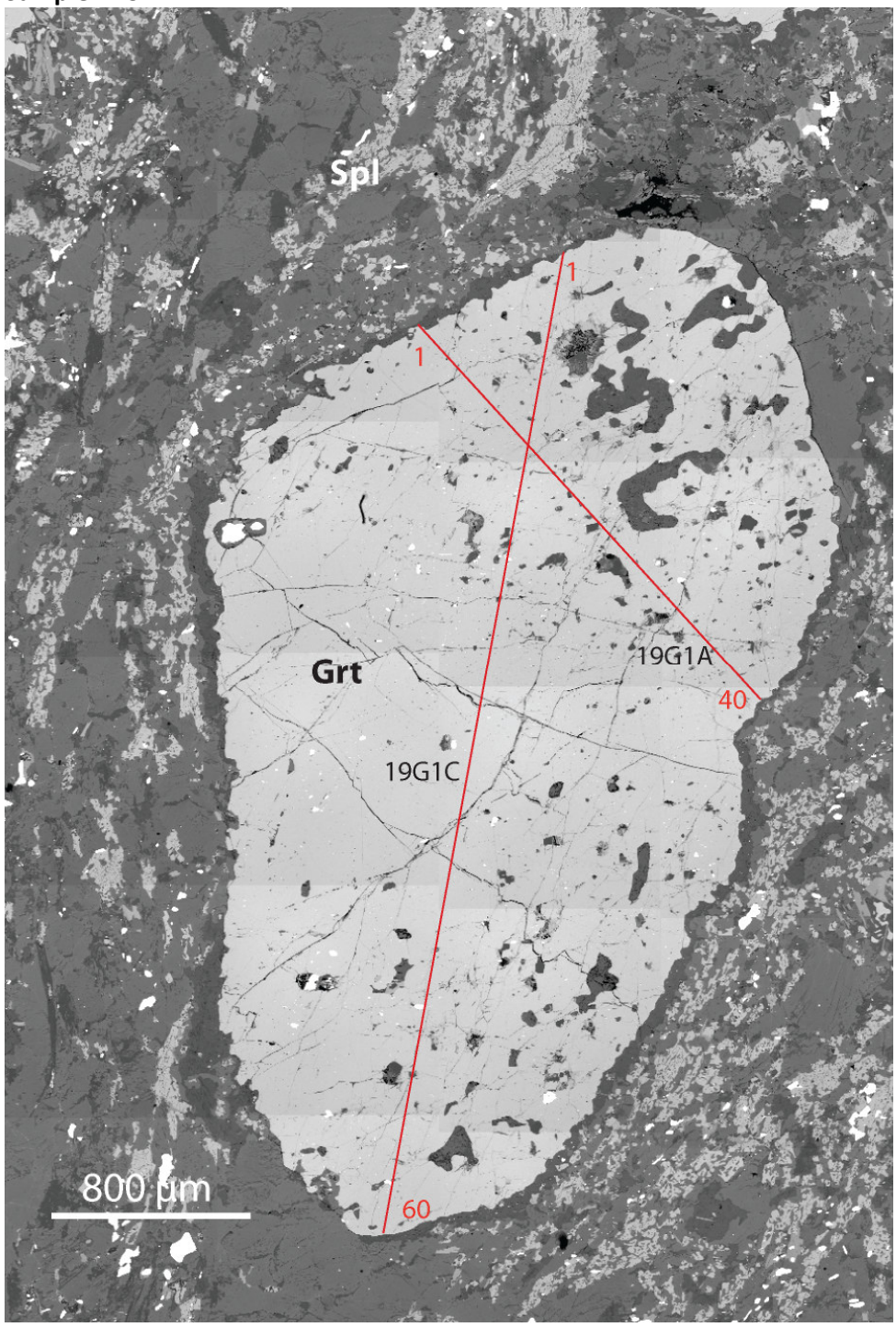

BSE image of location **19G1** in sample H19-H. The position of the zoning profiles through garnet are indicated with red lines.

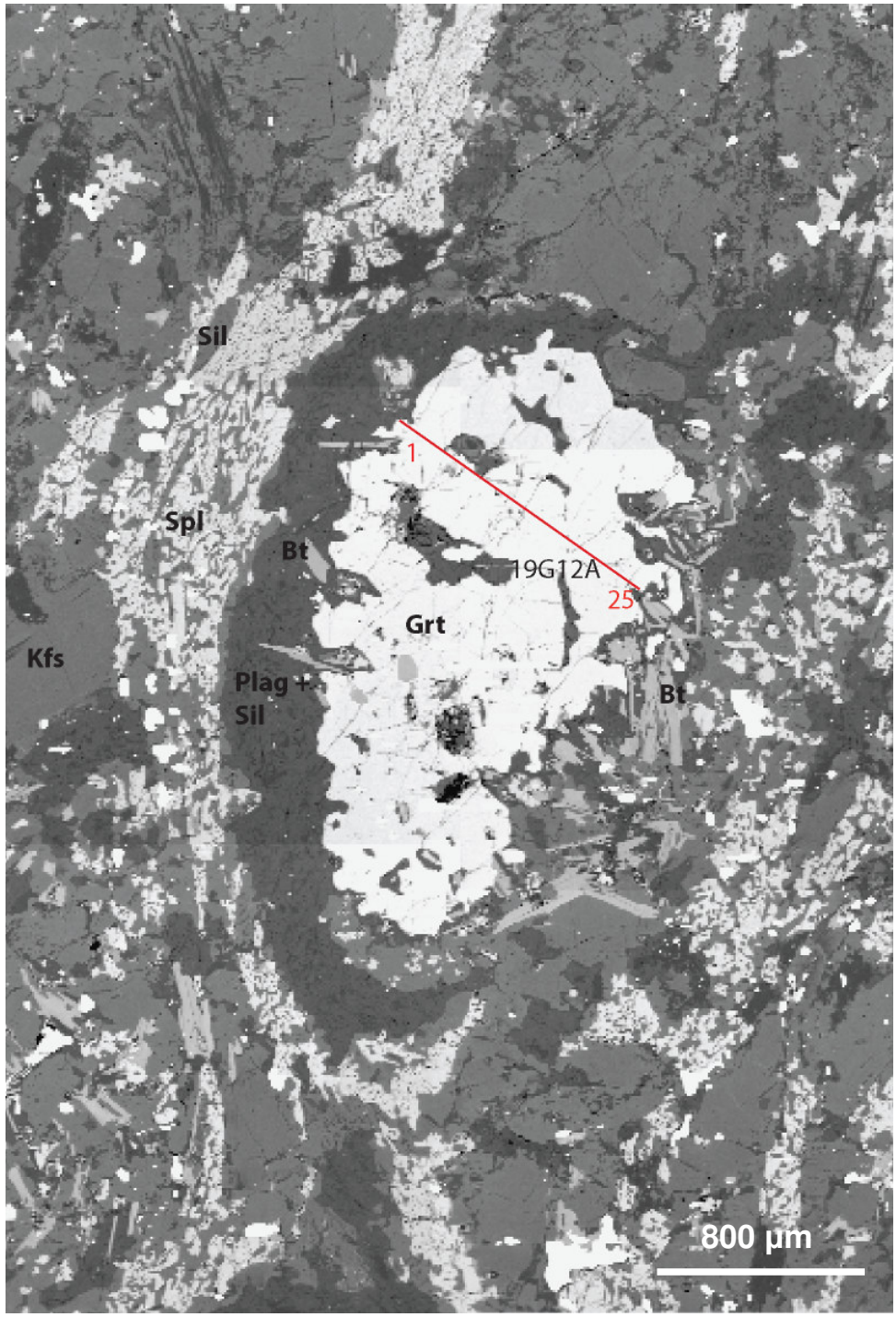

BSE image of location **19G12** in sample H19-H. The position of the zoning profile through the garnet is indicated with a red line.

Sample H20-C

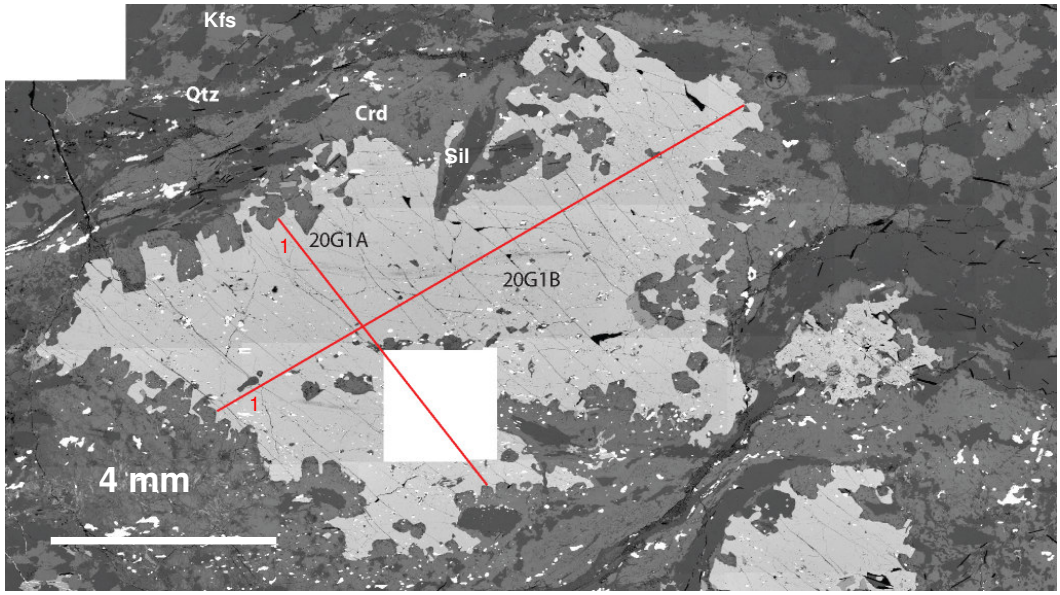

BSE image of location **20G1** in sample H20-C. The position of the zoning profiles through the garnet are indicated with red lines. Garnet is replaced by cordierite at the rims, showing well developed crystal faces. The foliation is formed by quartz + K-feldspar + sillimanite.

Sample K4

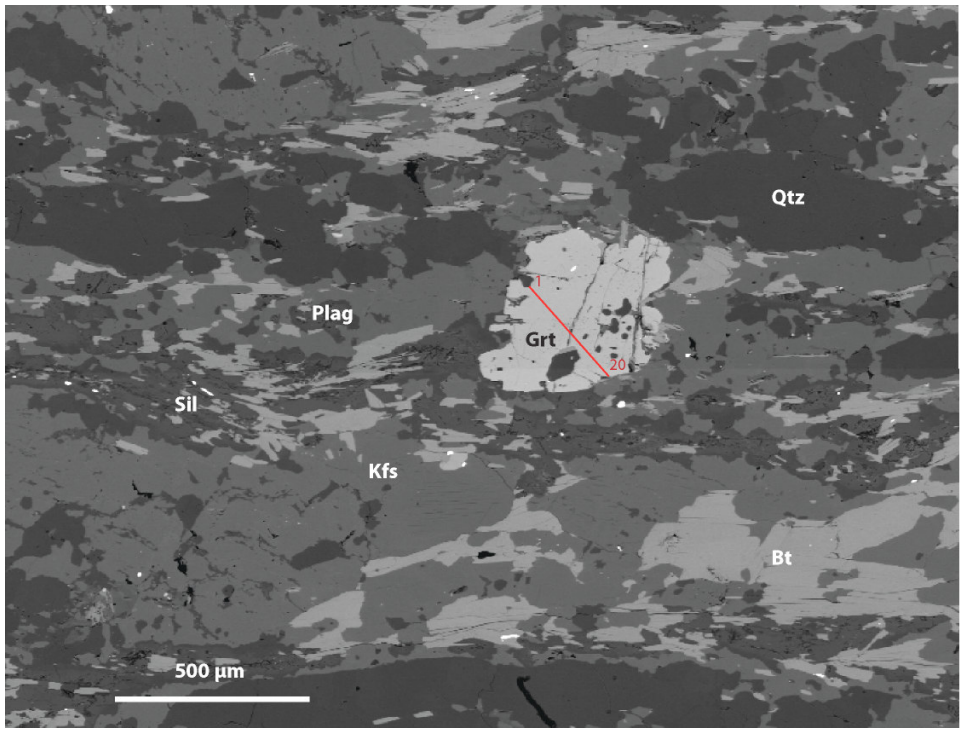

BSE image of location **K4G1** in sample K4. The position of the zoning profile through the garnet is indicated with a red line.

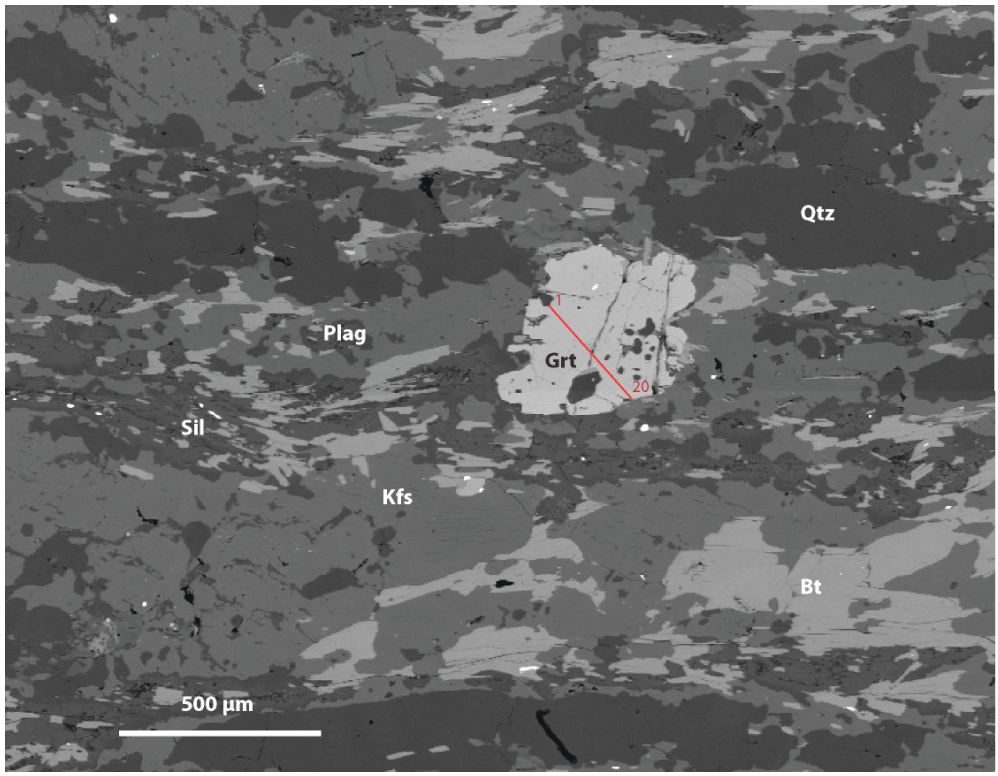

BSE image of location **K4G2** in sample K4. The position of the zoning profile through the garnet is indicated with a red line.

APPENDIX 6

Mineral abbreviations as used in the text and figures, based on Kretz (1983).

Abbreviation	Mineral name	Chemical formula	Number of cations per fixed number of oxygens
Als	aluminosilicate	Al_2SiO_5	3 cations/ 5 O
Bt	biotite	$K(Mg,Fe)_3(Si_3Al)O_{10}(OH,F)_2$	8-10 cations/ 10-12 O
Crn	corundum	Al_2O_3	2 cations/ 3 O
Cpx	clinopyroxene	$XYSi_2O_6$ where X=Ca,Na,Mg,Fe^{2+},Mn,Li and Y=Mg,Fe^{2+},Mn,Fe^{3+},Al,Cr,Ti diopside $CaMgSi_2O_6$, hedenbergite $CaFeSi_2O_6$, augite $(Ca,Na)(Mg,Fe,Al)(Si,Al)_2O_6$, jadeite $Na(Al,Fe)Si_2O_6$, aegirine $NaFe^{3+}Si_2O_6$	4 cations/ 6 O
Crd	cordierite	$Mg_2Al_4Si_5O_{18}$ (also $Fe_2Al_4Si_5O_{18}$*nH_2O)	11 cations/ 18 O
ep	epidote	$Ca_2(Fe^{3+},Al)_3(SiO_4)_3(OH)$ = $Ca_2(Fe,Al)Al_2(SiO_4)(Si_2O_7)O(OH)$	9 cations/ 13 O
Fsp	feldspar	see K-feldspar and plagioclase	
grt	garnet	$A_3B_2(SiO_4)_3$ where A=Mg,Fe,Mn,Ca and B=Al,Fe,Cr pyrope: prp $Mg_3Al_2(SiO_4)_3$, almandine (alm) $Fe_3Al_2(SiO_4)_3$, grossular (grs) $Ca_3Al_2(SiO_4)_3$, spessartine (spess) $Mn_3Al_2(SiO_4)_3$, uvarovite $Ca_3Cr_2(SiO_4)_3$, andradite $Ca_3Fe_2(SiO_4)_3$, schorlomite $Ca_3(Ti,Fe)_2((Si,Fe)O_4)_3$,	8 cations/ 12 O
Ilm	ilmenite	$FeTiO_3$	2 cations/ 3 O
Kfs	K-feldspar	$KAlSi_3O_8$: sanidine, orthoclase, microcline	5 cations/ 8 O
Mag	magnetite	Fe_2O_3	2 cations/ 3 O
Mnz	monazite	monazite-(Ce) $(Ce,La,Nd,Th)PO_4$, monazite-(La) $(La,Ce,Nd)PO_4$, monazite-(Nd) $(Nd,Ce,La)(P,Si)O_4$, monazite –(Sm) $SmPO_4$	2 cations/ 4 O
Mu	muscovite	$KAl_3Si_3O_{10}(OH,F)_2$	9 cations/ 11 O
Plag	plagioclase	end-members: albite $NaAlSi_3O_8$ and anorthite $CaAl_2Si_2O_8$	5 cations/ 8 O
Qtz	quartz	SiO_2	1 cation/ 2 O
Sil	sillimanite	Al_2SiO_5	3 cations/ 5 O
Spl	spinel	AB_2O_4 where A=Mg,Fe^{2+},Zn,Mn and B=Al,Fe^{3+},Cr 3 series determined by B-metal: spinel series with Al, magnetite series with Fe, chromite series with Cr. Spinel series: spinel $MgAl_2O_4$, hercynite $FeAl_2O_4$, galaxite $MnAl_2O_4$, gahnite $ZnAl_2O_4$	3 cations/ 4 O
Ttn	titanite	$CaTiO(SiO_4)$	3 cations/ 5 O
Wmca	white mica		9 cations/ 11 O
Zi	zircon	$ZrSiO_4$	2 cations/ 4 O

Mineral abbreviations as used in the text (corresponding to Kretz, 1983) with their corresponding names and chemical formulas. In the last column, the number of cations per number of oxygens in the formula is given, since this is useful during analyses with the EMP.

APPENDIX 7

Hand specimen of samples selected for PT analyses

Parts of the hand specimen used for bulk analyses are indicated with a box in the figures below (where necessary), otherwise a fragment as large as possible has been crushed and analysed.

Sample H12-G

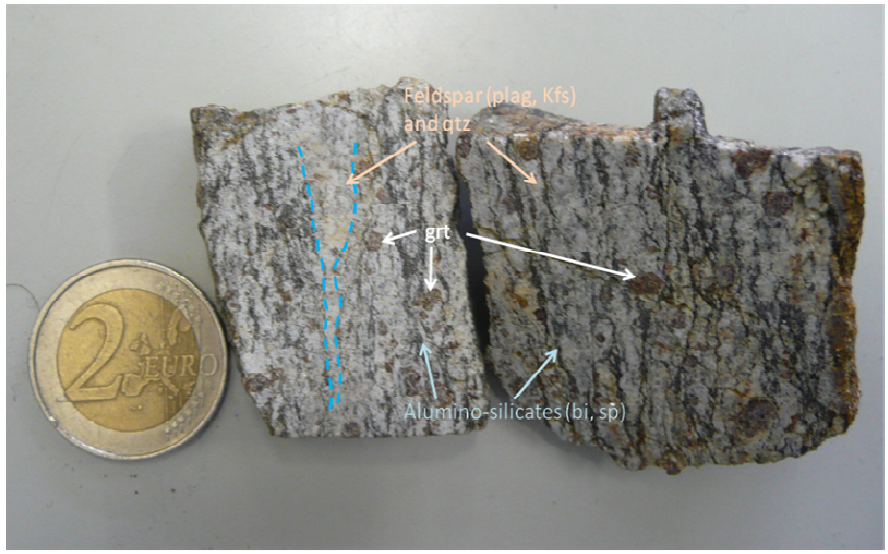

Sample H19-H

Sample H20-C

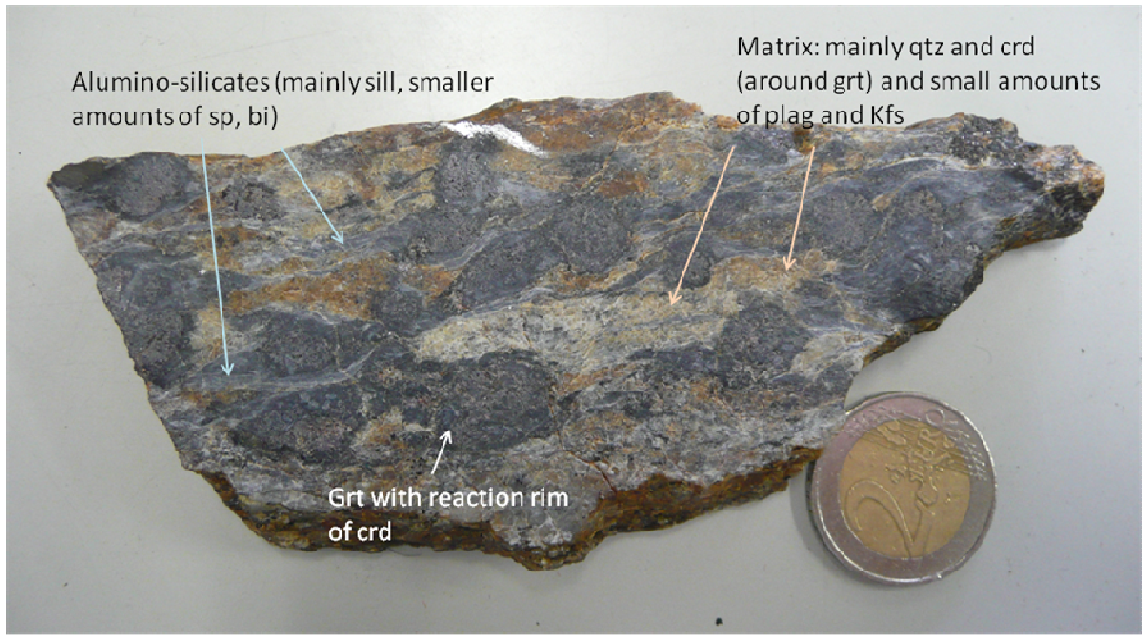

Sample K4

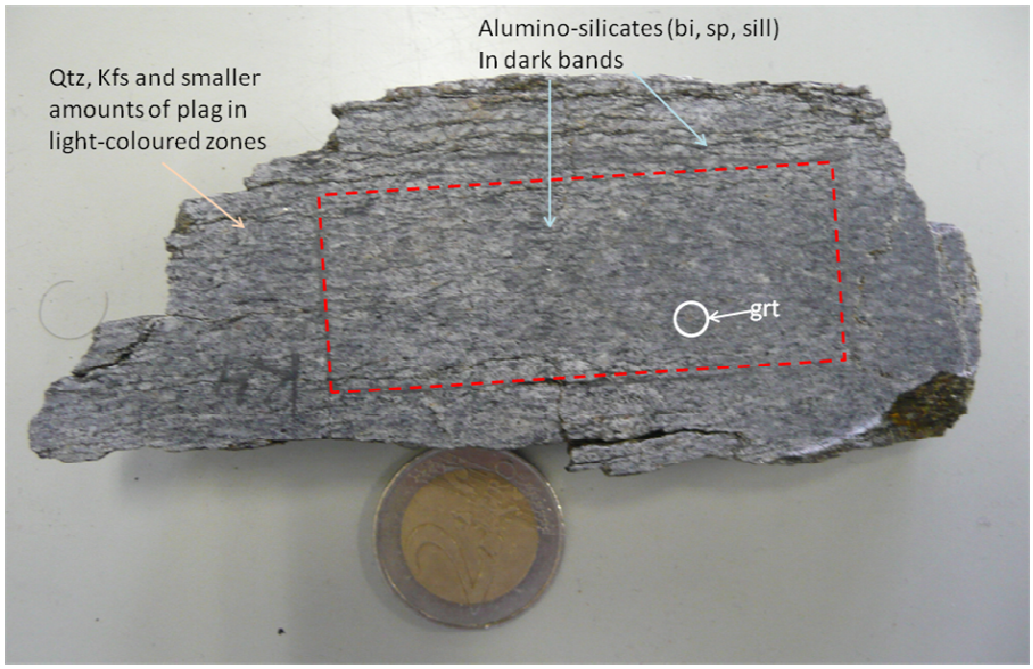

Sample K13

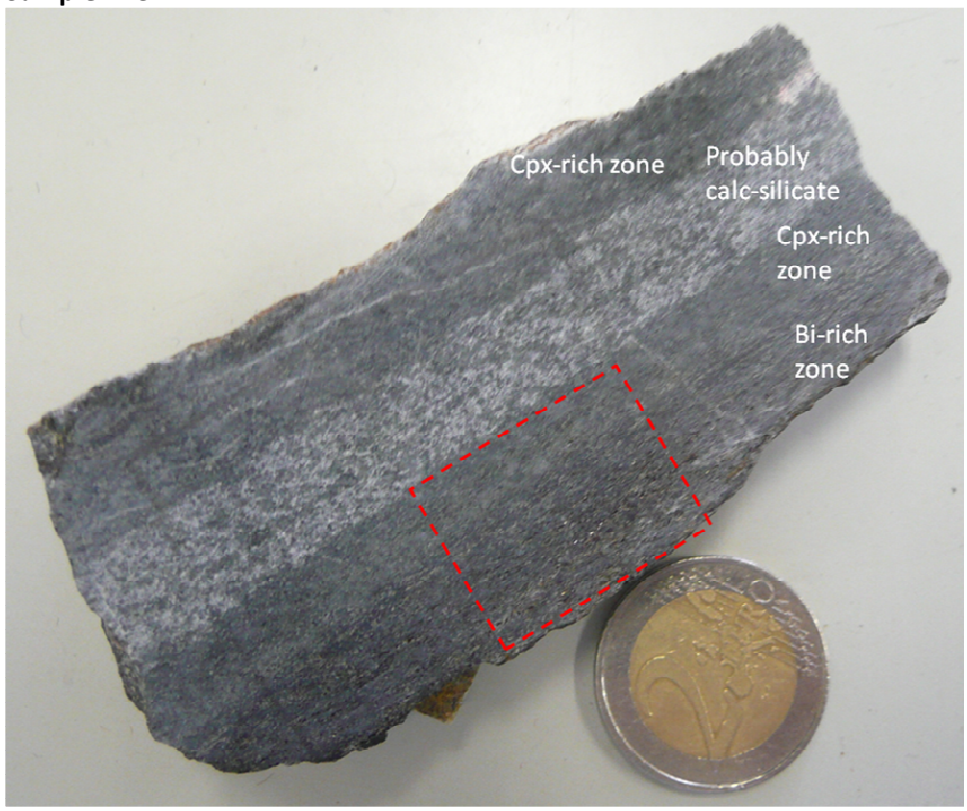

APPENDIX 8

Representative mineral analyses

Table 8.5. Representative analyses of **garnet**. Oxides in wt%, recalculated to 12 oxygens and 8 cations.

Mineral	Grt	Grt	Grt	Grt	Grt	Grt	Grt	Grt	Grt	Grt	Grt	Grt	Grt	Grt
Sample	H12-G	H12-G	H12-G	H19-H	H19-H	H19-H	H19-H	H19-H	H20-C	H20-C	H20-C	H20-C	K4	K4
EMP point	12G1A	12G3A	12G3A	19G1A	19G1A	19G1C	19G1C	19G12A	20G1A	20G1A	20G1B	20G1B	K4G1A	K4G1A
	average	core	rim	core	rim	core	rim	average	core	rim	core	rim	core	rim
SiO2	37.45	38.30	38.34	36.84	36.96	37.51	37.68	38.00	37.65	37.03	38.02	37.48	38.16	37.84
Al2O3	21.48	20.93	21.17	20.42	20.18	20.52	20.70	21.04	20.80	20.65	21.05	20.95	21.27	21.03
FeO	35.14	31.09	33.37	39.02	36.77	38.91	36.82	36.34	34.09	37.66	34.33	38.38	34.34	35.69
MnO	1.61	1.34	1.42	0.44	0.70	0.35	0.81	1.16	0.66	0.73	0.65	0.77	3.17	3.14
MgO	4.40	4.81	5.72	1.84	2.71	1.63	3.15	3.59	3.74	3.19	3.78	2.59	2.67	2.78
CaO	0.72	4.46	1.04	2.05	2.90	2.63	2.02	1.38	3.13	1.11	3.11	1.01	1.82	1.12
Na2O	0.00	0.02	0.01	0.01	0.01	0.01	0.01	0.01	0.01	0.02	0.01	0.01	0.01	0.00
TiO2	0.02	0.07	0.01	0.03	0.06	0.04	0.05	0.03	0.41	0.01	0.09	0.16	0.01	0.01
Cr2O3	0.01	0.00	0.01	0.00	0.01	0.00	0.00	0.00	0.01	0.01	0.02	0.01	0.01	0.00
Total	100.83	101.02	101.08	100.65	100.31	101.58	101.24	101.55	100.50	100.42	101.04	101.36	101.45	101.63
Si	2.98	3.01	3.01	2.99	2.99	3.01	3.01	3.01	3.00	2.99	3.01	3.00	3.03	3.01
Al	2.01	1.94	1.96	1.96	1.93	1.94	1.95	1.96	1.95	1.96	1.97	1.98	1.99	1.97
Fe-tot	2.34	2.04	2.19	2.65	2.49	2.61	2.46	2.41	2.27	2.54	2.27	2.57	2.28	2.38
Mn	0.11	0.09	0.09	0.03	0.05	0.02	0.05	0.08	0.04	0.05	0.04	0.05	0.21	0.21
Mg	0.52	0.56	0.67	0.22	0.33	0.20	0.38	0.42	0.44	0.38	0.45	0.31	0.32	0.33
Ca	0.06	0.38	0.09	0.18	0.25	0.23	0.17	0.12	0.27	0.10	0.27	0.09	0.15	0.10
Na	0.00	0.00	0.00	0.00	0.00	0.00	0.00	0.00	0.00	0.00	0.00	0.00	0.00	0.00
Ti	0.00	0.00	0.00	0.00	0.00	0.00	0.00	0.00	0.02	0.00	0.00	0.01	0.00	0.00
Cr	0.00	0.00	0.00	0.00	0.00	0.00	0.00	0.00	0.00	0.00	0.00	0.00	0.00	0.00
Cations	8.02	8.02	8.01	8.03	8.04	8.02	8.02	8.01	8.00	8.03	8.00	8.00	7.98	8.00
X(Mg)	0.17	0.18	0.22	0.07	0.10	0.06	0.12	0.14	0.15	0.12	0.14	0.10	0.11	0.11
X(Fe)	0.77	0.67	0.72	0.86	0.80	0.85	0.80	0.80	0.75	0.83	0.76	0.85	0.77	0.79
X(Ca)	0.02	0.12	0.03	0.06	0.08	0.07	0.06	0.04	0.09	0.03	0.09	0.03	0.05	0.03
X(Mn)	0.04	0.03	0.03	0.01	0.02	0.01	0.02	0.03	0.01	0.02	0.01	0.02	0.07	0.07
Fe/(Fe+Mg)	0.82	0.78	0.77	0.92	0.88	0.93	0.87	0.85	0.84	0.87	0.84	0.89	0.88	0.88

Table 8.6 (left). Representative analyses of **spinel**. Oxides in wt%, recalculated to 4 oxygens and 3 cations.

Table 8. 7 (right). Representative analyses of **sillimanite**. Oxides in wt%, recalculated to 5 oxygens.

Mineral	Spl	Spl	Spl
Sample	H12-G	H19-H	H20-C
SiO2	0.01	0.01	0.01
TiO2	0.04	0.05	0.04
Al2O3	59.12	58.14	57.21
Cr2O3	0.04	0.01	0.17
FeO	35.71	37.85	36.61
MnO	0.15	0.11	0.01
MgO	4.45	3.67	2.42
V2O3	0.11	0.06	0.37
NiO	0.00	0.01	0.10
ZnO	0.73	0.07	3.37
Total	100.35	99.99	100.32
Si	0.00	0.00	0.00
Ti	0.00	0.00	0.00
Al	1.95	1.94	1.93
Cr	0.00	0.00	0.00
Fe-tot	0.84	0.90	0.88
Mn	0.00	0.00	0.00
Mg	0.19	0.16	0.10
V	0.00	0.00	0.00
Ni	0.00	0.00	0.00
Zn	0.02	0.00	0.07
Cations	3.00	3.00	3.00
Xsp	0.18	0.15	0.11
Xherc	0.82	0.85	0.89

Mineral	Sil	Sil	Sil	Sil	Sil
Sample	H12-G	H12-G	H19-H	H20-C	K4
	inclusion	matrix	matrix	average	matrix
SiO2	36.24	35.77	35.81	36.33	35.58
TiO2	0.02	0.01	0.01	0.01	0.01
Al2O3	62.81	61.90	62.07	62.69	63.76
Cr2O3	0.02	0.01	0.00	0.04	0.00
FeO	0.88	0.25	0.27	0.32	0.31
MnO	0.04	0.01	0.01	0.00	0.00
MgO	0.01	0.01	0.01	0.01	0.03
CaO	0.00	0.01	0.01	0.00	0.04
Na2O	0.01	0.00	0.00	0.00	0.00
K2O	0.00	0.01	0.01	0.01	0.00
Total	100.03	97.97	98.20	99.42	99.73
Si	0.98	0.99	0.99	0.99	0.97
Ti	0.00	0.00	0.00	0.00	0.00
Al	2.01	2.01	2.01	2.01	2.04
Cr	0.00	0.00	0.00	0.00	0.00
Fe-tot	0.02	0.01	0.01	0.01	0.01
Mn	0.00	0.00	0.00	0.00	0.00
Mg	0.00	0.00	0.00	0.00	0.00
Ca	0.00	0.00	0.00	0.00	0.00
Na	0.00	0.00	0.00	0.00	0.00
K	0.00	0.00	0.00	0.00	0.00
Cations	3.01	3.01	3.01	3.01	3.01

Table 8.8. Representative analyses of **biotite**. Analyses in wt%, recalculated to 11 oxygens.

Mineral	Bt	Bt	Bt	Bt	Bt	Bt	Bt	Bt
Sample	H12-G	H19-H	H19-H	H20-C	H20-C	K4	K4	K13
EMP point	S1	S21	S18	Average	average	S10	average	average
	matrix	incl	matrix	matrix away from grt	matrix near grt	inclusion	matrix	matrix
SiO2	33.93	32.88	33.27	34.32	35.37	33.66	33.54	35.00
Al2O3	18.27	17.68	20.14	17.89	17.20	18.72	19.60	13.83
FeO	17.63	20.84	20.43	22.24	18.07	22.23	21.86	21.08
MnO	0.08	0.02	0.05	0.02	0.03	0.14	0.12	0.15
MgO	9.03	7.79	7.44	7.57	10.70	7.95	7.01	10.18
CaO	0.30	0.01	0.00	0.00	0.00	0.00	0.06	0.06
K2O	8.20	9.04	9.60	9.20	9.54	8.79	9.32	9.01
Na2O	0.14	0.30	0.16	0.15	0.16	0.32	0.10	0.05
TiO2	4.50	5.40	3.22	3.36	3.31	3.21	2.09	4.07
Cr2O3	0.02	0.00	0.00	0.06	0.05	0.01	0.00	0.08
Total	92.10	93.94	94.30	94.81	94.44	95.04	93.70	93.50
Si	2.65	2.58	2.59	2.67	2.71	2.61	2.64	2.76
Al	1.68	1.63	1.85	1.64	1.55	1.71	1.82	1.29
Fe-tot	1.15	1.37	1.33	1.45	1.16	1.44	1.44	1.39
Mn	0.01	0.00	0.00	0.00	0.00	0.01	0.01	0.01
Mg	1.05	0.91	0.86	0.88	1.22	0.92	0.82	1.20
Ca	0.02	0.00	0.00	0.00	0.00	0.00	0.00	0.01
K	0.82	0.90	0.95	0.91	0.93	0.87	0.94	0.91
Na	0.02	0.04	0.02	0.02	0.02	0.05	0.01	0.01
Ti	0.26	0.32	0.19	0.20	0.19	0.19	0.12	0.24
Cr	0.00	0.00	0.00	0.00	0.00	0.00	0.00	0.01
Cations	7.67	7.76	7.79	7.78	7.80	7.80	7.80	7.81

Table 8.9. Representative analyses of **plagioclase**.
Analyses in wt%, recalculated to 8 oxygens.

Mineral	Plag	Plag	Plag	Plag	Plag	Plag
Sample	H12-G	H19-H	H19-H	H20-C	K4	K4
	matrix	inclusion	matrix	matrix	inclusion	matrix
SiO2	56.59	58.43	60.43	56.59	65.44	65.39
Al2O3	26.97	25.31	23.98	26.97	21.35	21.28
FeO	0.15	0.56	0.18	0.15	0.31	0.08
MnO	0.01	0.02	0.01	0.01	0.01	0.02
MgO	0.01	0.00	0.00	0.01	0.00	0.00
CaO	8.85	6.96	5.16	8.85	2.03	2.31
K2O	0.08	0.28	0.22	0.08	0.12	0.14
Na2O	6.38	7.34	8.37	6.38	10.43	10.33
TiO2	0.00	0.02	0.03	0.00	0.01	0.01
Cr2O3	0.01	0.01	0.01	0.01	0.02	0.00
Total	99.05	98.92	98.38	99.05	99.72	99.57
Si	2.56	2.64	2.73	2.56	2.89	2.89
Al	1.44	1.35	1.28	1.44	1.11	1.11
Fe-tot	0.01	0.02	0.01	0.01	0.01	0.00
Mn	0.00	0.00	0.00	0.00	0.00	0.00
Mg	0.00	0.00	0.00	0.00	0.00	0.00
Ca	0.43	0.34	0.25	0.43	0.10	0.11
K	0.00	0.02	0.01	0.00	0.01	0.01
Na	0.56	0.64	0.73	0.56	0.89	0.88
Ti	0.00	0.00	0.00	0.00	0.00	0.00
Cr	0.00	0.00	0.00	0.00	0.00	0.00
Cations	5.00	5.01	5.01	5.00	5.01	5.00
Xan	0.43	0.34	0.25	0.43	0.10	0.11
Xab	0.56	0.65	0.74	0.56	0.90	0.88
Xor	0.00	0.02	0.01	0.00	0.01	0.01

Table 8.10. Representative analyses of **muscovite**.
Analyses in wt%, recalculated to 11 oxygens.

Mineral	Ms	Ms	Ms	Ms
Sample	H19-H	H19-H	H20-C	K4
EMP point	S2	S16	S37	S8
	inclusion	matrix	matrix	matrix
SiO2	47.92	46.31	45.07	35.96
Al2O3	30.76	36.79	34.74	30.19
FeO	2.82	0.78	1.44	4.23
MnO	0.01	0.02	0.00	0.01
MgO	0.79	0.14	0.64	0.88
CaO	0.05	0.03	0.02	2.84
K2O	8.93	9.46	9.90	2.14
Na2O	0.10	0.11	0.66	0.38
TiO2	2.02	0.01	0.09	0.02
Cr2O3	0.01	0.00	0.00	0.01
Total	93.39	93.64	92.56	76.65
Si	3.24	3.09	3.08	2.93
Al	2.45	2.90	2.80	2.90
Fe-tot	0.16	0.04	0.08	0.29
Mn	0.00	0.00	0.00	0.00
Mg	0.08	0.01	0.06	0.11
Ca	0.00	0.00	0.00	0.25
K	0.77	0.81	0.86	0.22
Na	0.01	0.01	0.09	0.06
Ti	0.10	0.00	0.00	0.00
Cr	0.00	0.00	0.00	0.00
Cations	6.82	6.87	6.99	6.76

Table 8.11. Representative analyses of **K-feldspar**.
Analyses in wt%, recalculated to 8 oxygens.

Mineral	Kfs	Kfs	Kfs	Kfs	Kfs	Kfs	Kfs
Sample	H12-G	H12-G	H19-H	H19-H	H20-C	K4	K13
	inclusion	matrix	inclusion	matrix	matrix	matrix	matrix
SiO2	63.10	62.94	63.01	62.52	63.22	63.68	61.35
TiO2	0.04	0.04	0.03	0.01	0.02	0.00	0.07
Al2O3	18.77	18.73	18.63	18.70	18.73	18.30	18.38
Cr2O3	0.01	0.00	0.00	0.00	0.00	0.00	0.00
FeO	0.52	0.05	0.41	0.29	0.00	0.10	0.06
MnO	0.02	0.00	0.00	0.01	0.00	0.01	0.01
MgO	0.01	0.00	0.02	0.00	0.00	0.01	0.00
CaO	0.12	0.22	0.06	0.08	0.12	0.02	0.02
Na2O	1.93	2.22	1.51	1.82	1.84	0.98	1.10
K2O	13.84	13.46	14.70	14.17	14.03	15.67	14.44
Total	98.35	97.67	98.37	97.61	97.97	98.77	95.42
Si	2.94	2.95	2.94	2.93	2.96	2.97	2.96
Ti	0.00	0.00	0.00	0.00	0.00	0.00	0.00
Al	1.03	1.03	1.03	1.03	1.03	1.01	1.04
Cr	0.00	0.00	0.00	0.00	0.00	0.00	0.00
Fe-tot	0.02	0.00	0.02	0.01	0.00	0.00	0.00
Mn	0.00	0.00	0.00	0.00	0.00	0.00	0.00
Mg	0.00	0.00	0.00	0.00	0.00	0.00	0.00
Ca	0.01	0.01	0.00	0.00	0.01	0.00	0.00
Na	0.17	0.20	0.14	0.17	0.17	0.09	0.10
K	0.82	0.80	0.88	0.85	0.84	0.93	0.89
Cations	5.00	5.00	5.00	5.00	5.00	5.00	5.00
Xan	0.01	0.01	0.00	0.00	0.01	0.00	0.00
Xab	0.17	0.20	0.13	0.16	0.17	0.09	0.10
Xor	0.82	0.79	0.86	0.83	0.83	0.91	0.90

Table 8.12. Representative analyses of **cordierite**.
Analyses in wt%, recalculated to 18 oxygens.

Mineral	Crd	Crd
Sample	H20-C	H20-C
EMP point	average inclusions	average matrix
SiO2	47.55	46.91
TiO2	0.00	0.00
Al2O3	32.54	32.10
Cr2O3	0.00	0.01
FeO	10.82	12.60
MnO	0.08	0.09
MgO	6.92	5.58
CaO	0.00	0.02
Na2O	0.07	0.10
K2O	0.00	0.13
Total	97.99	97.56
Si	4.97	4.97
Ti	0.00	0.00
Al	4.01	4.01
Cr	0.00	0.00
Fe-tot	0.95	1.12
Mn	0.01	0.01
Mg	1.08	0.88
Ca	0.00	0.00
Na	0.01	0.02
K	0.00	0.02
Cations	11.03	11.04
Xcrd	0.53	0.44
Xfcrd	0.47	0.56

Table 8.13. Representative analyses of **clinopyroxene.**
Analyses in wt%, recalculated to 6 oxygens and 4 cations.

Mineral	Cpx	Cpx
Sample	K13	K13
EMP point	cpx-band	bt-band
SiO2	50.33	49.48
TiO2	0.07	0.07
Al2O3	0.90	0.39
Cr2O3	0.01	0.00
FeO	16.04	34.78
MnO	0.45	0.86
MgO	8.37	13.30
CaO	22.60	0.77
Na2O	0.20	0.00
Total	98.97	99.66
Si	1.97	1.97
Ti	0.00	0.00
Al	0.04	0.02
Cr	0.00	0.00
Fe-tot	0.52	1.16
Mn	0.02	0.03
Mg	0.49	0.79
Ca	0.95	0.03
Na	0.01	0.00
Cations	4.00	4.00
Fe3+ (Droop, 1987)	0.03	0.04
Fe2+	0.49	1.12

Table 8.14. XRF analyses for the samples from the Hırkadağ (H12-G, H19-H, H20-C) and Kırşehir (K4 and K13) massifs. Analyses in wt% and normalised to 100%, assuming that $Fe^{total} = Fe^{2+}$.

Sample name		**K4**	**K13**	**H12-G**	**H19-H**	**H20-C**
SiO2	**wt%**	69.70	62.97	61.70	49.78	62.94
AlO3	**wt%**	14.71	14.39	19.44	29.20	21.95
TiO2	**wt%**	0.44	0.70	0.86	1.10	1.49
FeO	**wt%**	4.45	5.85	5.78	8.34	9.17
MnO	**wt%**	0.06	0.14	0.15	0.08	0.12
CaO	**wt%**	0.78	7.94	1.09	0.68	0.55
MgO	**wt%**	1.38	2.56	1.38	0.99	1.30
Na2O	**wt%**	1.74	2.32	3.53	2.68	0.53
K2O	**wt%**	6.75	3.13	6.06	7.15	1.95
Total		100	100	100	100	100